THREE-DIMENSIONAL WAKES IN LINEARLY STRATIFIED LIQUIDS

by

CHARLES B. CLARK

B.S. University of Massachusetts
(1964)

PHILIP J. STOCKHAUSEN

S.B. Massachusetts Institute of Technology
(1964)

submitted in partial fulfillment of
the requirements for the degree of
Master of Science

at the

Massachusetts Institute of Technology

June 1966

Signature of Authors . . . . . .
Department of Civil Engineering, May 26, 1966

. . . . . .
Department of Civil Engineering, May 26, 1966

Certified by . . . . . .
Thesis Supervisor

Accepted by . . . . . .
Chairman, Departmental Committee on Graduate Students

ACKNOWLEDGMENTS

Sincere thanks are extended to Associate Professor John F. Kennedy for his valuable advice and assistance throughout the tenure of this study. The authors also wish to thank Miss Ruth Frazer for her excellent job of typing this thesis and Mrs. Alice Clark for her encouragement and support.

This project was financed with funds from the Office of Naval Research as administered by the M.I.T. Division of Sponsored Research under designation DSR 8228.

ABSTRACT

THREE-DIMENSIONAL WAKES IN LINEARLY STRATIFIED LIQUIDS

by

Philip J. Stockhausen, Charles B. Clark

Submitted to the Department of Civil Engineering on May 26, 1966, in partial fulfillment of the requirements for the degree of Master of Science.

The wake and the zone of turbulently mixed fluid behind a three-dimensional body in a liquid with a linear density gradient were studied. The objective of this investigation was to determine the configuration of the wake and the mixed zone it generated as a function of distance behind the body, and to examine the interaction of the wake and the free surface. In the course of the investigation, an efficient method was developed for generating a linearly stratified fluid from an initially two-layered fluid.

All experiments were conducted in a tank 50' long, and 4.5' wide, which contained linearly stratified salt water to a depth of 30". A self-propelled model, 2 1/2' long and 4 1/2" in diameter with a 6-inch diameter circular disc mounted on the bow, was used to generate the wake. Specially designed conductivity probes were used to measure the salt concentration distribution behind the body. A motion picture study was conducted to obtain data on surface movements. The average Reynolds number for the experiments, based on the disc diameter, was 8.9×10^4. Most experiments were conducted with a density gradient of

$$\frac{1}{\rho_o}\frac{d\rho}{dy} = -0.003\ (\text{ft})^{-1},$$

although supplementary surface motion experiments were made with gradients of zero and $-0.0015\ (\text{ft})^{-1}$, to determine the effect of the strength of the stratification on the surface motion.

The principal results obtained from the experiments are as follows:

1. The initial turbulent expansion of the wake, immediately behind body, was almost uniform in all directions, similar to the wake generated in a homogeneous fluid. At approximately 50 disc diameters behind the model, turbulent diffusion had subsided to the point that a significant role was played by gravity forces, which acted on the fluid placed in density disequilibrium by the turbulent mixing. The gravitational forces propelled

the mixed fluid back toward a level of density equilibrium. This resulted in a rapid vertical collapse of the mixed region. The collapse was complete at a distance of about 75 disc diameters behind the model.

2. A continued horizontal expansion of the mixed region was detected throughout all stages of wake generation and collapse, governed at first by turbulent diffusion, and during later stages by the collapsing of the mixed-fluid zone, which expanded laterally at about the level of the model path. The horizontal extent of the mixed zone increased almost linearly with time.

3. During the wake collapse, a convergence of fluid toward the vertical plane of the model path was detected at the free surface. This converging fluid replaced the mixed fluid which settled vertically toward density equilibrium.

4. An argument based on energy considerations was presented to show that the convergence of surface particles can occur only if the turbulent wake extends to the free surface.

5. The rate of horizontal transverse convergence of fluid at the free surface decreased as the density gradient, $\frac{1}{\rho_o}\frac{d\rho}{dy}$, was decreased.

6. The passage of the model and ensuing wake collapse generated many modes of internal gravity waves.

Thesis supervisor: John F. Kennedy

Title: Associate Professor

TABLE OF CONTENTS

LIST OF FIGURES AND TABLES

CHAPTER I

INTRODUCTION

The behavior of wakes in density stratified fluids has become a subject of increasing interest in recent years, as more attention has been directed toward understanding all phenomena associated with the interaction between a submarine and its environment. A wake generated in a density stratified fluid demonstrates several peculiar characteristics which do not occur in homogeneous fluids. The purpose of this report is to present the results of a laboratory investigation into the configuration of the wake generated by a self-propelled body moving in a laboratory tank containing a fluid whose density is linearly stratified. In addition, attention was directed to fluid displacements generated at the free surface by the moving body.

Previous investigations have been conducted to study the wake behavior of both two and three-dimensional bodies in homogeneous and in stratified fluids. A brief review of these studies is helpful in understanding the current investigation.

A submerged body moving in an otherwise quiescent fluid, or a body held stationary in a moving fluid, will generate a zone of turbulent mixing behind it. This zone of mixing is defined as the wake region, and its width is denoted by some lateral dimension, b. As the wake grows laterally behind the body, it transmits its momentum to the surrounding fluid. For a homogeneous fluid, b may be defined by noting the region where mean fluid velocities differ from those of the surrounding fluid, as illustrated by the example in Figure 1. In the case of a density stratified fluid, it is possible to define a wake width in terms of the variations in the concentration of the density biasing agent. In this case, the wake width is associated with the lateral dimension of the region where concentrations vary by some fixed amount from their initial values.

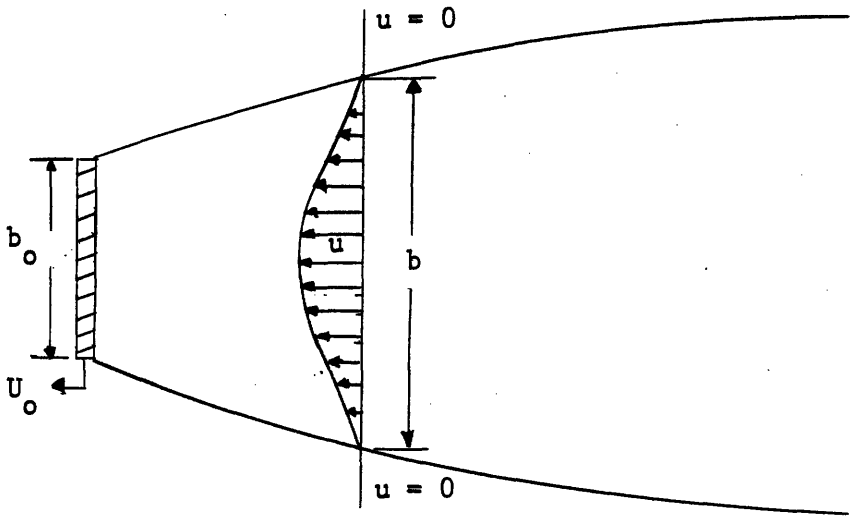

Definition Sketch of the Wake Width, b, for a Moving Body in a Still Homogeneous Fluid

Figure 1

The classical analyses of a two-dimensional wake in a homogeneous fluid are summarized by Schlichting[1]. He reports that the width of the wake of a two-dimensional body is proportional to $x^{1/2}$, where x is the distance behind the body. Such, however, is not the case for a two-dimensional wake in a density stratified fluid. As fluid globules or "puffs" of one density are displaced by turbulent mixing, they are surrounded by fluid of a different density. Turbulent and molecular mixing will bring the eddy and surrounding fluids to a new equilibrium density. In this manner, the horizontal momentum of the displaced fluid is transferred to the surrounding fluid, which is the mechanism by which the width of the momentum wake increases. This mixing process, however, is not instantaneous, and before complete mixing is accomplished, the displaced fluid is subjected to a gravitational force pulling it back toward a position of density equilibrium. Gravity, therefore, exhibits an inhibiting effect on the lateral transfer of momentum to the surrounding fluid and, consequently, suppresses the wake growth. The wake width may attain a maximum value a short distance behind the body, and then diminish as the gravity effects dominate the turbulent mixing. This phenomenon, referred to as "wake collapse", was observed in experimental studies at M.I.T. by Prych, Harty, and Kennedy[2], and by Kennedy and Froebel[3]. Both groups used the

same experimental equipment consisting of a flat plate of height, $b_o = 4.13$ inches, towed broadside to the direction of travel at the interface of a two-layered density stratified fluid. The Reynolds numbers for the experiment ranged from 2.1×10^4 to 4.7×10^4. Measurements were made of the variation of concentration and velocity profiles as the plate traveled the length of the laboratory tank. Prych, et al., defined a characteristic wake half-width, b_c', as the height above or below the original interface where

$$C_* = \frac{C - C_T}{C_B - C_T} = 0.25,\ 0.75 \qquad (1)$$

where

C = absolute concentration

C_T = concentration at the free surface

C_B = concentration at the bottom of the tank

C_* = normalized concentration

In order to include the effect of differences in concentration between the two layers, a stratification parameter, J, was defined:

$$J = \sqrt{\frac{\frac{\Delta\rho}{\rho} g\, b_o}{C_D\, U^2}} \qquad (2)$$

where

ρ = mass density of upper layer

$\Delta\rho$ = mass density difference of lower and upper layer

g = a gravitational constant

b_o = height of the plate

C_D = drag coefficient of the plate

U = velocity of the plate

The results of their experiments are summarized in Figure 2[2]. Referring to the figure, it is seen that the width of the concentration wake initially increases with distance behind the plate and then subsequently decreases, due to the gravitational effects described above. Prych and co-workers also noted that the degree of vertical mixing decreased as the initial concentration difference between the two layers was increased. This fact reinforces the notion that increased stability is associated with an increase in the degree of stratification.

The data obtained by Kennedy and Froebel[3] for the momentum wake are plotted in Figure 3 and are compared with Schlichting and Reichardt's[1] relation for circular cylinders of diameter, b_o, in a homogeneous fluid. The equation referred to in the figure is

$$b_{1/2} = 0.25(x\, C_D\, b_o)^{1/2} \qquad (3)$$

It is interesting to note that the wake collapse here is preceded by a region in which the wake width is greater for the stratified than for the homogeneous case. This is contrary to what is expected and has not yet been explained.

The behavior of three-dimensional axi-symmetric wakes is somewhat different than the behavior described above for simple two-dimensional wakes. According to Schlichting's[1] description, the width, b, of a circular wake in a homogeneous fluid increases as $x^{1/3}$ rather than $x^{1/2}$. A three-dimensional turbulent wake in a density stratified liquid would be expected to collapse at a greater rate than a two-dimensional wake because of the lateral expansion of the mixed zone into the unmixed fluid, and corresponding vertical collapse necessitated by continuity considerations. Immediately behind the body, turbulent mixing dominates the wake growth, and the wake should expand almost uniformly in all directions. At greater distances behind the body, where the mixing is less intense and fluid is displaced farther from density equilibrium, gravity effects become dominant, and the lateral spreading and associated vertical collapse of the mixed zone are the salient

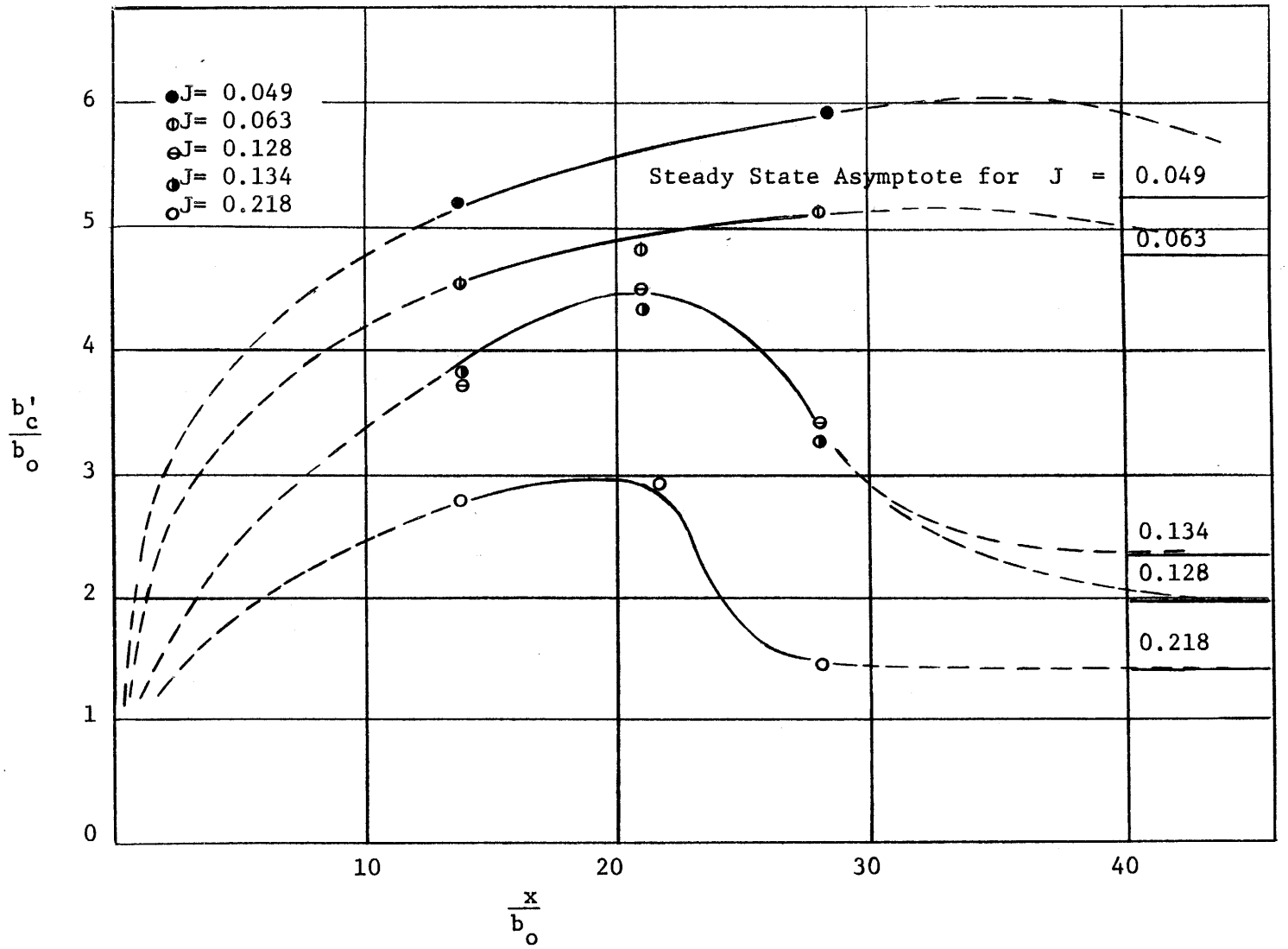

Figure 2 Variation of wake width with distance behind plate for different values of the stratification parameter J.

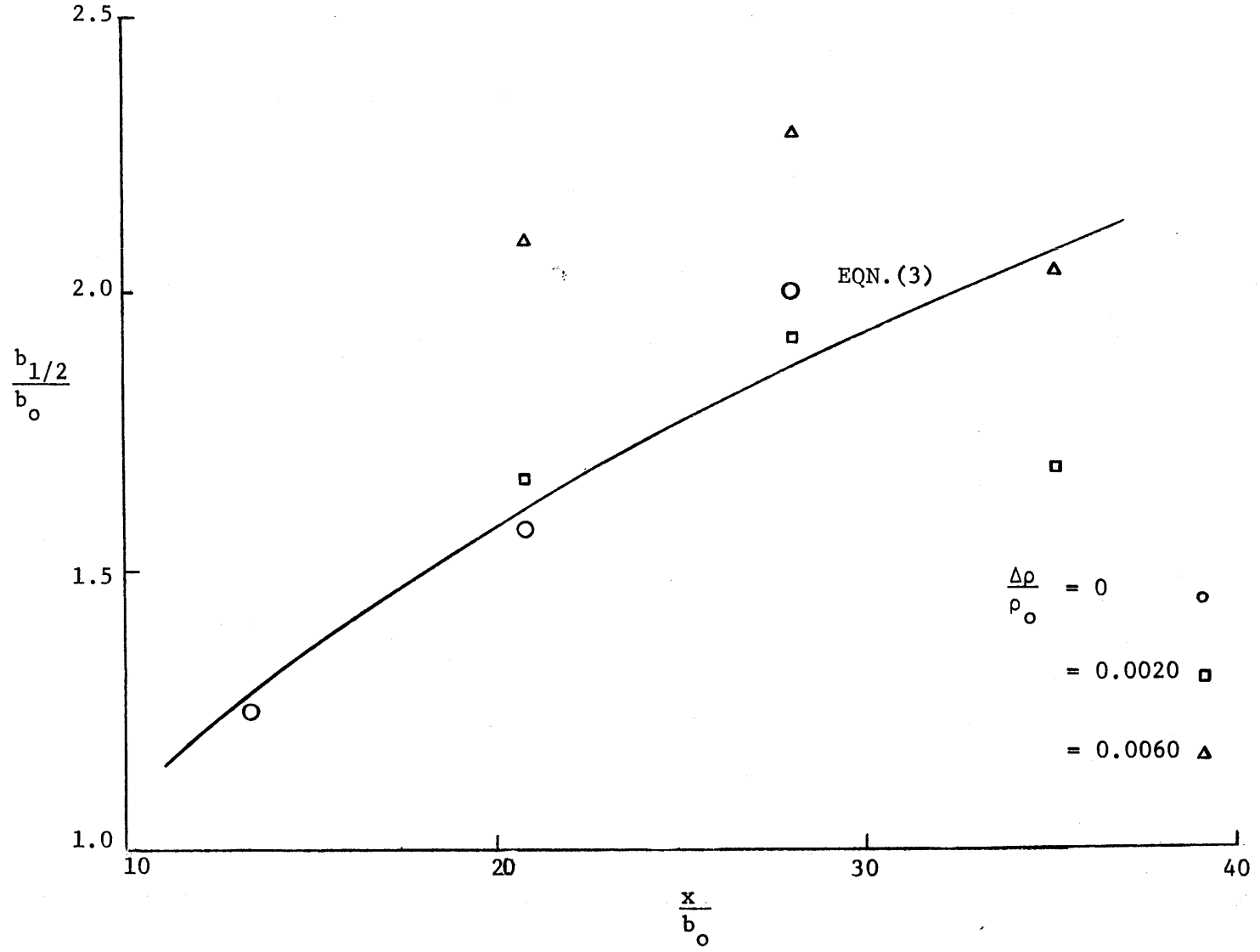

Variation of Wake Half-Width with Distance

Figure 3

features of the wake configuration. In this zone, the motion is probably nearly two-dimensional and in the plane normal to the wake axis, longitudinal gradients having negligible effects. It should be noted that this type of vertical collapse, associated with lateral spreading, cannot occur in the case of a two-dimensional wake; in that case, the collapse is due to the displaced fluid returning to a level of density equilibrium before becoming mixed with surrounding fluid.

Schooley and Stewart[4] investigated the behavior of a wake generated by a self-propelled body in a linearly density stratified fluid having a density gradient

$$\frac{1}{\rho_o}\ \frac{d\rho}{dy} = -.1585\ (\text{ft})^{-1}$$

where

ρ_o = mass density of fresh water

y = vertical dimension

It should be noted that a self-propelled body such as the one used by Schooley and Stewart will transmit no net momentum to the surrounding fluid because the drag on the body is equal in magnitude to the thrust imparted to the fluid by the body. A self-propelled body is said, therefore, to generate a "momentumless" wake. For simplicity of analysis, Schooley and Stewart assumed that their model, which was cylindrical and oriented with its axis parallel to the direction of travel, generated an initially axisymmetric wake. Horizontal and vertical wake widths were obtained by injecting dye tracer from the model into the mixed region and visually measuring the extent of the mixing zone. Schooley and Stewart were able to measure the rate of vertical wake collapse and horizontal expansion, and found that the vertical collapse generated many modes of internal waves. A significant finding of their study was that the vertical collapse also caused a convergence, perpendicular to the axis of travel, of fluid at the free surface.

A highly idealized study of the mixed regions associated with wakes in stratified fluids was conducted by Wu[5]. He simplified the study by assuming that a wake generated by a moving body is circular and homogeneous throughout. He further assumed that such a problem could be studied by examining the behavior of a transverse cross-section of the wake. Wu wanted only to study the gravitational and inertial effects associated with the wake collapse and excluded all effects arising from turbulent diffusion. His experimental setup consisted of a cylindrical "slice" of quiescent homogeneous fluid encased within a fluid having a linear density profile. By using colored fluids, he was able to study the wake collapse phenomenon when the mixed zone was allowed to spread in a stratified liquid. While his results may not apply directly to the actual case of the wake of a moving self-propelled body, he clearly demonstrated the wake collapse phenomenon and its influence on the generation of internal waves. He was also able to make precise measurements of the horizontal expansion of the mixed region associated with the vertical decrease in wake width.

The study reported herein was a further investigation of momentumless three-dimensional wakes in linearly density stratified fluids. The primary objective was to ascertain the configuration of the mixed region in the turbulent wake, and to study the interaction of the wake collapse and the free surface movements. Experiments were conducted in a rectangular tank, 4.5 feet wide and 50 feet long. The wake was generated by a twin-screw plastic model, 2.5 feet long and 4.5 inches in diameter. The model was self-propelled and capable of speeds up to three feet per second. To facilitate the experiments, a simplified method was developed to generate a linear density profile in the tank by mixing an initially two-layered fluid in a special way. Sodium chloride was used as the density biasing agent in the water and acted as a tracer which enabled concentration measurements to be made with specially designed conductivity probes. Variations in salinity were measured in the zone of mixing as the model passed. The resulting data were plotted as normalized isochler distributions for transverse cross-sections at various

distances behind the model. Free surface motion was studied by placing small particles on the free surface and taking motion pictures of the particle movements during a passage of the model.

The investigation revealed that a definite vertical collapse of the wake or mixed region occurs, commencing at a distance of about ten model lengths behind this body for the value of the density gradient investigated, $\frac{1}{\rho_o}\frac{d\rho}{dy} = -0.003\ (\text{ft})^{-1}$. The wake collapse is virtually complete at about fifteen model lengths behind the body, a time duration of 16 seconds after passage of the body. This is a relatively slow time of collapse compared to the value of 2.5 seconds reported by Schooley and Stewart[4]; however, the density gradient used by them was of the order of 50 times greater than that used in the present study, which of course increased the stability of their density profile. Immediately after passage of the model, the mixed region directly behind the model expanded almost uniformly in all directions, due principally to turbulent diffusion. After the onset of the wake collapse, however, the gravitational force responsible for the collapse rapidly became dominant, and was the primary factor controlling the rate of lateral expansion of the wake region during the later stages of the motion. The motion picture studies indicated good correspondence between the time of initiation of the wake collapse, determined from the density configuration studies, and the beginning of convergence of fluid at the free surface toward the region above the model path. An investigation of three different density gradients, with all other quantities held constant, showed that the rate of convergence of surface particles decreases with decreasing density gradient.

Chapter II gives a detailed description of the self-propelled model, instrumentation, and other equipment used in the experiments. It also describes an efficient method developed for generating a linear density profile, and the procedure used in the conduct of the experiments.

Chapter III presents an analysis of the laboratory data, a description of the data reduction calculations, and an error analysis. Chapter IV contains the presentation and a critical analysis of the results obtained. Chapter V summarizes the principal results and conclusions of the investigation.

CHAPTER II

APPARATUS AND PROCEDURE

This chapter presents a description of the apparatus used in the experiments, and a detailed description of the operational procedures. Before proceeding, it is helpful to present a brief outline of the experimental procedure so that the functions of the various components of the apparatus will be more clearly understood.

A. Brief Outline of Procedure

A linear profile was produced in the tank before each series of runs in the following way. The tank was filled to half depth, and the salt tracer was added and mixed into solution; then the upper half of the tank was filled with tap water. A flat plate, oriented normal to the direction of motion and located at the interface, and a rod, located three inches below the surface, were passed through the two-layered system. A linear profile resulted after the profile reached a state of equilibrium. The runs were then begun. The recording probes were mounted on a movable carriage and placed at desired positions before the submerged model was launched. As the model passed the recording probes, changes in the local salt concentration, due to the mixing of the wake, were continuously recorded with an electronic recorder. By combining the results of a large number of such runs, a time history of the density configuration in the wake was concentructed.

B. Apparatus

The principle items of apparatus used in the experiments consisted of a large tank, a movable carriage, conductivity probes, and a self-propelled body. The other appurtenances, which complemented the principle apparatus and were required to conduct the experiments, are described jointly with the

principle items of apparatus in the following paragraphs.

1. Tank and Carriage

The steel tank, in which the experiments were conducted is 50 feet long, 4.5 feet wide, and 3.5 feet deep. The front side-wall of the tank contained a 10-foot section of 1/4-inch glass. Vertical rows of drain cocks are located at three locations along the sides of the tank: one at each end of the front of the tank; and one row at the center of the back wall. The density (salinity) profile was determined prior to each run by measuring the salt concentration of the samples withdrawn through the drain cocks.

The launcher, used to bring the self-propelled body rapidly to its operating speed, is spring activated and is located at one end of the tank (see Figure 4). When it was activated, it propelled the model forward, and simultaneously engaged a toggle switch which started the model's battery-driven motors. As the model approached the other end of the tank, it passed under a vertical staff which engaged the switch and turned off the motors. The body then came to rest against the foam rubber cushion shown in Figure 5. The model was supported from a pair of 3/32-inch solid stainless steel wires extending along the full length of the tank.

The movable carriage, shown in Figure 6, spanned the width of the tank and rode on one-inch diameter rails mounted on the flanges at the top of the tank. It was used to carry its power supply, speed control, and the bridge boxes used in conjunction with the recording device. The mixing plate and rod were mounted on the carriage during their pass through the two-layered fluid system to generate the linear density profile. During an experiment, the plate and rod were detached from the carriage, and the salinity probes were mounted to it. The power supply for propelling the carriage along the tank was a 1/8-horsepower d.c. reversible motor. A 5/64-inch stainless steel wire, spanning the length of the tank, was wrapped around a pulley connected to the motor's drive shaft, and the carriage advanced along the tank as the pulley revolved. The speed of the motor and

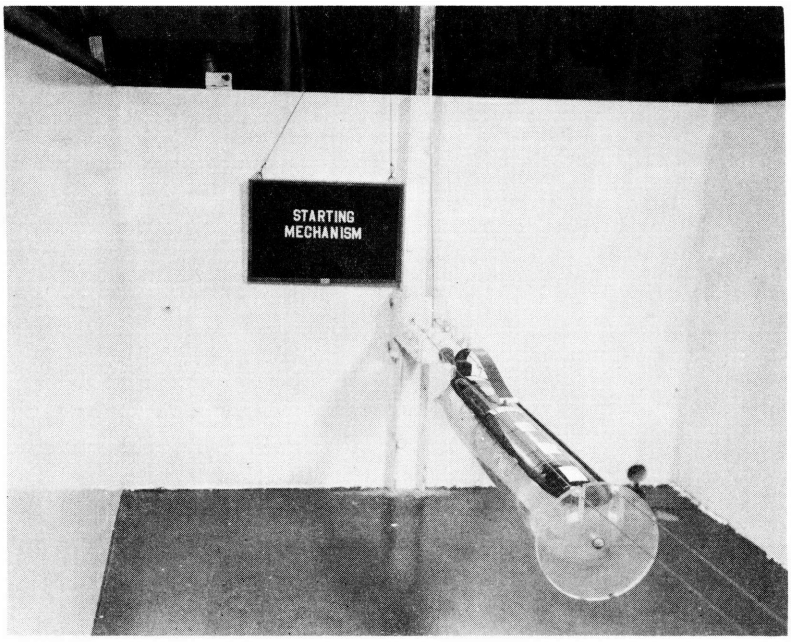

Figure 4 Spring-Loaded Launching Mechanism

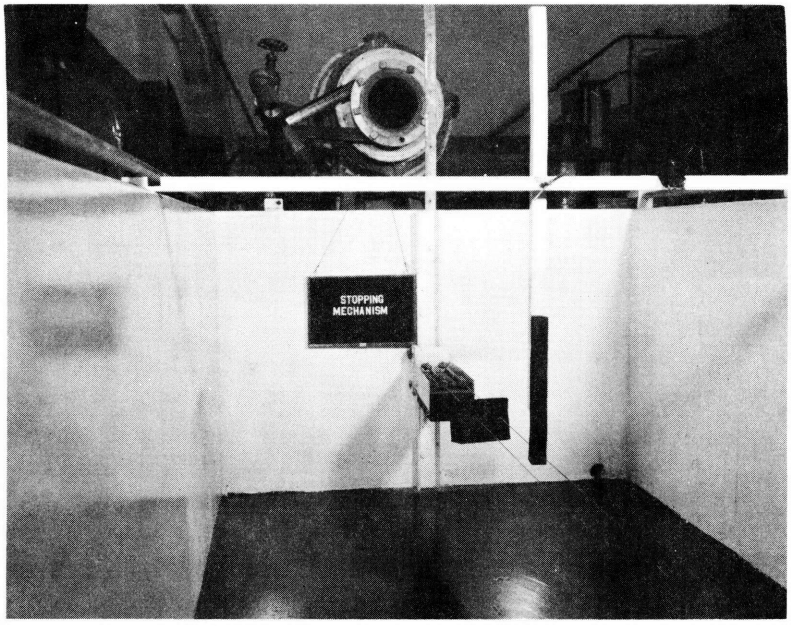

Figure 5 Device for Stopping Model

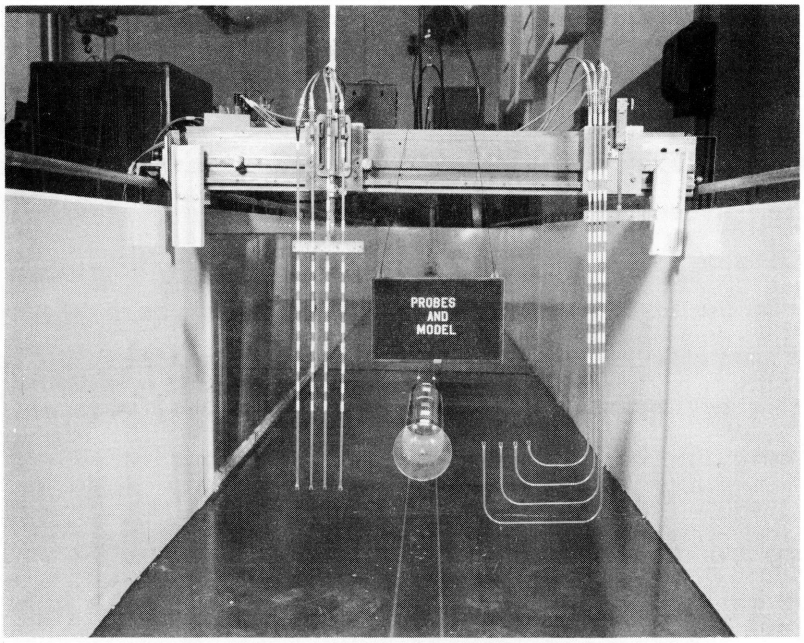

Figure 6 General view of interior of tank (drained) showing movable carriage, model, and typical probe array.

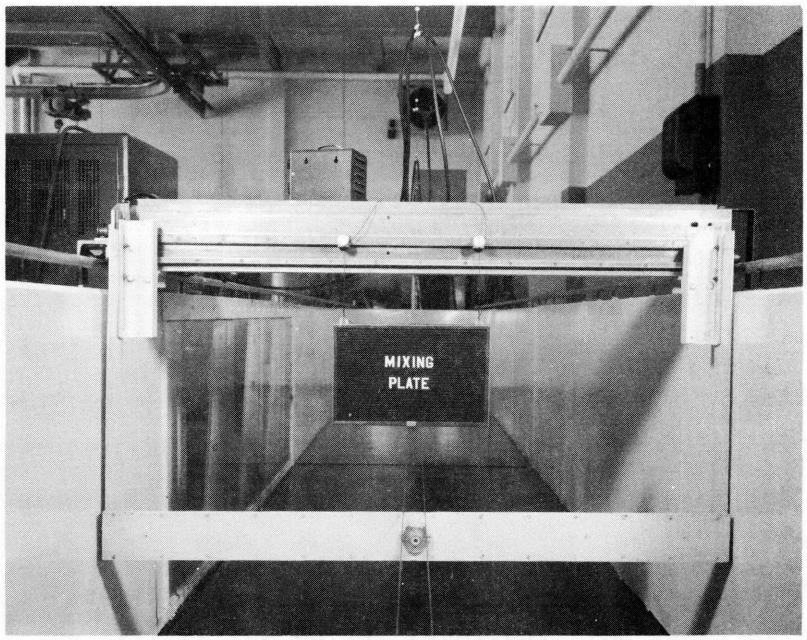

Figure 7 Mixing Plate attached to movable carriage (without rod)

carriage were varied by a Minarik speed control. Constant speeds from 0.05 fps to 2.00 fps could be obtained with this apparatus by varying the size of the pulley and adjusting the speed control. A movable carriage was required not only for moving the mixing plate and rod, but also to insure that the fluid was constantly flushed between the faces of the probes during the runs.

The mixing plate, shown in Figure 7 is the same plate that was used by Prych, Harty, and Kennedy[2]. It is 53 inches wide, 4.13 inches high, and is attached to the carriage by vertical supports and centered at the level of the initial interface. A 53-inch long, 1.5-inch diameter rod, used in conjunction with the plate, was positioned 3 inches below the water surface. It was found by trial and error that this array of the plate and rod combination gives the desired linear profile for a carriage speed of 1.0 fps.

2. The Model

The self-propelled body, referred to as the model and shown in Figures 8a and 8b, is a self-driven electro-mechanical device used to generate the turbulent wake. It has two propellers powered by four twelve-volt rechargeable nickel-cadmium batteries. A schematic drawing of the electrical arrangement is presented in Figure 8c. A six-inch diameter disc, oriented perpendicular to the direction of motion, is attached to the front of the model to give a fully turbulent wake.

3. Measurement System

Conductivity probes were used to measure the salt concentration, and thereby the density, in the turbulent wake behind the model. From these measurements, the wake configuration was inferred. The two models of probes used and their dimensions are shown in Figures 9a and 9b. Type B probes were developed in order to obtain data from the area directly below the model At the end of each probe, there are two 0.1-inch diameter platinum surfaces spaced 1/8 of an inch apart, which act as one arm of a bridge circuit (see Figure 10). The electrical resistance of the probes varies linearly with

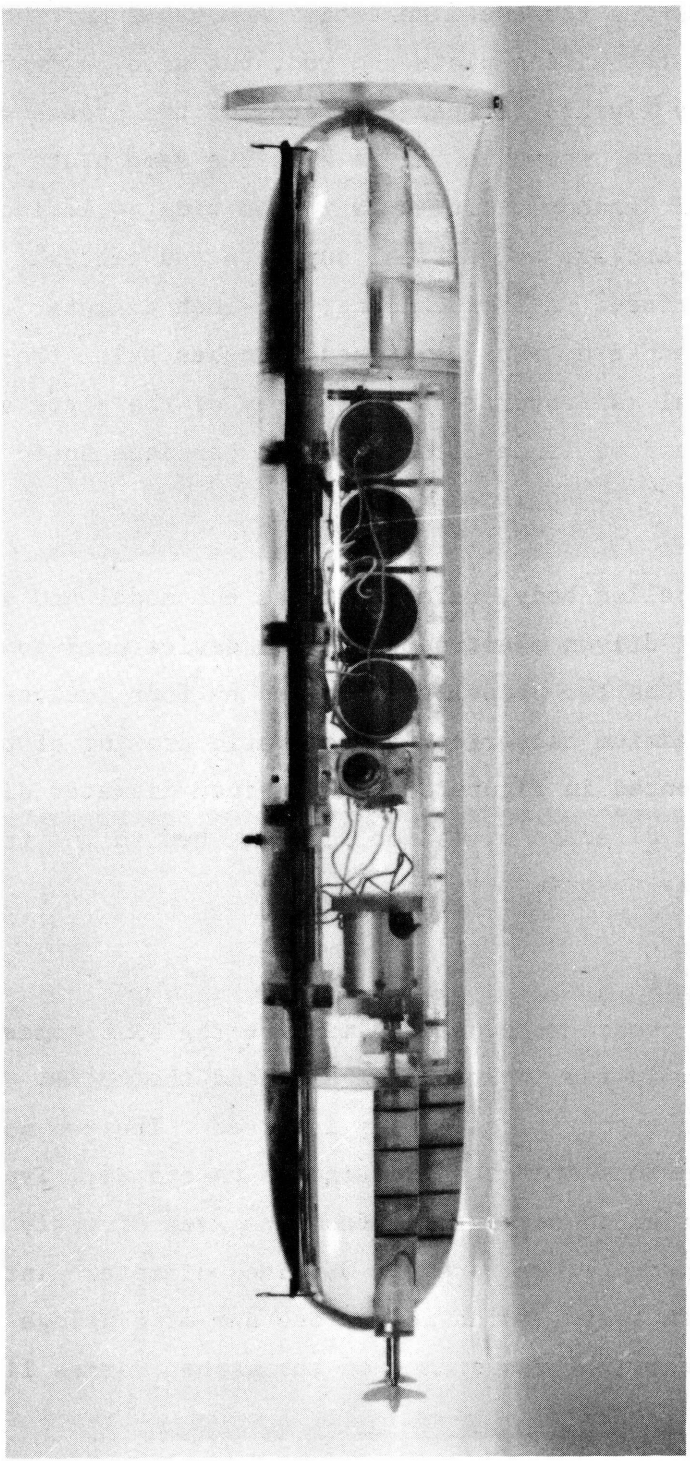

Figure 8a Self-Propelled Model

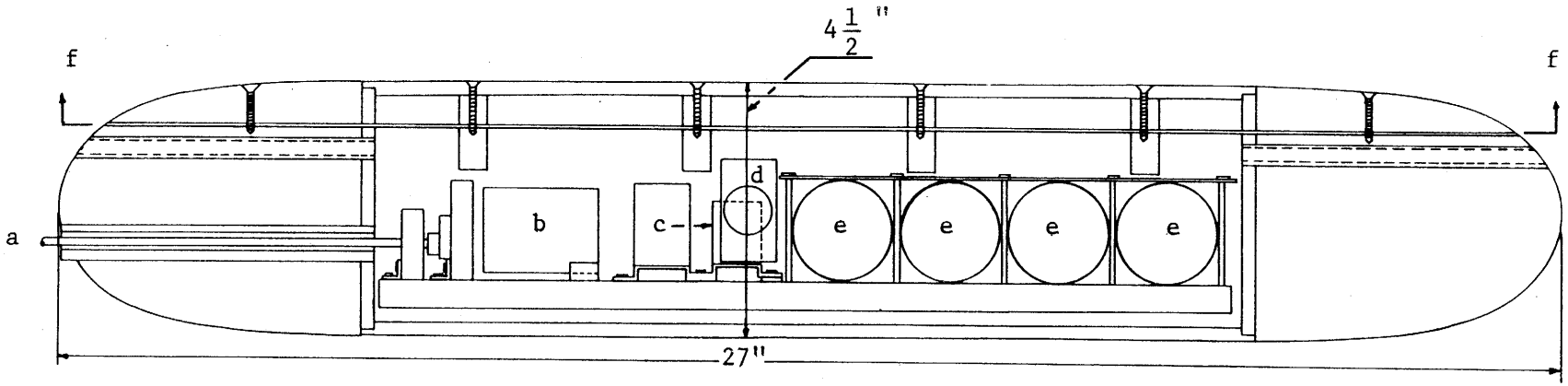

(a) Propeller Shaft
(b) Motor
(c) Relays 1 and 2
(d) Phono-Plug and Support
(e) Battery
(f) Removable Hatch

1"

Scale Drawing of Self-Propelled Model

Figure 8b

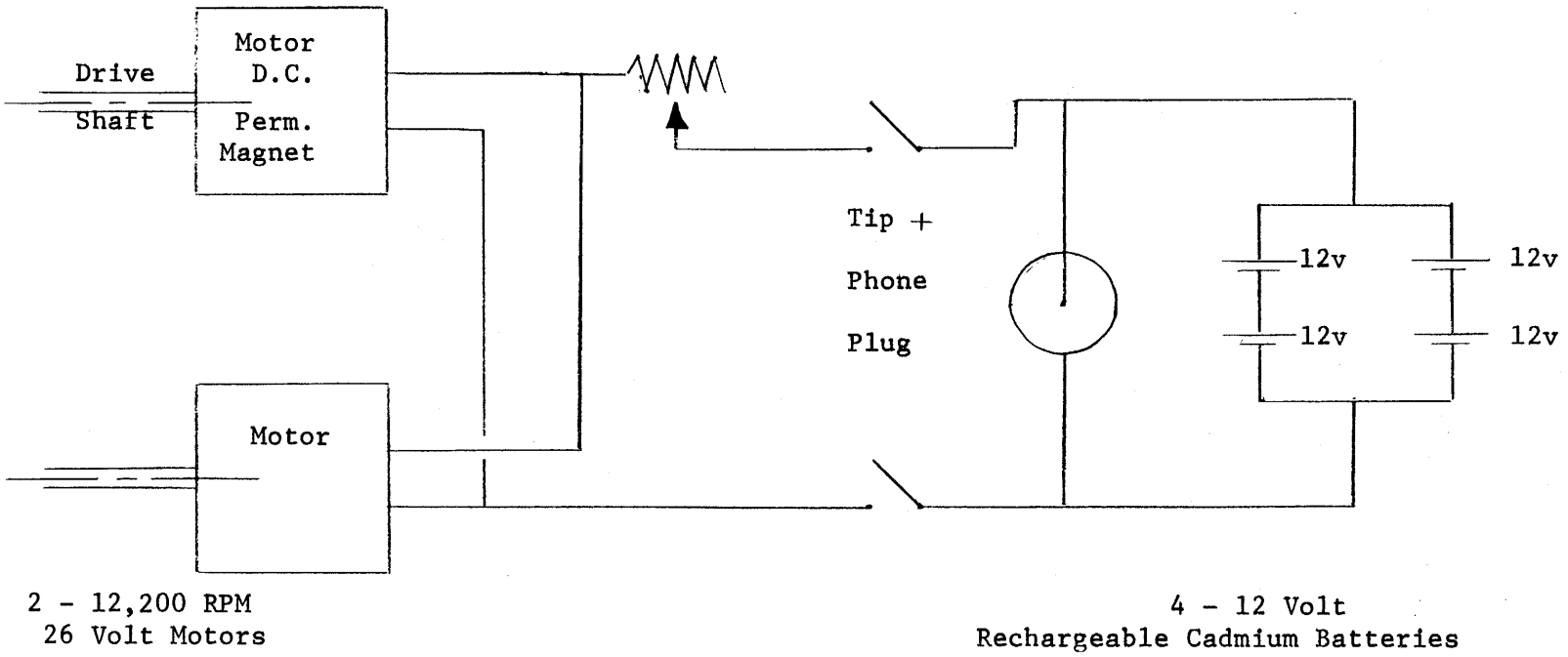

Schematic of Electrical Circuitry in the Model

Figure 8c

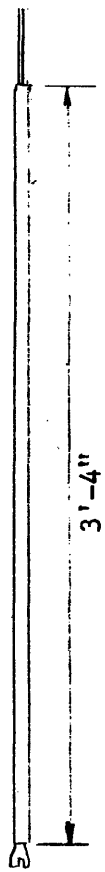

Figure 9a Probe Type A

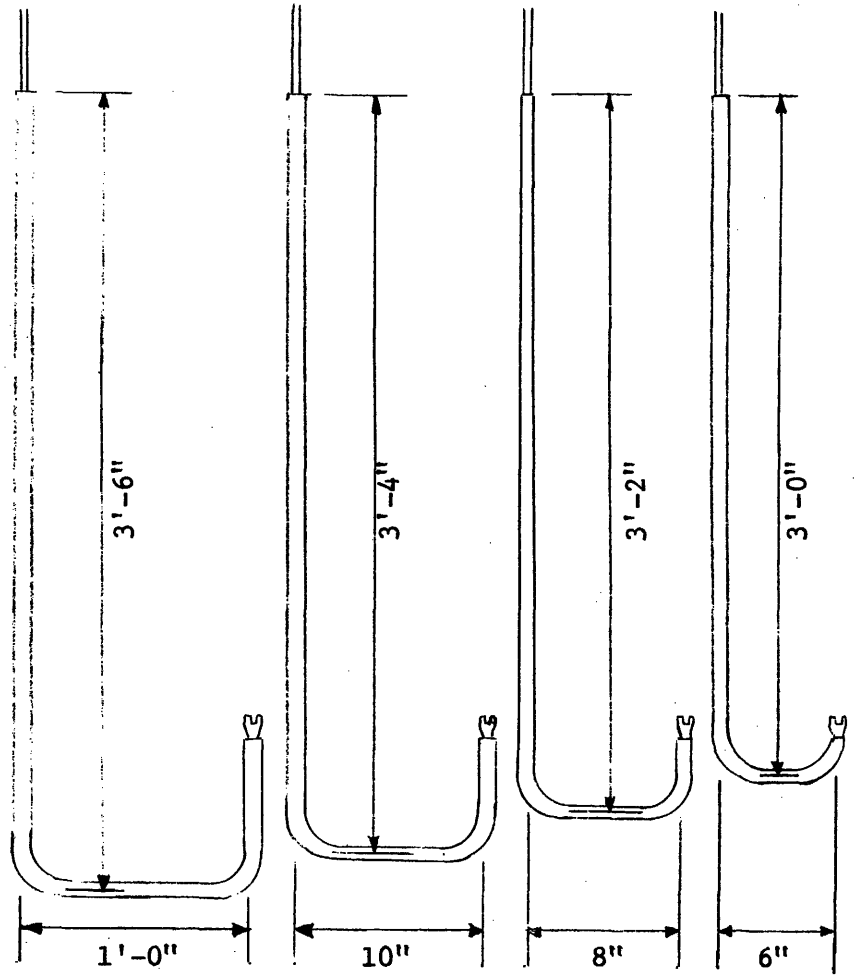

Figure 9b Probe Type B

Conductivity Probes

Figure 9(a and b)

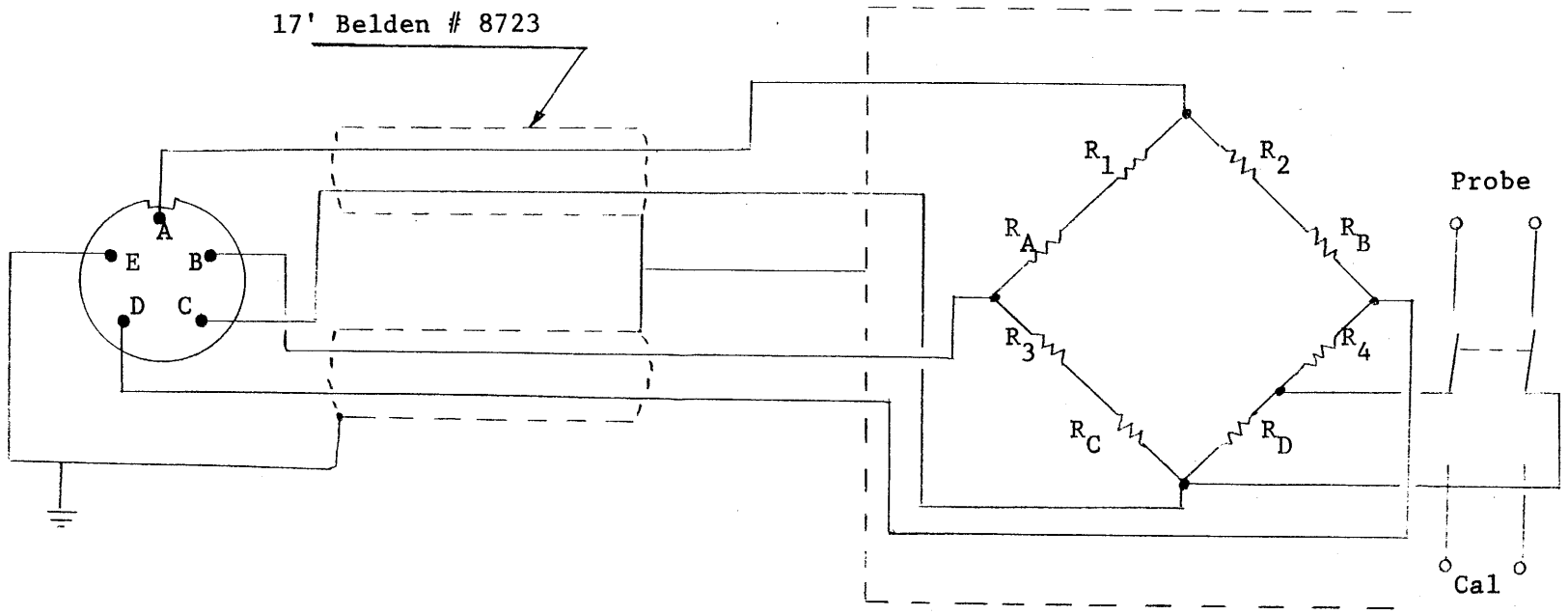

$R_{1,2,3,4}$	100 ohms
$R_{A,B,C,D}$	10 ohms
All Resistors	I.R.C. WW4J

Complete Bridge Circuit for Probes

Figure 10

the salt concentration of the fluid between the platinum surfaces, as will be discussed in Chapter III. The probes were securely attached to the carriage by two plexiglass brackets mounted on a cathetometer, which it turn was attached to a traverse track on the carriage. The probes were positioned vertically by shifting them in the plexiglass holders and with the cathetometer, and horizontally by moving their mount along the traverse track on the carriage. The performance of the probes, with respect to time response, temperature response, speed vs fluid entrainment, and the interaction between probes is contained in Chapter III. It was found that these sources of error were of inconsequential magnitude when compared to the responses due to the concentration changes in the wake.

Two four-channel Sanborn recorders were used to record the salinity data. One of the recorders has an averaging option that averages the response over the preceding one second. This was of great assistance in reducing the data, because any outside, periodic, electrical noise was completely eliminated from the recorder output.

C. Procedure

1. Preparation of the Linear Density Profile

Before a series of experiments could be run, it was necessary to generate a linear density profile in the tank. The usual procedure for doing this is to place in the tank a series of fluid layers with an incremental density difference between successive layers, and then allow molecular diffusion to smooth the profile. However, this is a very tedious and time consuming procedure, and it was judged impractical for the large tank used in the present investigation. A series of experiments was therefore conducted to develop an improved method of generating linear density profiles. The method finally developed and adopted proceeds as follows.

The tank was initially filled to a depth of fifteen inches, one-half of the final depth, and enough salt was added to give a sodium chloride concentration of 0.6 percent by weight. Two 0.5 horsepower, 1,750 rpm

electric motors with twin-bladed propellers were used to mix the salt into homogeneous solution. The flat plate and the rod described in section B were then attached to the movable carriage and positioned vertically, as shown in Figure 7, and the carriage, plate, and rod were moved to the end of the tank. A four-foot square sheet of 1/4-inch plywood was floated on the salt water at the center of the tank, and secured to prevent horizontal drift. Fibrous material was placed in a loose layer on the top of the flotation board. Tap water was allowed to run through the fibrous material, which acted as an energy dissipator, onto the flotation board at a rate of about 16 ft^3/hr until the tank was filled to a final depth of 30 inches, after which the flotation board and the energy dissipator were removed from the tank. Figure 11 illustrates the procedure used in depositing the fresh water layer.

The flat plate and rod were then passed through the two-layered fluid at a speed of one foot per second. When the fluid again came to rest and reached equilibrium, a linear profile existed. Figure 12 shows a typical density profile and illustrates the mixing method employed to obtain it. The entire procedure for establishing the linear profile took approximately 28 hours, most of which was required to place the upper fluid layer.

To measure the resulting density profiles, samples were taken from the drain cocks, and their conductivity, thus salt concentration, was determined with a conductivity bridge. Special care had to be taken to withdraw the samples slowly, so that the fluid sample was selectively withdrawn at just the level of the drain cock. The concentration of the samples was found from graphs of conductivity vs sodium chloride concentration for different temperatures, prepared from data available in many physical handbooks.

2. The Wake Experiments

The form of the density profile existing in the tank was checked prior to each run by taking fluid samples from the drain cocks and plotting the resulting profiles. The profile was considered satisfactory if a linear profile existed over the range of depths where probe measurements were to be

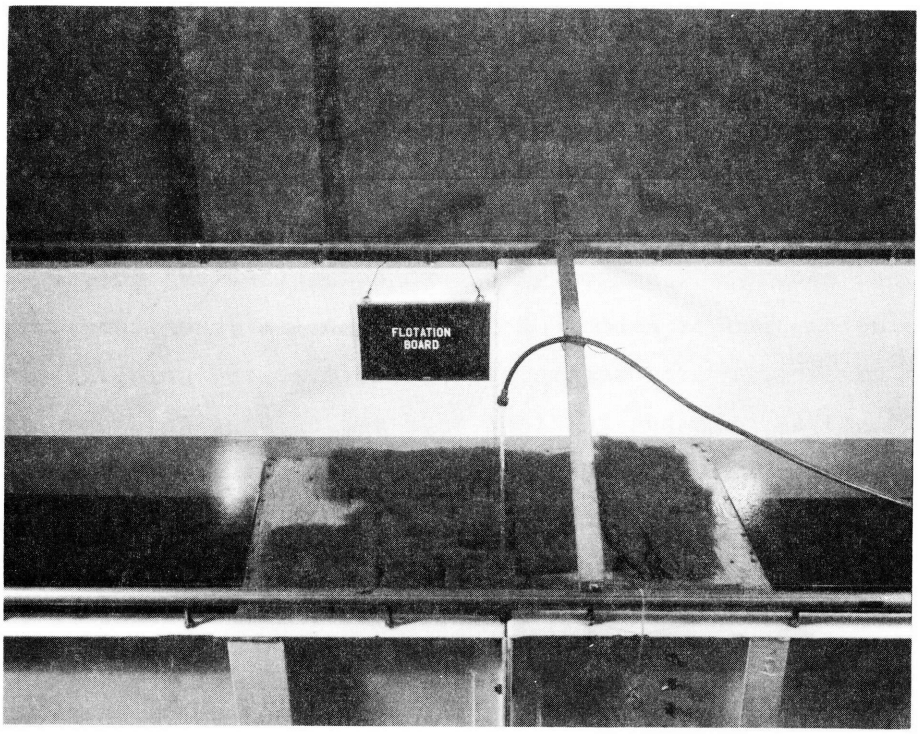

Figure 11 Method of Depositing Fresh Water Layer

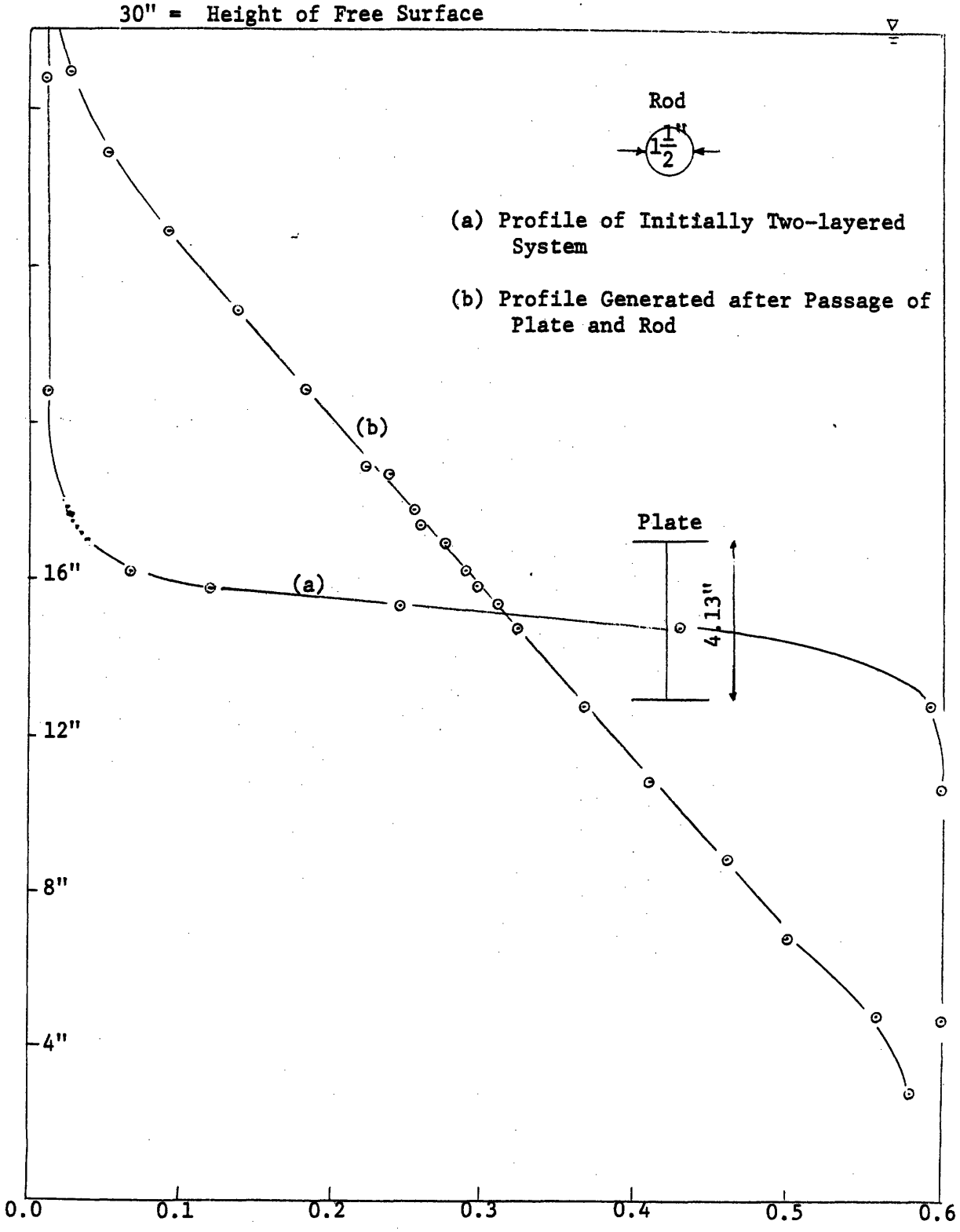

Profiles Generated over Depth of Tank Showing Positions of Plate and Rod

Figure 12

taken. These depths ranged from ten inches above to ten inches below the centerline of the model. The model was then positioned for launching and the conductivity probes were placed at the locations where concentration measurements were to be taken. The bridges of the probes were balanced by adjusting the variable resistance and capacitance built into the recorders until the initial concentration at each probe position corresponded to zero deflection on the recorder. The height of the probes above or below the centerline of the model where these initial adjustments were made is referred to as the"balance" position. A reference concentration was determined by first raising or lowering the probes 1.5 inches and noting the corresponding deflections on the recording paper. The deflections were then adjusted by varying the gain of the recorder until they were 20 percent of the recording paper width. This procedure was called "zeroing", and the new position of the probes was referred to as the zero position. Knowing the concentration as a function of depth, as determined from the drain cock samples, and knowing the deflection caused by moving the probes from the balance to zero positions, a linear relation between concentration change and recorder deflection was developed. The probes were then moved through a 5-foot section of the tank at the zero position and also at the balance position, the data from which was used to obtain an average recorder deflection between the two positions. If the variation in recorder deflection at either the zero or balance positions, which was measured during the two traverses at these constant depths, corresponded to more than 1/3 of the total average deflection between these two positions, the density profile was considered nonuniform, the tank was drained, and a new profile was generated.

The apparatus was then in a state of readiness to record experimental data, provided the recorder had experienced no drift during the zeroing procedure. The probes were then moved at their balance position to the beginning of the test section. During the entire balancing and zeroing procedure, as well as during the experiment, the probes were moved at a constant speed of 0.085 fps. This insured a continuous exchange of fluid

between the probe faces, thus preventing fluid from being retained in the probe and yielding erroneous results.

The probes were then started forward as was the recorder data paper. As the probes passed the first reference point, x = 0, a remote marker button was depressed giving a mark on the recorder data strip. To insure uniformity of the experiments, the model was launched as the probes passed the point x = 3 inches. This occurrence was also remotely recorded on the recorder paper. Other points recorded during the progress of the run were the time when the model passed the probes, the time when the model passed x = 20 feet, and times when the probes passed x = 5 feet and x = 10 feet. These data were necessary to determine the carriage and the model velocities. The velocities of the model and the probes were relatively constant throughout the experiments; average velocities were 1.92 fps and 0.085 fps respectively.

In general, eight to ten runs were performed with each profile before the tank was drained and refilled. Although considerable disturbance was generated by the model, when a quiescent state returned, the profile was still nearly linear, but with a slightly reduced gradient. A new profile was required when nonlinearities began to appear in the drain cock data or during the balancing and zeroing procedure.

3. Surface Motion Experiments

During this series of experiments to investigate surface motions induced by the moving body, two different density gradients were used, in which the initial sodium chloride concentrations of the lower layer were 0.6 and 0.3 percent by weight. In addition, a series of runs was performed using homogeneous tap water. A 16 mm Bell and Howell motion picture camera was mounted approximately 5 1/2 feet above the free surface. Prior to each experiment, a reagent to reduce surface tension, "Surfonic LF7" manufactured by the Jefferson Chemical Company, was applied to the free surface in order to prevent mutual attraction of the small paper particles which were then placed individually on the free surface throughout the area to be photographed.

After drain-cock samples had been taken to check the linearity of the density profile, the model was launched and motion picture photographs of the free-surface and particle movement were made at various camera speeds. The velocity of the model was the only additional item of data taken for this series of experiments. Quantitative data on the particle movements were extracted from the motion picture films with the aid of a Bell and Howell 16 mm Time-and-Motion-Study projector. The film was projected directly onto a large sheet of paper, and the movements of the individual particles were traced by hand-winding the projector and marking the particle positions on the paper every 16 (or other number, depending on the camera speed) frames, to give one second real-time increments. The relative particle positions were then measured, using as a scale the one-inch-division measuring tape which was placed just above the water surface and photographed during the experiments. A clock was also placed in the camera field to give an additional check on elapsed times.

CHAPTER III

ANALYSIS OF DATA

A. Concentration Profiles

The method used to generate a linear density profile in the laboratory tank proved to be quite satisfactory, both from the standpoint of ease and speed of generation and the results obtained. A typical concentration profile is shown in Figure 12. The average density gradient over the linear range was $-0.003\ (\text{ft})^{-1}$ for all experiments. As can be seen from the sample profile in Figure 12, nonlinearities did exist very near the free surface and close to the bottom of the tank. These nonlinearities did not interfere with the study of wake configurations, because concentration variation measurements were confined to the region over which the density profile was linear.

The concentration profile remained stable over a long period of time, and a passage of the model did not significantly alter the profile after the fluid had returned to equilibrium. This fact enabled several experiments to be conducted with each profile before the tank had to be drained and refilled. Shown in Figure 13 is a sample density profile from the drain cock samples taken six days after the original profile generation, and after fourteen passages of the model. The data for this sample profile appear in Table I. A nearly linear region still persists over the central portion of the tank; however, such a profile would have warranted draining of the tank and generation of a new density profile.

B. Analysis of Data

Salinity concentration (density) measurements were made at 1 1/2-inch intervals, both vertically and horizontally, throughout the region of measurable concentration change in the wake. At each of these points, salinity probe readings were recorded continuously as the model passed. Each

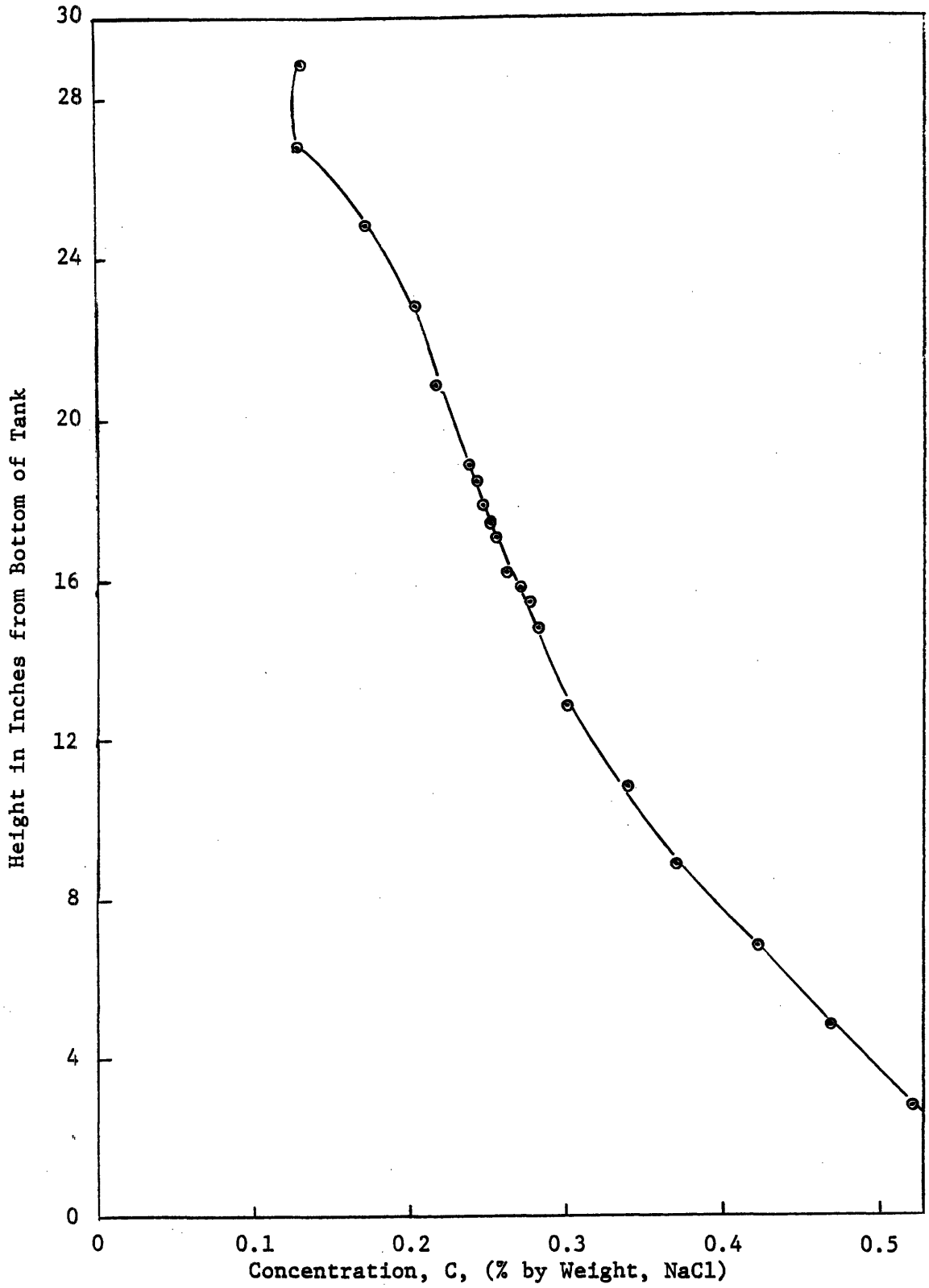

Existing Concentration Profile, Six Days after Generation and after Fourteen Passages of the Model

Figure 13

TABLE I

Drain Cock Sample Data Sheet for Determination

of Pre-Run Concentration Profile

Run No. X2 4 January 1966

Drain Cock No.	Height above tank bottom (inches)	Conductivity of Sample $(ohms)^{-1}$	Temperature (° C)	Concentration (% NaCl)
3	28 7/8	2,390	22.0	.132
4	26 7/8	2,440	21.9	.1325
5	24 7/8	3,200	22.0	.174
6	22 7/8	3,640	21.9	.205
7	20 7/8	4,000	22.2	.22
8a	18 7/8	4,360	22.1	.24
8b	18 7/16	4,400	22.0	.244
9a	17 3/4	4,480	22.0	.249
9b	17 3/8	4,520	21.9	.253
9c	17	4,700	22.4	.260
10a	16 1/4	4,820	22.5	.265
10b	15 7/8	4,920	22.4	.273
10c	15 7/16	5,000	22.4	.278
11	14 3/4	5,100	22.3	.284
12	12 7/8	5,400	22.4	.301
13	10 7/8	6,100	22.8	.340
14	8 7/8	6,650	22.8	.372
15	6 7/8	7,520	22.9	.424
16	4 7/8	8,350	23.0	.470
17	2 7/8	9,280	23.1	.523

measurement yielded a record of the time variation of concentration at that point. To relate recorder deflections to changes in concentration, the bridges connecting the probes to the recorder were balanced at their respective initial concentrations, as described in Chapter II. The resistance measured between the electrodes of each probe then corresponded to zero deflection on the recorder at the balance positions of the probes; all quantitites measured at this position are denoted by the subscript, b. Reference concentrations and corresponding recorder deflections were then taken by shifting the probes to the zero position, denoted by the subscript, o. Shown below is a schematic of the external leg of the electrical bridge across which the probe was connected.

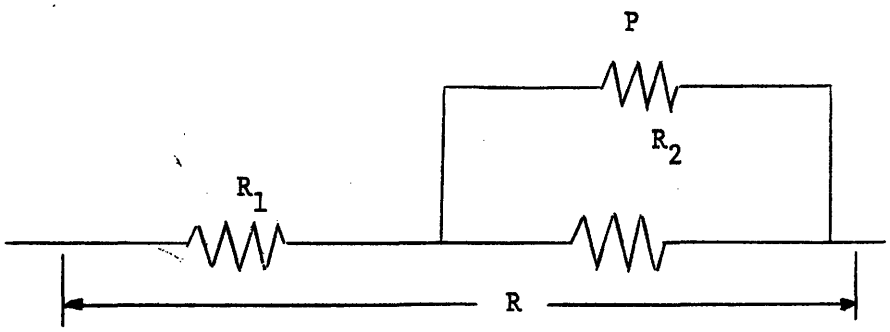

R_1 = 90.0 ohms

R_2 = 10.0 ohms

External Leg of Bridge Connecting the Probe to the Recorder

Figure 14

In the circuit shown in Figure 14, P is the resistance between the probe electrodes,and the total resistance, R, is the resistance across the entire leg of the bridge. Hence,

$$R = R_1 + \frac{PR_2}{P + R_2} \tag{4}$$

The deflection, δ, registered on the recorder is proportional to a change in resistance, ΔR, in the entire leg,

$$\Delta R = \alpha\delta \tag{5}$$

where α is a constant. In the range of interest, it was found that the concentration of salinity in the fluid entrained in the probe is inversely proportional to the resistance across the probes,

$$C \propto \frac{1}{P}$$

where P is the resistance between the probe electrodes. Therefore,

$$\frac{C - C_b}{C_o - C_b} = \frac{\frac{1}{P} - \frac{1}{P_b}}{\frac{1}{P_o} - \frac{1}{P_b}} = \frac{P_b - P}{P_b - P_o}\left(\frac{P_o}{P}\right) = \frac{\Delta P}{\Delta P_o}\left(\frac{P_o}{P}\right) \tag{6}$$

When a fluid of different salinity concentration than the initial balance concentration enters the probes, the change in resistance across the external leg of the bridge is

$$\Delta R = R - R_b = \frac{R_2 P}{R_2 + P} - \frac{R_2 P_b}{R_2 + P_b} =$$

$$\frac{R_2^2 P + R_2 P P_b - R_2^2 P_b - R_2 P P_b}{(R_2 + P)(R_2 + P_b)} = \frac{R_2^2 \Delta P}{(R_2 + P_b)(R_2 + P)} \tag{7}$$

Since R_2 is small compared to P and P_b, equation (4) can be approximated by

$$\Delta R = \frac{R_2^2 \Delta P}{P_b P} \tag{8}$$

Combining (5), (6), and (8), it is seen that

$$\frac{C - C_b}{C_o - C_b} = \frac{\alpha P_b}{R_2^2} \frac{P_o}{\Delta P_o} \delta = \beta\delta$$

where β is constant for each probe during each individual experiment.

Thus, it has been shown that, to a close approximation, the value of the normalized concentration parameter, $\frac{C - C_b}{C_o - C_b}$, is directly proportional to the recorder deflection, the constant of proportionality being determined by the condition that at the zero position, $C = C_o$, and $\delta = \delta_o$; hence,

$$\frac{C_o - C_b}{C_o - C_b} = \beta\delta_o = 1$$

or

$$\beta = \frac{1}{\delta_o}$$

which yields

$$\frac{C - C_b}{C_o - C_b} = \frac{\delta}{\delta_o} \tag{9}$$

The results from any individual experiment did not provide enough information to describe the configuration of the mixed region behind the body. Therefore, it was necessary to combine the results obtained from all of the experiments to produce plots of cross-sectional normalized isochlor configurations at various distances behind the model. The parameter chosen

to portray the salinity distribution is

$$C_* = \frac{C - C_T}{C_B - C_T}$$

where

C = concentration at any point at any time, t

C_T = concentration at the upper limit of the linear density profile, determined from the drain cock samples

C_B = concentration at the lower limit of the linear density profile, also determined from the drain cock samples.

In order to obtain values of $\frac{C - C_T}{C_B - C_T}$ from the experimentally determined value of $\frac{C - C_b}{C_o - C_b}$, the following relation was used:

$$\frac{C - C_T}{C_B - C_T} = \left[\frac{C_o - C_b}{C_B - C_T}\right]\left[\frac{C - C_b}{C_o - C_b}\right] + \left[\frac{C_b - C_T}{C_B - C_T}\right] \qquad (10)$$

For any individual experiment, the constants, $\frac{C_o - C_b}{C_B - C_T}$, and $\frac{C_b - C_T}{C_B - C_T}$ could be determined from the initial density profile obtained from the drain-cock samples. Cross-sectional normalized isochlor maps were constructed for distances of 2.5, 5, 7.5, 10, 12.5, 15, 17.5, 20, 22.5, 25, 30, 35, and 40 model lengths behind the model. During each passage of the submerged model, the conductivity probes, although remaining fixed with respect to cross-sectional coordinates, moved slowly along the tank. This resulted in a distortion of the time scale recorded on the recorder data strip, which was compensated for when the data were transcribed from the recorder charts.

C. Error Analysis

A linear relation between recorder deflection and change in the normalized concentration was demonstrated in the preceding section. From (5), it is seen that this also implies a linear dependence of ΔR, the change in resistance across the entire external leg of the connecting bridge, on normalized concentration. Equation (9), from which values of the normalized concentrations were calculated, can therefore be rewritten as

$$\frac{C - C_b}{C_o - C_b} = \frac{\Delta R}{\Delta R_o} \tag{11}$$

This result was checked for accuracy by measuring the value of $\frac{C - C_b}{C_o - C_b}$ at various depths, as computed from (11), and comparing these values with the exact values obtained from (6). The probe resistance, P, was measured over a 1 1/2-inch range of depth in which the density profile was linear. This was done by noting the deflection on the recorder that corresponded to a certain probe resistance. This resistance was then measured independently by replacing the probe with a decade resistance box measuring the resistance that caused the same deflection on the recorder. The quantity, ΔR, could also be easily calculated from (7), knowing R_2 (= 10.0 ohms). With ΔR and ΔR_o known, values of $\frac{C - C_b}{C_o - C_b}$ were obtained from (11). The results of several of these experiments are presented in Figure 15, which shows a plot of values of $\frac{C - C_b}{C_o - C_b}$ obtained from (11) vs corresponding exact value obtained from (6). The linear correspondence is quite good, verifying the validity of (9) and (11).

Several sources of error in data measurement occurred, some of which necessitated modification of the way in which data were taken. The primary concern was whether the conductivity probes were actually recording changes

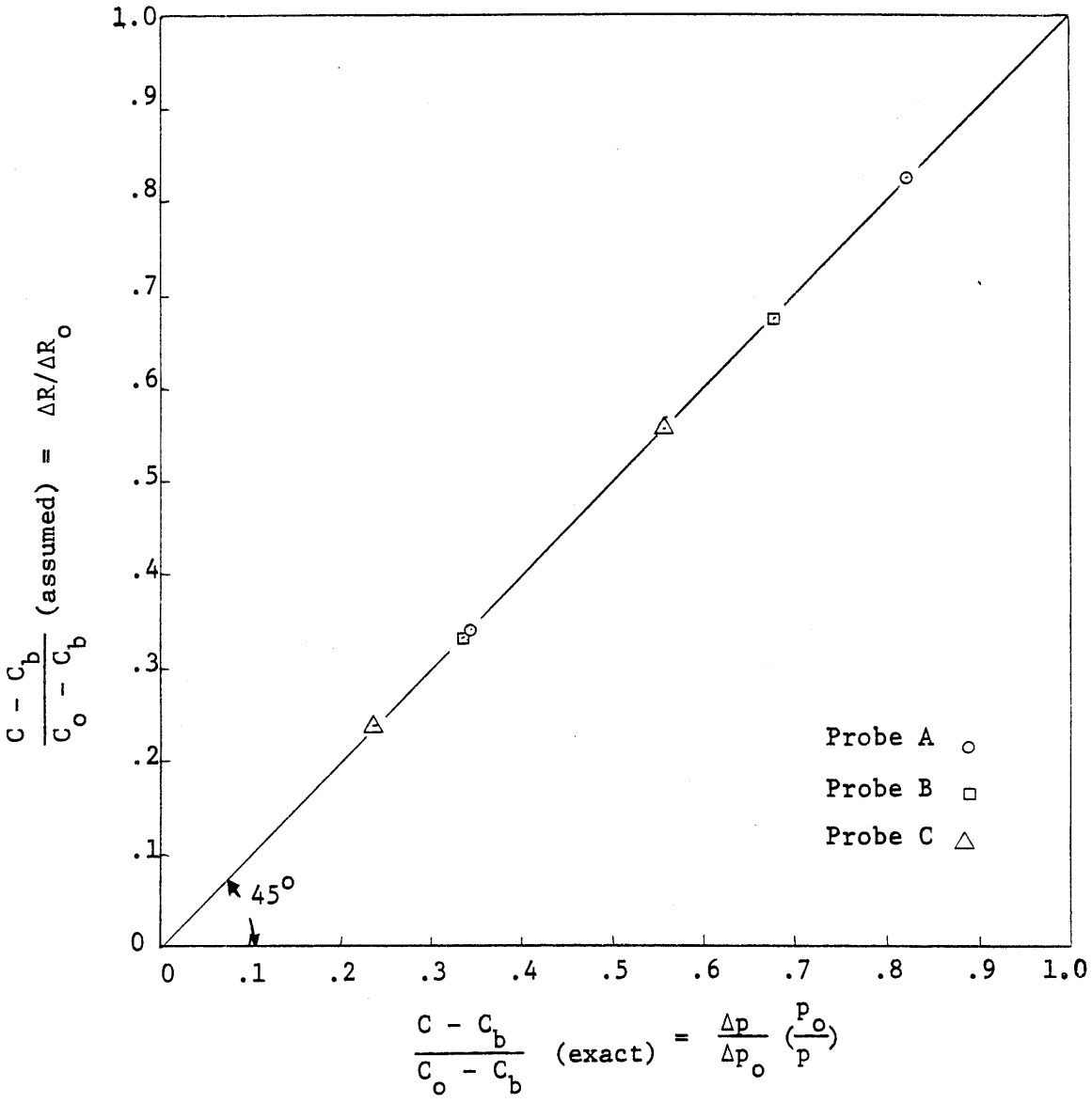

Assumed Values of $\frac{C - C_b}{C_o - C_b}$ vs Exact Values over

1 1/2-inch Depth Range

Figure 15

in fluid concentration, or other related phenomena such as temperature fluctuations due to heating of the fluid between the probe electrodes, which would also influence fluid resistance. The magnitude of this and other sources of error was determined by the series of experiments described below.

In order to test the effect of velocity fluctuations on probe readings, the sensing devices were placed in a fluid with a fixed homogeneous salt concentration. Fluid turbulence was generated with a magnetic mixer. The deflections noted on the data recording strip indicated that the probes were insensitive to velocity fluctuations at the level of recorder sensitivity used in the tank experiments with the moving body.

During the preliminary stages of the tank experiments, the probes were held stationary as the model passed. In this case, it was found that the fluid in the vicinity of the sensing device of each conductivity probe was heated due to the current passing through the fluid between the electrodes. Since this affected fluid resistance significantly, it was necessary to take measures to eliminate this effect. Related to this phenomenon was the fact that the stationary probes did not respond immediately to a change in local concentration because they were not continuously flushed with the local fluid. It was not possible to isolate these two different effects, and they were, therefore, treated simultaneously. A correction was sought by continuously moving the probes longitudinally down the tank at a high enough speed that the spaces between legs of the electrodes were continuously flushed with local fluid. This prevented heating and also resulted in the probes sensing the resistance of the local fluid. The description of how the probes were moved is given in Section B of Chapter II. It was found that a probe speed of 0.085 fps was sufficient to accomplish this purpose and eliminate any measurable recorder drift resulting from heating of the entrained fluid.

The conductivity probes were found to interact slightly with each other; however, the interaction was periodic and could be easily detected and eliminated when the data were transcribed from the recorder tape. As mentioned previously, one of the Sanborn recorders was equipped with an

averaging option that averaged the resistance readings over the previous one second. This eliminated all periodic disturbances on the data recording strip of that recorder.

The last experiment conducted in this series was to test the probes for time response to an instantaneous change in concentration. For this test, the probes were moved from air into salt water, and the time for the recording device to reach a steady state deflection was noted. The time response for all of the probes was of the order of 1/20 second, which was considered inconsequential for the present application.

The normalized concentration reported for each point, in Tables B-I to B-XIII represent the average concentration obtained from two to four different experiments in which a measurement was made at that point. The objective of obtaining repeated measurements at each point was to reduce the effects of various sources of error, such as random internal waves and turbulent fluctuations, which could not be directly compensated for, and thereby to obtain more meaningful data. The discrepancies between different runs at the same point varied from less than 10 percent at large distances from the path of the model, up to 100 percent and more, occasionally, at short distances behind and in the path of the model, where the turbulent mixing was most intense and the fluid motion quite random. More measurements were made in these latter regions. By averaging the results of several measurements, and discarding an occasional measurement that appeared especially erratic, it is believed that the data in all regions, with the possible exception of the near-wake of the body, are accurate to 10 percent or less.

CHAPTER IV

PRESENTATION AND DISCUSSION OF RESULTS

A. Summary of Experiments

Continuous records of salinity concentration were obtained at 1 1/2-inch vertical and horizontal intervals throughout the region of significant salinity variation. Two to four measurements were obtained and averaged for each point. A brief summary of the principle descriptive parameters for the salinity-contour experiments follows:

Average velocity:	$\overline{U} = 1.92$ fps
Maximum and minimum velocity:	$U = 1.59$ fps to 2.22 fps
Bow-disc diameter:	$b_o = 6.0$ inches
Fluid kinematic viscosity:	$\nu = 1.08 \times 10^{-5}$ ft^2/sec
Average Reynolds number:	$R = \frac{Ub_o}{\nu} = 8.9 \times 10^4$
Density gradient:	$\frac{1}{\rho_o}\frac{d\rho}{dy} = -0.003$ (ft)$^{-1}$
Densimetric Froude number:	$F = U\sqrt{-\frac{1}{\rho_o g}\frac{d\rho}{dy}} = 0.0185$
Väisälä frequency:	$N = \sqrt{-\frac{g}{\rho_o}\frac{d\rho}{dy}} = 0.31$ (sec)$^{-1}$
Model length:	$L = 2.5$ ft
Model body diameter:	$d = 4.5$ inches
Fluid depth:	$y = 2.5$ ft

B. Density Configuration behind the Model

Tables B-I through B-XIII, presented in Appendix B, summarize the salinity concentration data. The data are presented in the previously discussed normalized form, $C_* = \frac{C - C_T}{C_B - C_T}$, for various distances behind the

model and at all points on the data grid. There is an absence of data in Table B-I, for a distance of 2 1/2 model lengths behind the body, in the path where the model passed because the probes could not be moved into the model path fast enough after it had passed the probes to obtain measurements at this short distance.

Graphical representations of the data from Tables B-I to B-VI, B-VIII, B-XI, and B-XIII are shown in the isochlor maps for various distances behind the model presented in Figures 16a through 16i. These isochlor charts consist of lines connecting points of equal normalized concentration, C_*, in each of nine different sections behind the model. The light horizontal lines superimposed on the maps show the positions of the initial normalized isochlors, prior to the passage of the model, and the semi-circle on each map indicates the outline of the path of the circular disc mounted on the model bow. The heavy dashed lines on the maps enclose what were judged to be the zones of principal mixing and disruption of the stratification. Individually, these envelopes are necessarily somewhat subjective and arbitrary; as a collective set, however, they are quite systematic in their definition of the mixed zone. The envelopes can no longer be meaningfully defined after about fifteen model lengths (75 disc diameters) behind the body, because of the diminished effects of turlulent mixing in the wake; additionally, the lateral extent of the zone of disruption goes beyond the region over which data were obtained. In all cases, the lateral extent of disruption is difficult to define because of its narrow vertical extent, and the superimposed wave motion that was excited by the model. Moreover, to the sides of the model there is much less variation of C_* from its initial value than there is above and below the body since the mixed fluid spreading laterally has nearly the same concentration as the initial concentration at that level.

The influence of the disruptive forces and the gravitational forces on the density stratification is made clearer by examining the fluctuations of the vertical positions and orientations of the normalized isochlors at the

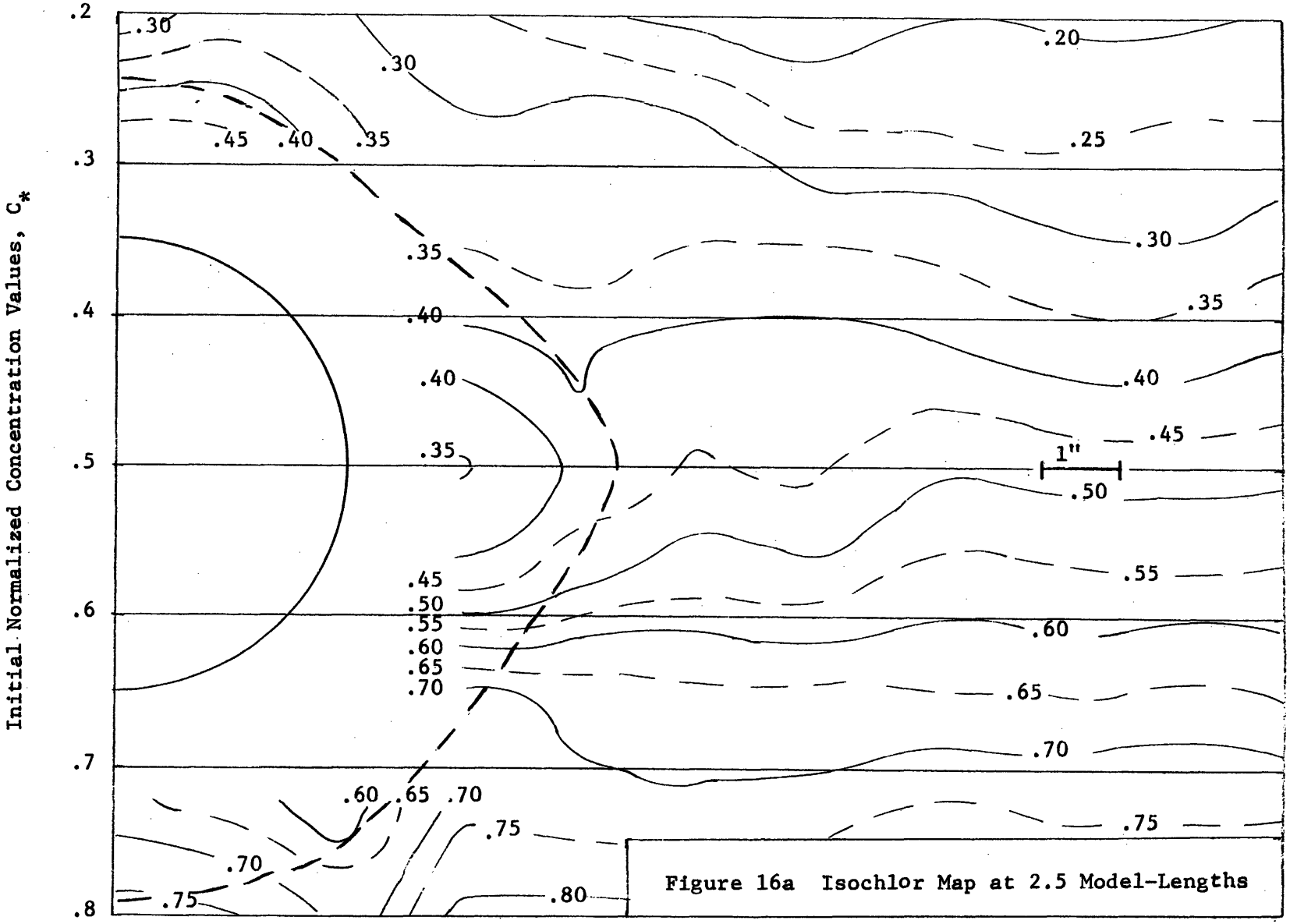

Figure 16a Isochlor Map at 2.5 Model-Lengths

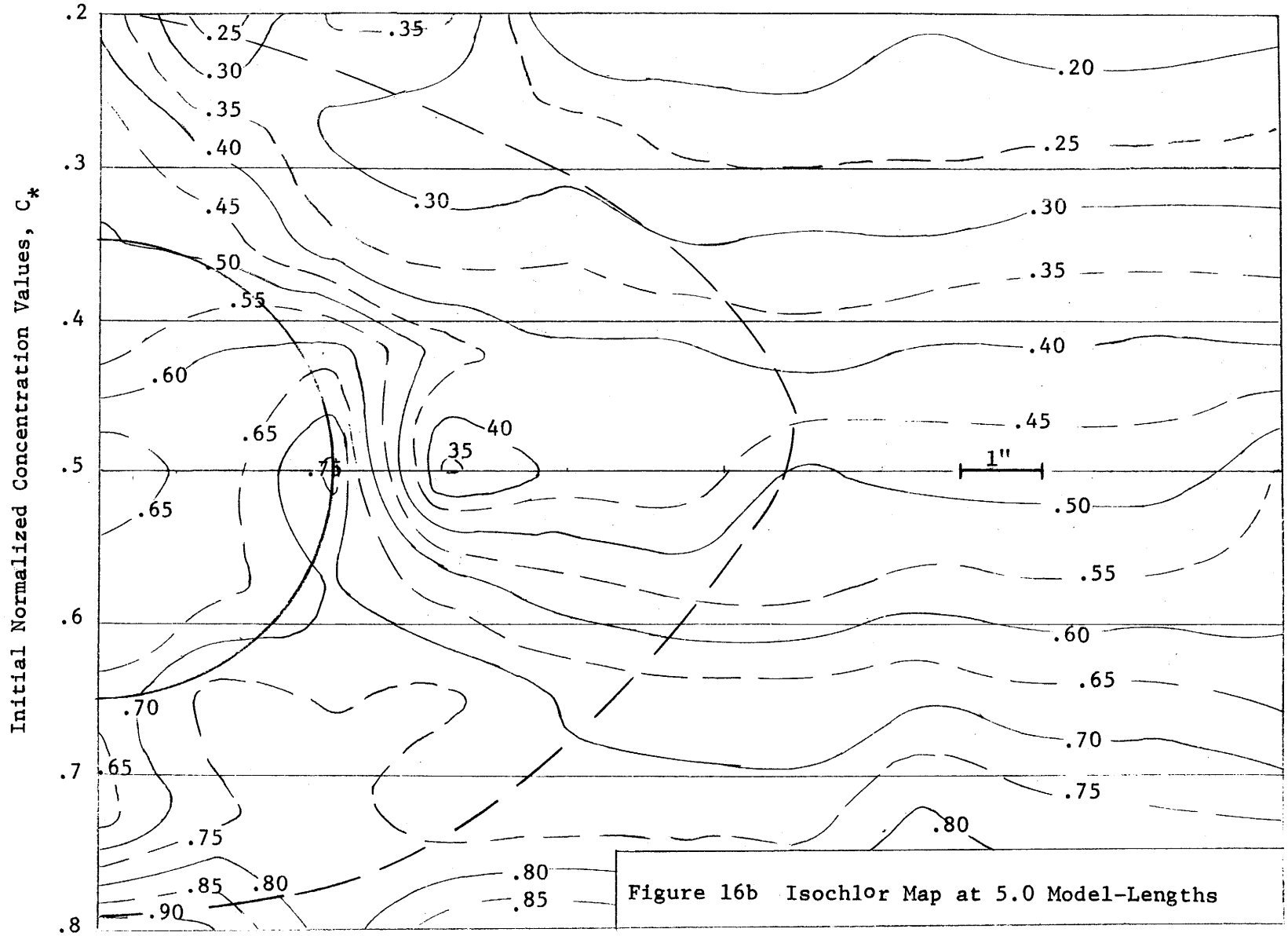

Figure 16b Isochlor Map at 5.0 Model-Lengths

Figure 16c Isochlor Map at 7.5 Model-Lengths

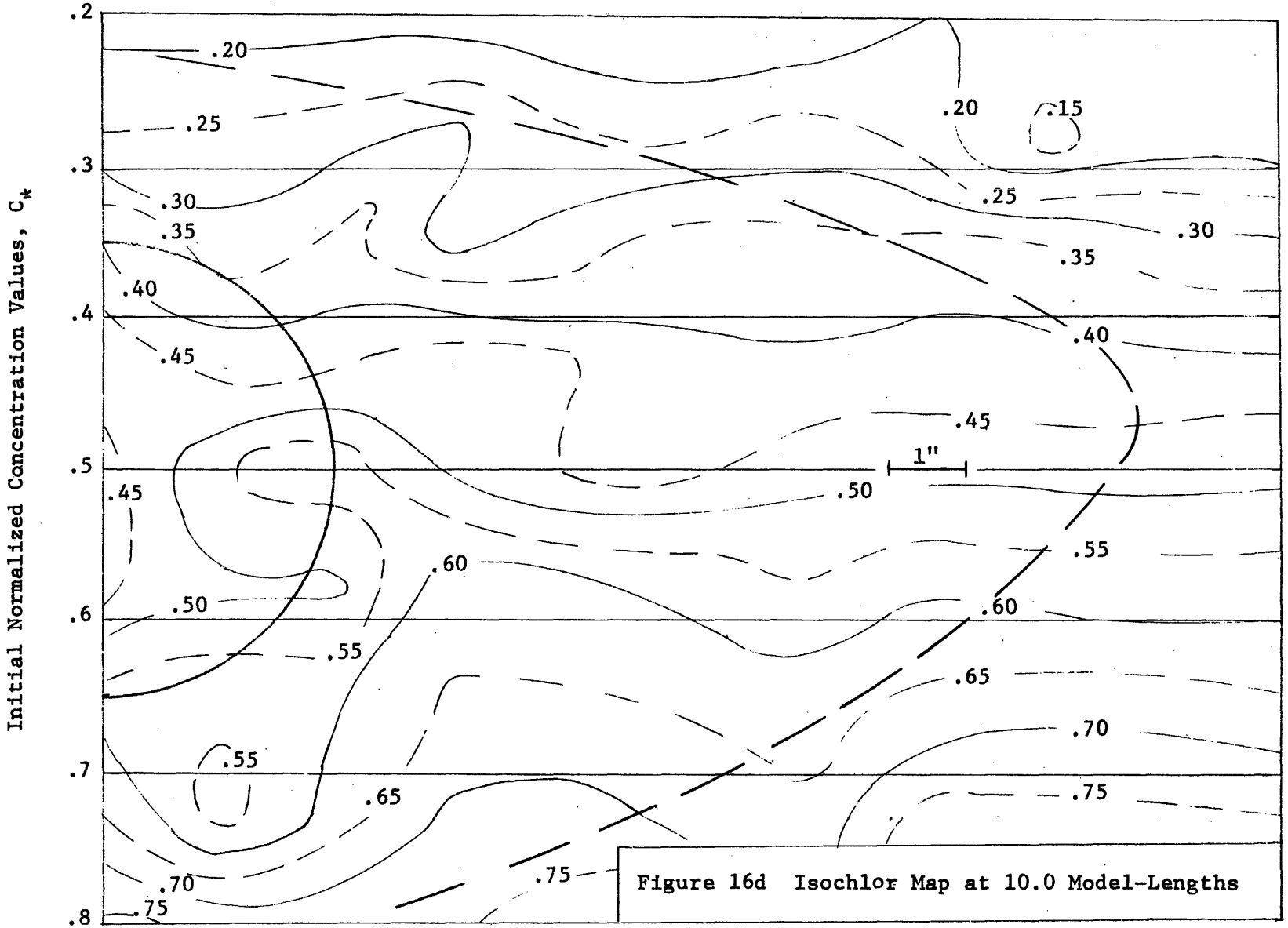

Figure 16d Isochlor Map at 10.0 Model-Lengths

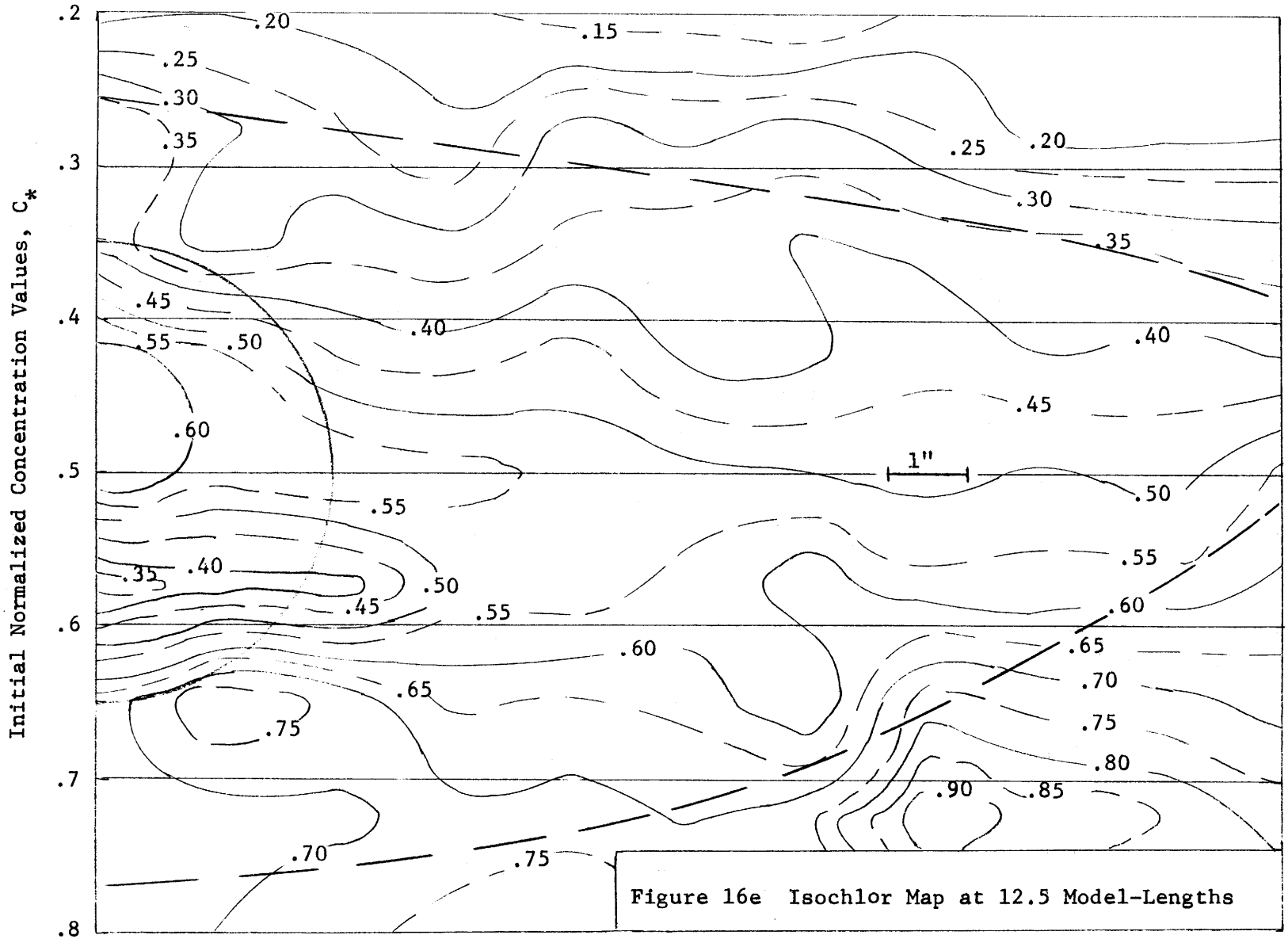

Figure 16e Isochlor Map at 12.5 Model-Lengths

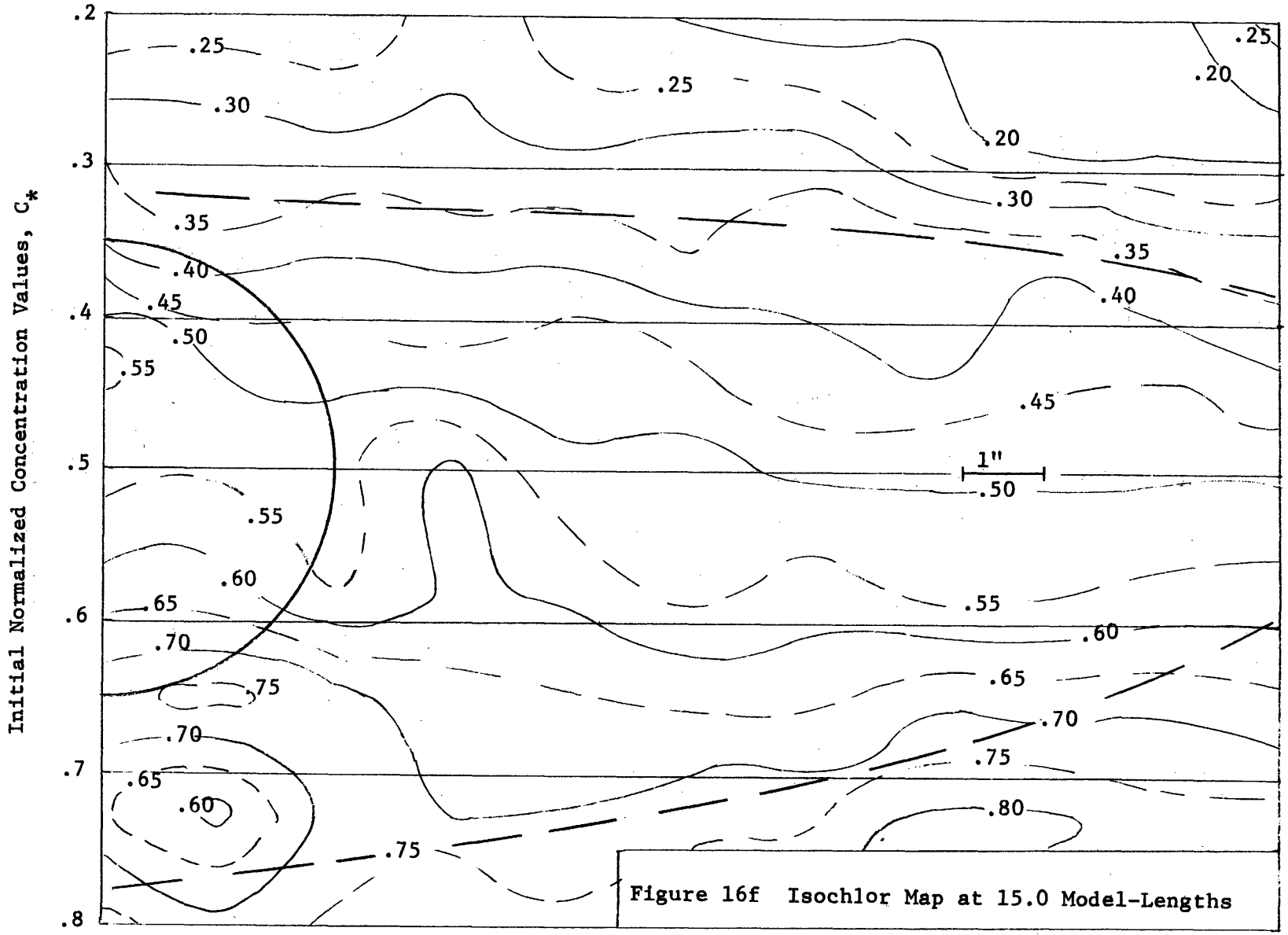

Figure 16f Isochlor Map at 15.0 Model-Lengths

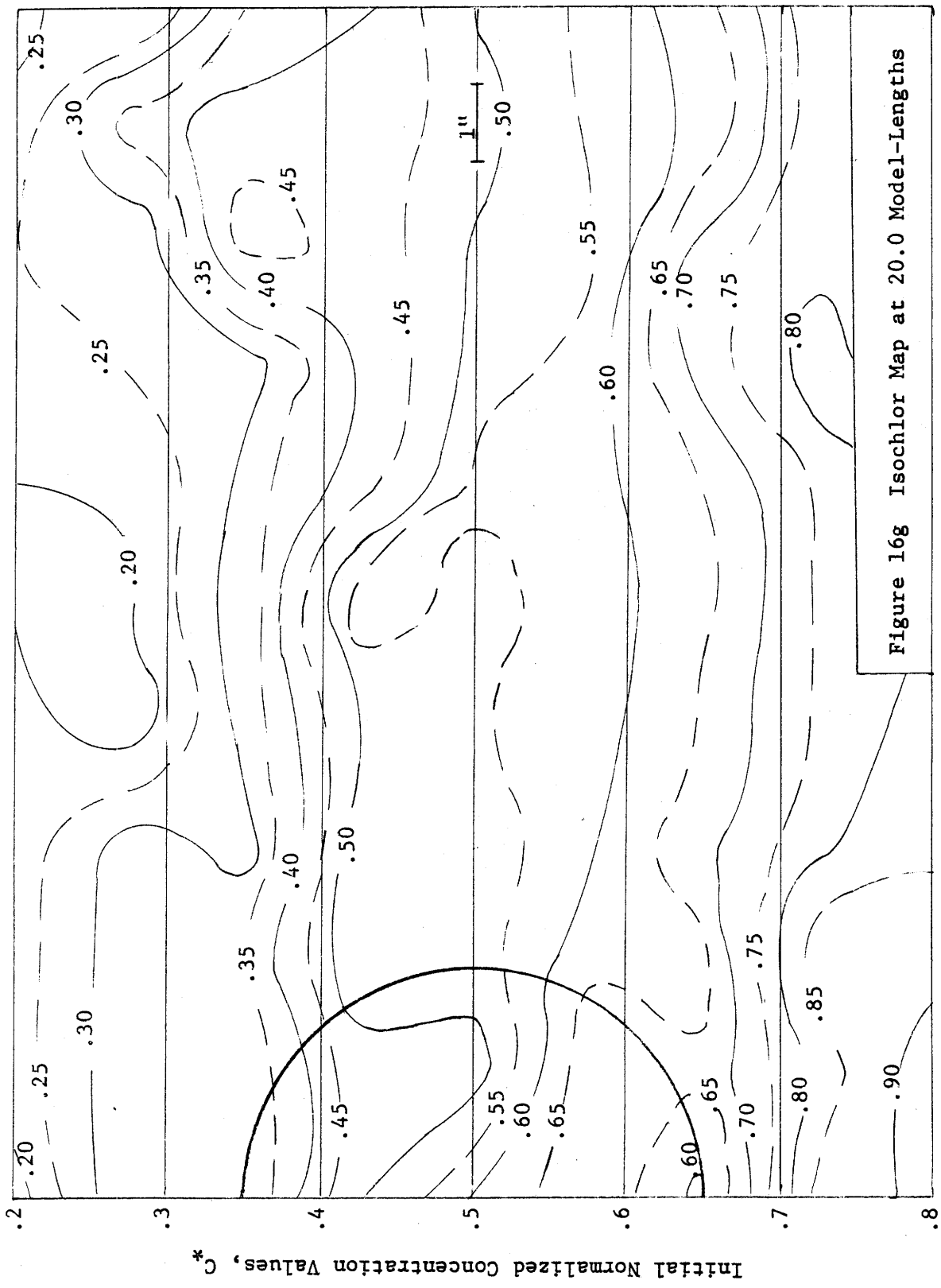
Figure 16g Isochlor Map at 20.0 Model-Lengths
1"
Initial Normalized Concentration Values, C*
.2
.3
.4
.5
.6
.7
.8
.20
.25
.30
.35
.40
.45
.50
.55
.60
.65
.70
.75
.80
.85
.90

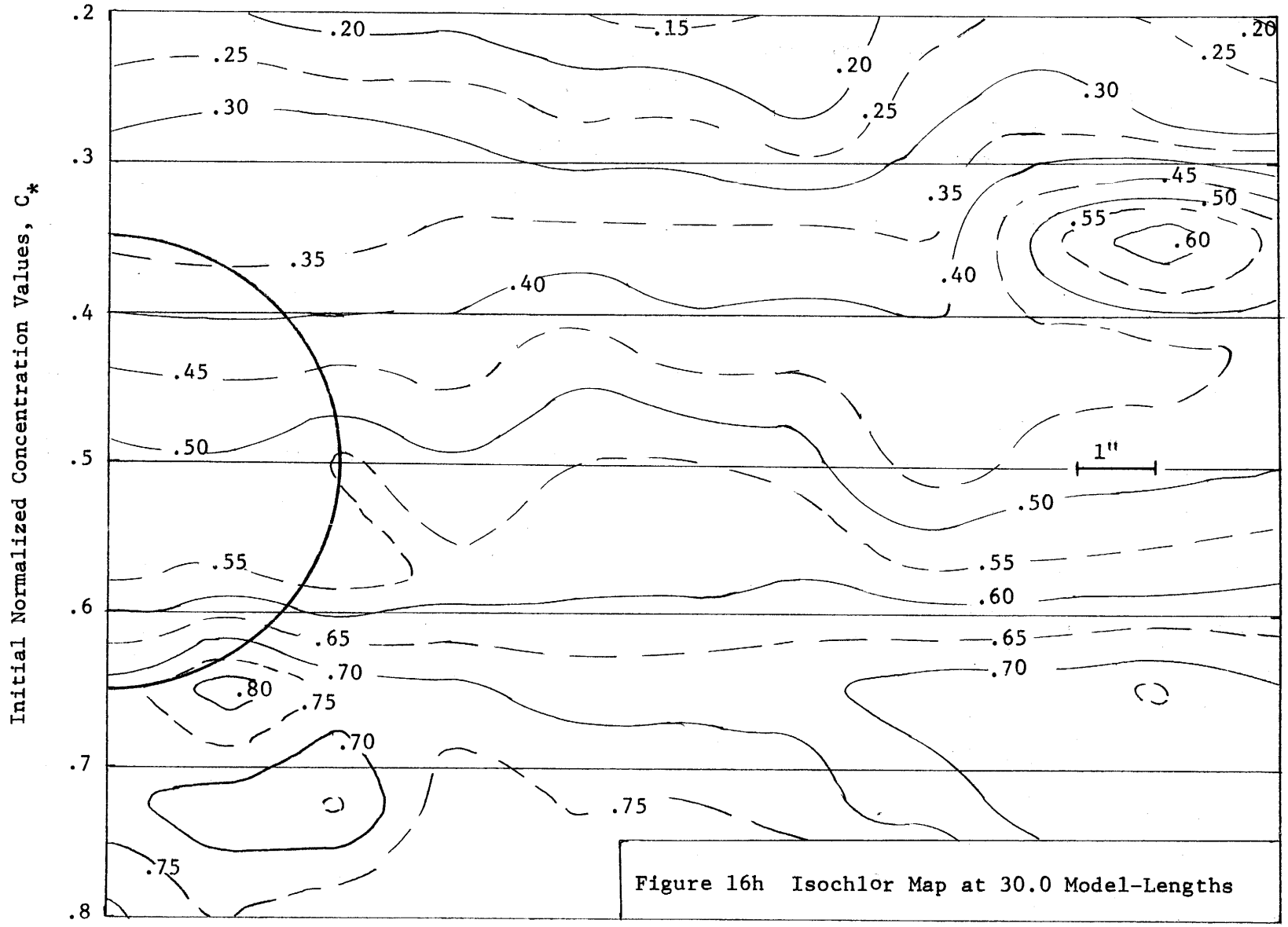

Figure 16h Isochlor Map at 30.0 Model-Lengths

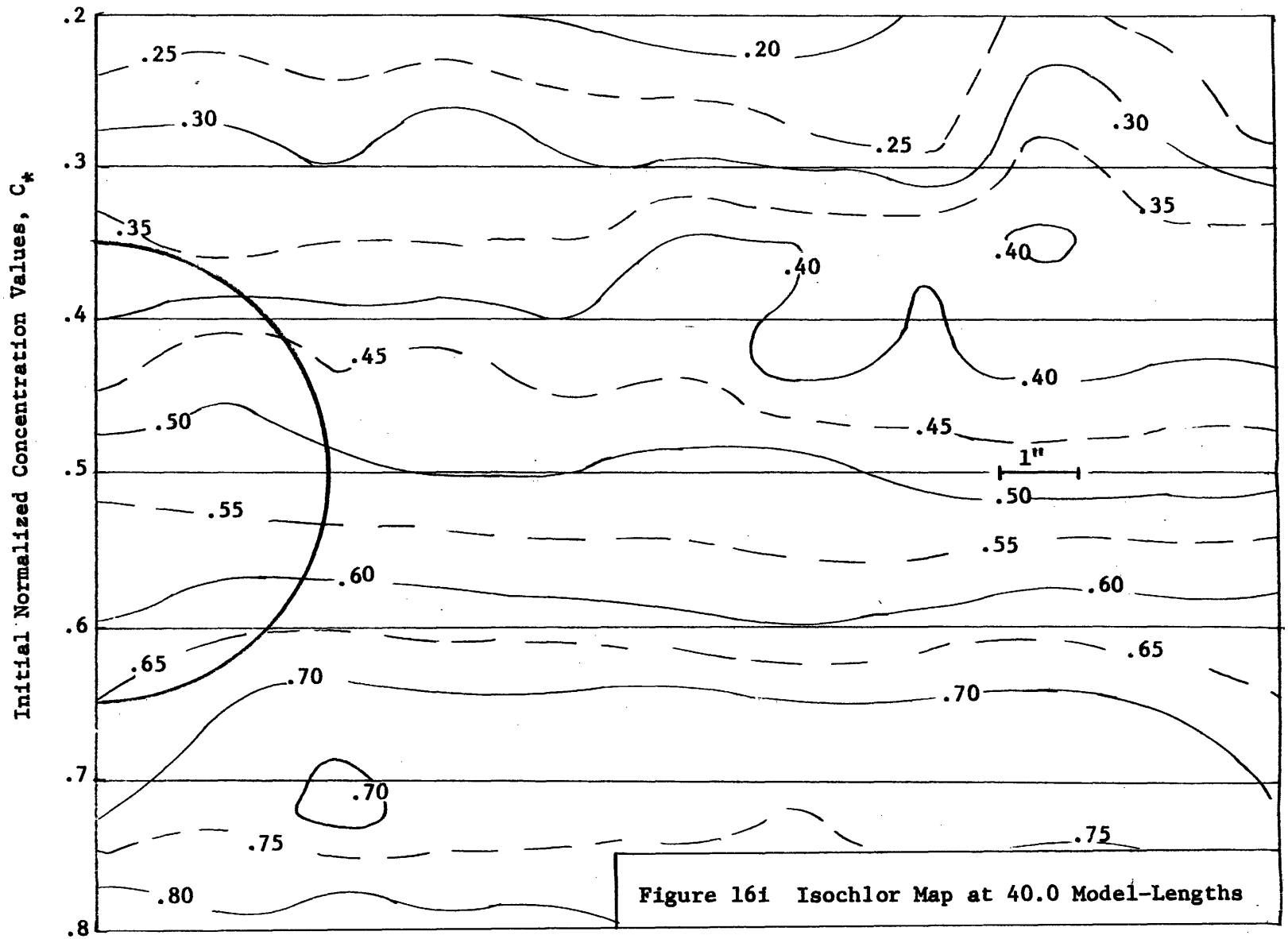

Figure 16i Isochlor Map at 40.0 Model-Lengths

vertical centerline (℄) in Figures 16b, 16d, 16e, and 16f. Looking now at the isochlors above the model in Figure 16b, it is observed that the isochlors are inclined upward near the ℄, indicating that the wake is expanding vertically. In this instance, the turbulent mixing is dominant, and there is a net upward flux of salinity above the model at the ℄. The closed and semi-closed isochlors in and near the path of the disc are another manifestation of the turbulent mixing.

In Figure 16d, the effects of gravity and turbulent mixing are both in evidence, both above and below where the model passed. At this distance, ten model-lengths or fifty disc diameters behind the body, the vertical wake collapse has begun. Gravity now is influencing the .2, .25, .6, .65, and .7 isochlors, which have become either horizontal or inclined back toward the level of the body, while the mixing is still influencing the .4, .45, and .5 isochlors, which are more strongly affected by the wake turbulence. At larger distances behind the body, gravity forces start to become dominant throughout the disturbed region, and by 12.5 model-lengths (62.5 disc diameters,see Figure 16e) the vertical collapse of the mixed region appears to be well developed, corresponding isochlors above and below the body having moved closer together. The semi-closed contours extending away from the ℄ suggest that well mixed fluid from this region is moving laterally away from the body at levels of density equilibrium. The collapse is practially complete by 15 model-lengths or 75 disc diameters, Figure 16f, and at this point, turbulent mixing apparently ceases to be one of the dominant features of the motion except in a few isolated regions. By 40 model-lengths or 200 disc diameters behind the body, Figure 16i, the fluid system has nearly returned to equilibrium, and only a few disruptions, presumably due to internal waves, remain.

Data obtained from the envelopes of the zones of mixing in Figures 16a to 16i are displayed in Figure 17, which is a plot of the heights and widths of the envelopes of the zone of disruption vs distance behind the model. These plots substantiate the conclusions inferred from the isochlor

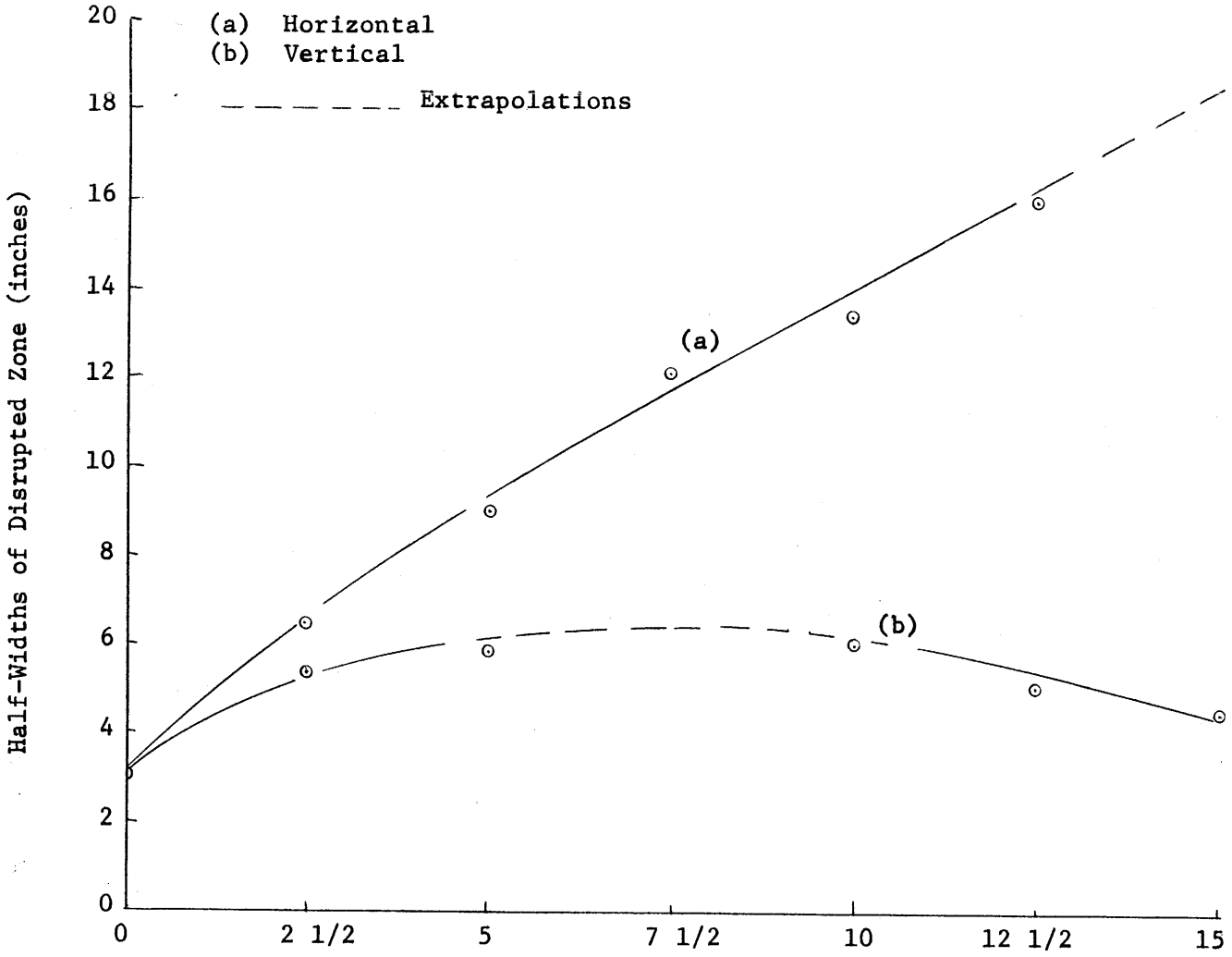

Horizontal and Vertical Half-Width of Disrupted Zone vs
Distance Behind Model in Multiples of Model-Length

Figure 17

maps; that is, the turbulent mixing dominates the vertical wake height initially, while at larger distances, the gravity forces and associated wake collapse appear to be the dominant features. By 7 or 8 model-lengths, gravity forces have suppressed the vertical growth of the mixed region at the $\mathcal{L}$,and by 15 model lengths have nullified its initial growth. The horizontal extent of influence of the body on the stratification appears to increase almost linearly with time.

Unfortunately, it was not found possible to define wake widths in the usual sense of a distance between points where the concentration has some prescribed departure from its initial value. Vertical concentration profiles were drawn for several distances behind and to the sides of the body. Typical examples of such profiles are shown in Figures 18a and 18b. In practically all cases, the concentration departures from the initial profile were too small and/or erratic to yield a meaningful definition of a wake height. The erratic variations noted were no doubt due to the internal waves in the fluid.

It is interesting to compare the results presented in Figure 17 on the vertical extent of the mixed region with the results reported by Schooley and Stewart[4]. They defined the extent of the wake by measuring the extent of the dispersion of a dye tracer injected into the wake of a self-propelled body in a fluid with a constant density gradient of $\frac{1}{\rho_o}\frac{d\rho}{dy} = -0.1585\ (ft)^{-1}$. In their work, gravity forces would be expected to be more significant than in the present study since their density gradient was 50 times greater than that of this investigation. This notion is substantiated by Prych, Harty, and Kennedy[2], see Figure 2, who found that the wake collapse occurs at smaller distances behind the body as the stratification parameter, $J \propto (\frac{\Delta\rho}{\rho_o})^{1/2}$, increases. The larger density gradient used by Schooley and Stewart should, therefore, result in a larger gravitational effect which would be accompanied by a more rapid inception of wake collapse than was found in the present study. A brief comparison of the results of Schooley and Stewart and those of the

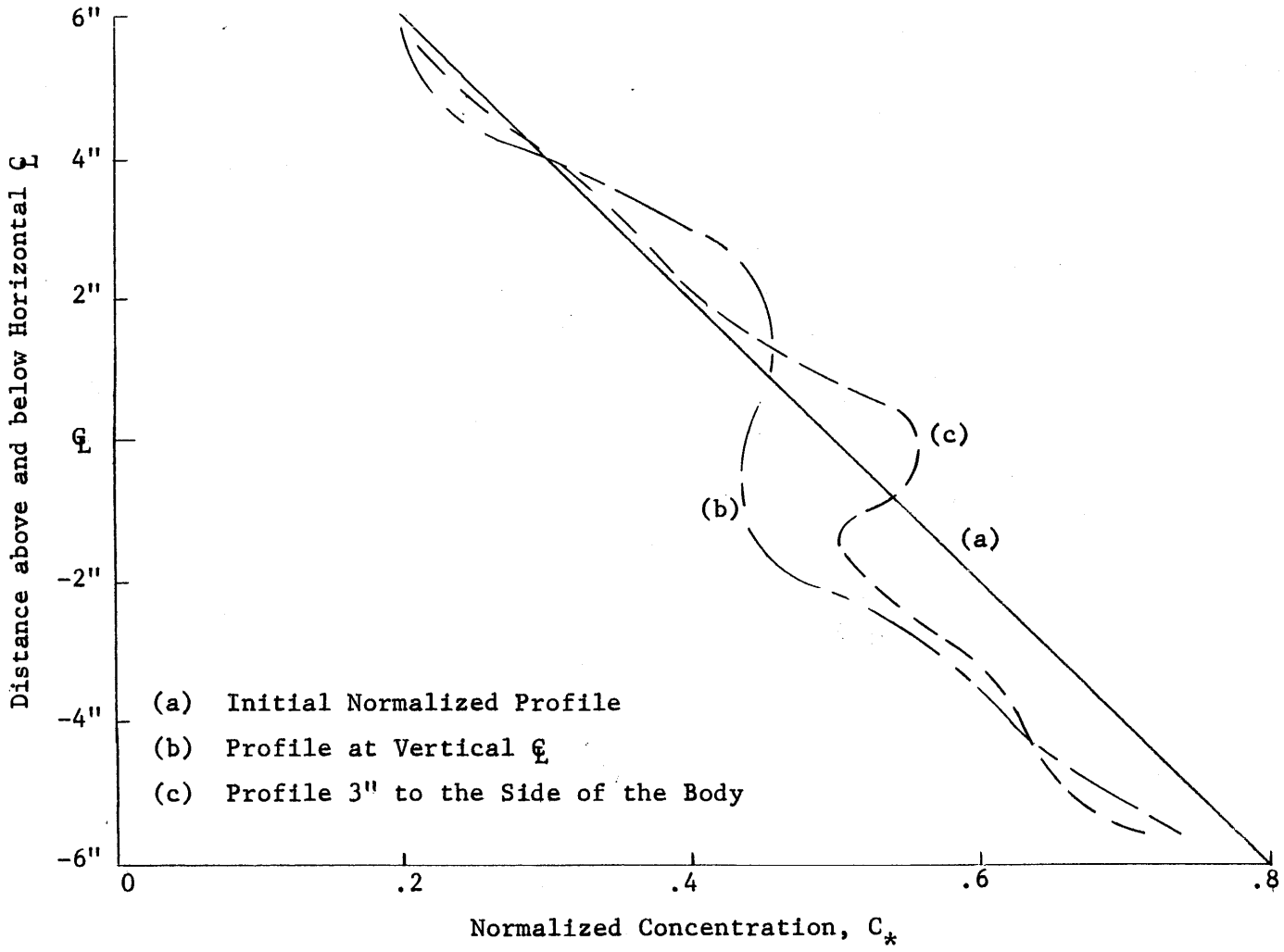

Vertical Concentration Profiles at 10 Model-Lengths behind the Model

Figure 18a

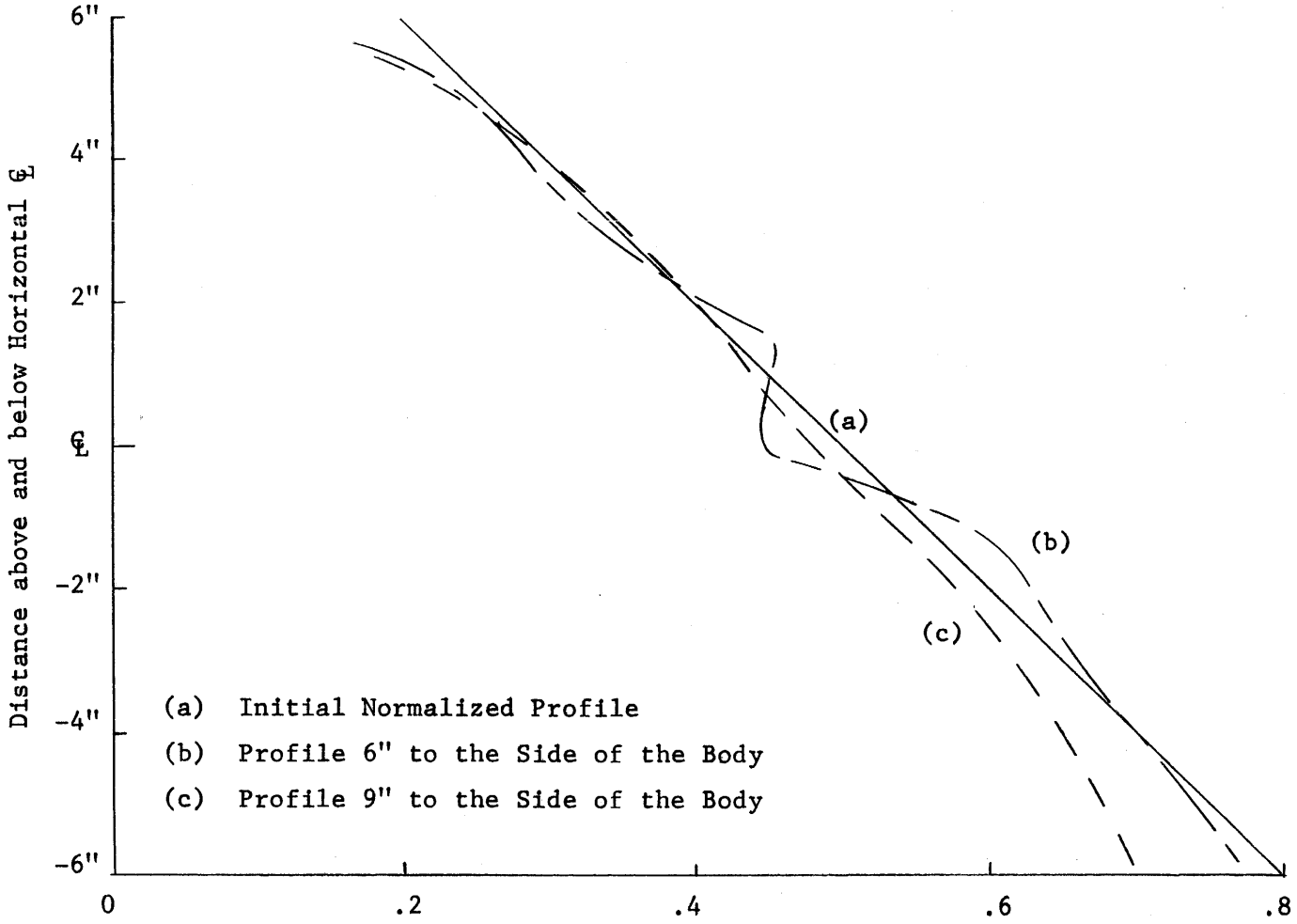

Vertical Concentration Profiles at 10 Model-Lengths behind the Model

Figure 18b

present study is as follows:

Schooley and Stewart	Present Study
$\frac{1}{\rho_o}\frac{d\rho}{dy} = -0.1585\ ft^{-1}$	$\frac{1}{\rho_o}\frac{d\rho}{dy} = -0.003\ ft^{-1}$
$R = 10^4$	$R = 8.9 \times 10^4$
$T^* = 1.0$ sec.	$T^* = 9.75$ sec.
$D^* = 20.4$	$D^* = 37.5$
$\frac{b^*}{b_o} = 2.16$	$\frac{b^*}{b_o} = 2.17$
$b_o = 2.2$ cm	$b_o = 6.0$ in.
$d^* = 7.5$ cm	$d^* = 16.5$ in.

where

R = Reynolds number

T^* = time to maximum vertical wake width

D^* = distance in body diameters that model travels in T^*

b^* = maximum vertical extent of the wake

b_o = diameter of disrupting body (disc diameter in the present study)

d^* = depth of submergence

The much larger value of T^* in the present study supports the obvious idea that the gravitational effects increase with increasing density gradient. This time to the maximum extent of the vertical wake should also increase with the intensity of turbulent mixing and hence the Reynolds number.

In both investigations, it is somewhat surprising how fast the wake attains its maximum vertical dimension. The close agreement between the values of b^*/b_o for the two studies is probably little more than coincidence.

It would be expected that as the density gradient is decreased, the vertical extent of the wake would increase, which would make a stronger wake collapse possible. However, the diminished density gradient reduces the gravity effect. Hence, there must be an optimum combination of Reynolds number (as a measure of the turbulent mixing) and density gradient that maximizes the wake collapse phenomena. Either a zero or infinite density gradient precludes a wake collapse.

Figures 19a, 19b, and 19c are plots of the normalized distance between isochlors vs distance behind the model for various horizontal distances from the vertical ℄. To normalize the isochlor spacing, the measured vertical distances between the isochlors were divided by their original spacing. It is observed in each of the figures that there is an initial increase of the isochlor spacing at the ℄ , which is accompanied by a small but consistent decrease in spacing at the various horizontal distances from the ℄ . The first minimum spacing at the ℄ occurs at about fifteen model lengths, and this minimum is accompanied by a maximum or an increasing trend in the isochlor spacing at the various distances from the ℄ . These observations are consistent with what one would expect from continuity considerations; that is, a collapse in the vertical wake-height should be accompanied by an extension of its horizontal extent as the fluid from above and below the level of the body spreads laterally, increasing the isochlor spacing at the side of the body. The maximum spacing at the ℄ occurs at about five to eight lengths behind the body; this is consistent with Figure 17. In Figure 19a, it is seen that after about fifteen model-lengths, a periodic variation suggesting internal wave motion appears to be the predominant influence.

The envelopes of the vertical extent of the motion of the .3, .5, and .7 isochlors over the full period of time studied is shown in Figure 20. This plot demonstrates the decreasing magnitude of the isochlor motion with increasing distance from model. The magnitude of the isochlor motion fifteen inches from the model ℄ is probably comparable to the magnitude of the internal waves.

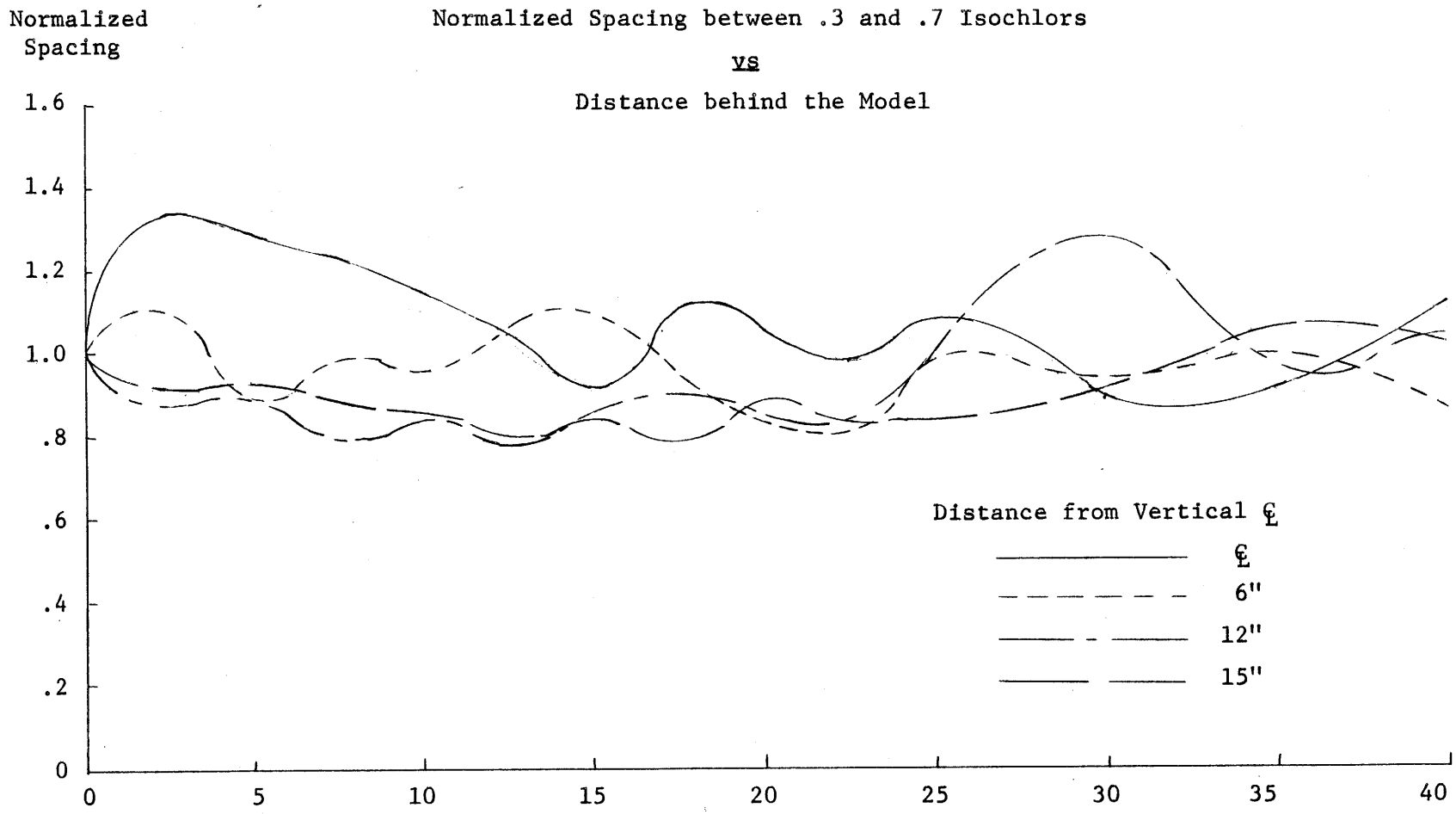
Normalized Spacing
Normalized Spacing between .3 and .7 Isochlors
vs
Distance behind the Model
1.6
1.4
1.2
1.0
.8
.6
.4
.2
0
0
5
10
15
20
25
30
35
40
Distance from Vertical ℄
℄
6"
12"
15"
Distance behind Model in Multiples of Model-Length

Figure 19a

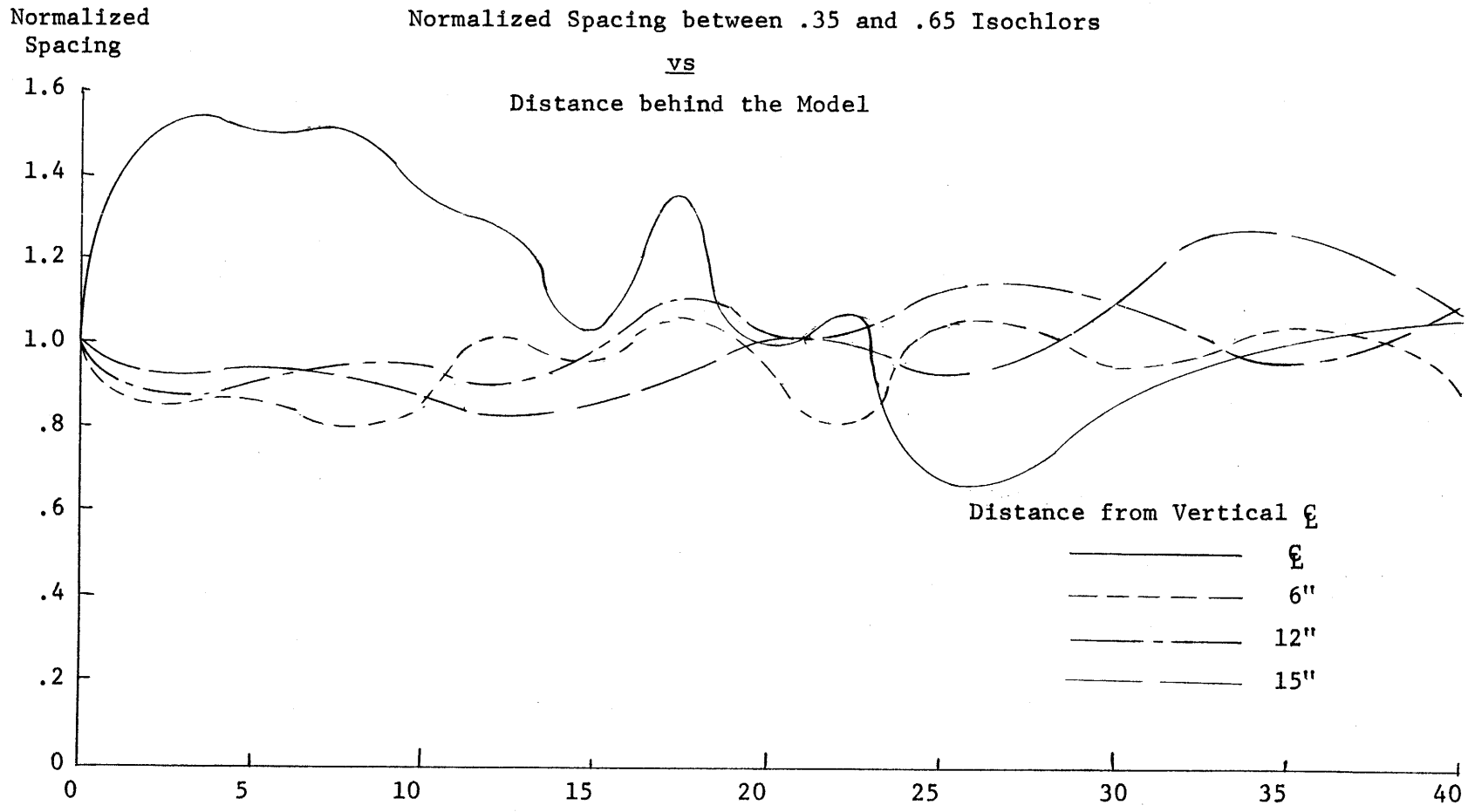
Normalized Spacing
Normalized Spacing between .35 and .65 Isochlors
vs
Distance behind the Model
1.6
1.4
1.2
1.0
.8
.6
.4
.2
0
0
5
10
15
20
25
30
35
40
Distance from Vertical ℄
℄
6"
12"
15"
Distance behind Model in Multiples of Model-Length

Figure 19b

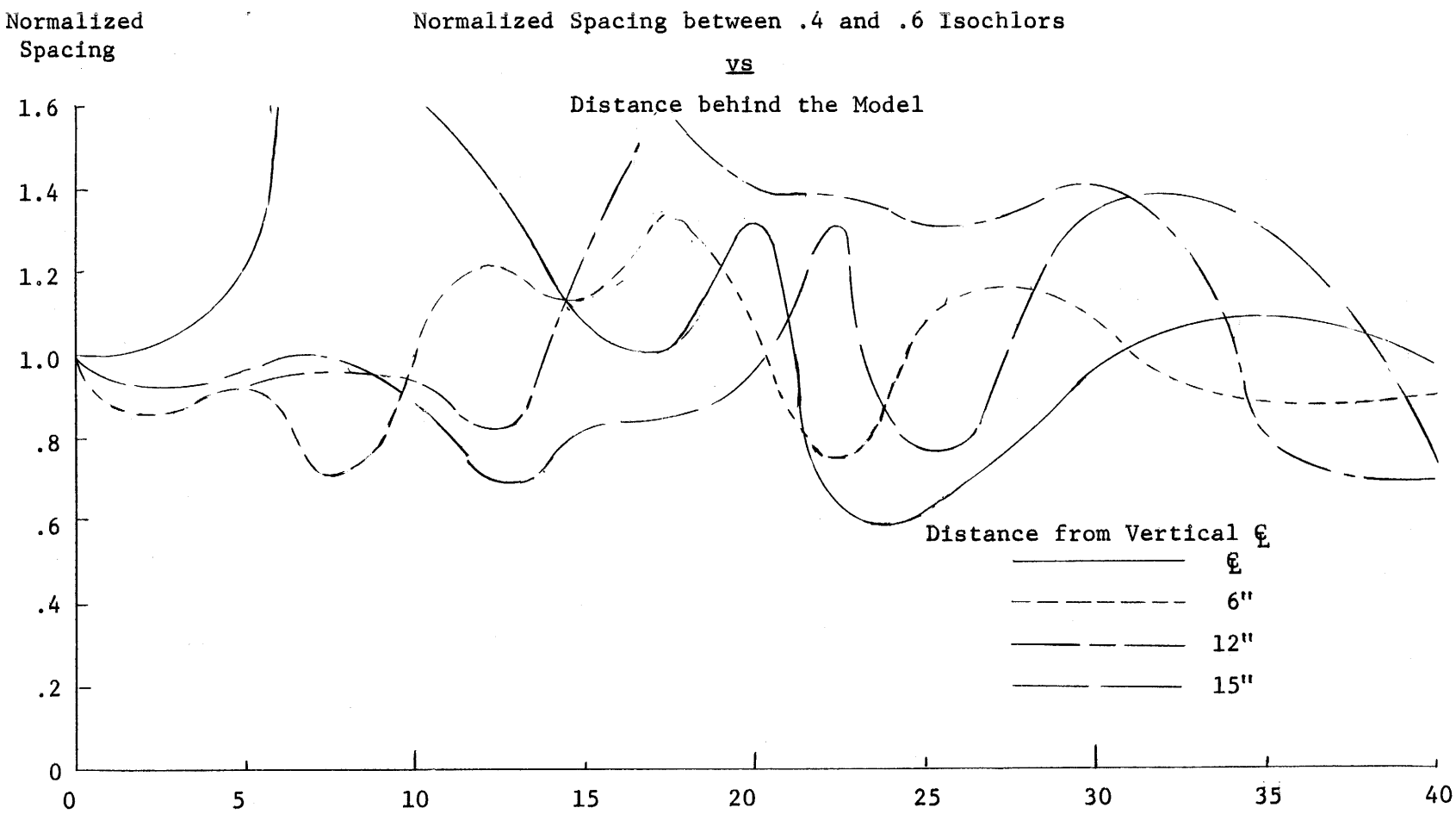
Normalized Spacing
Normalized Spacing between .4 and .6 Isochlors
vs
Distance behind the Model
1.6
1.4
1.2
1.0
.8
.6
.4
.2
0
0
5
10
15
20
25
30
35
40
Distance from Vertical ℄
℄
6"
12"
15"
Distance behond Model in Multiples of Model-Length

Figure 19c

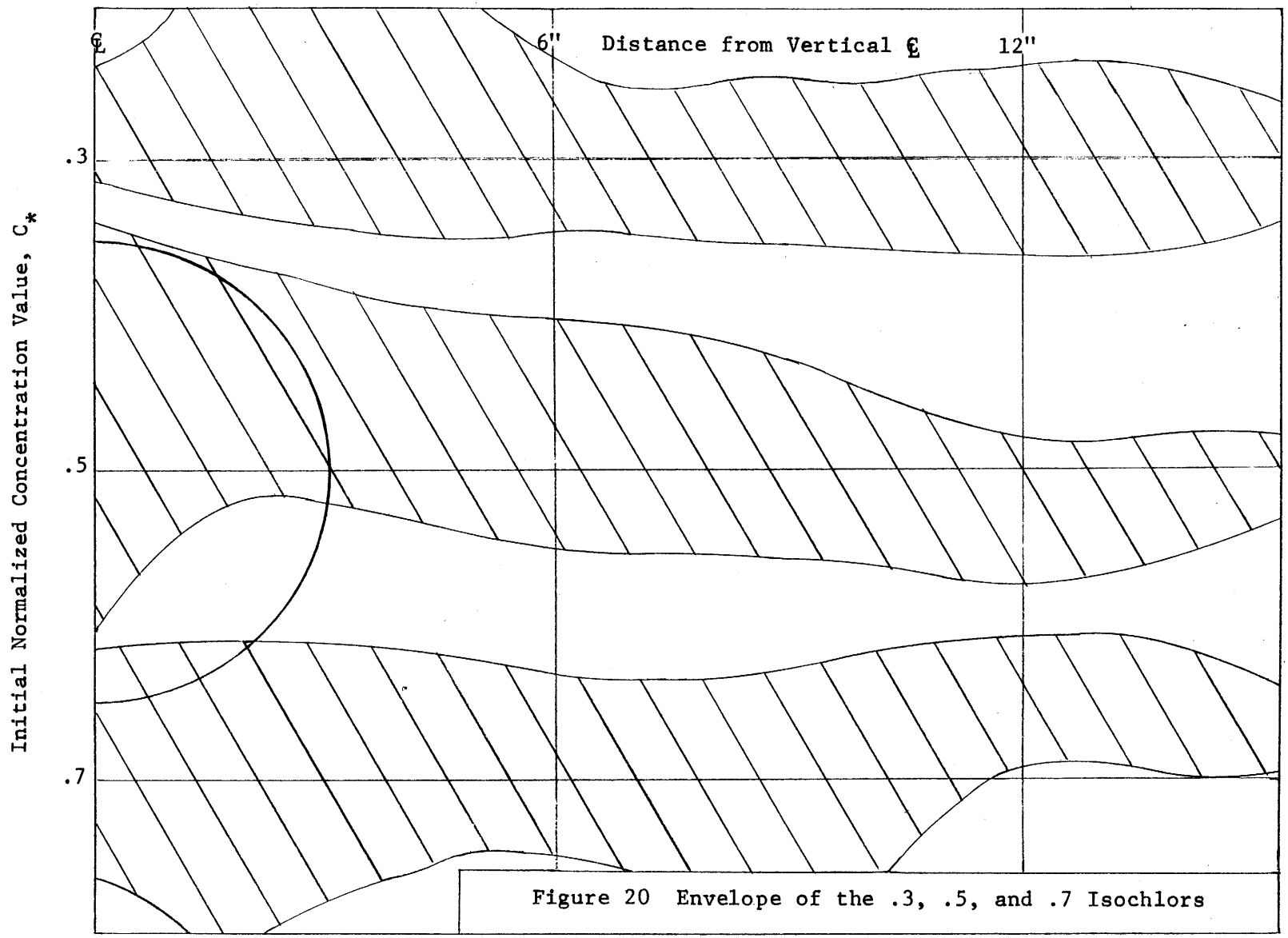

Figure 20 Envelope of the .3, .5, and .7 Isochlors

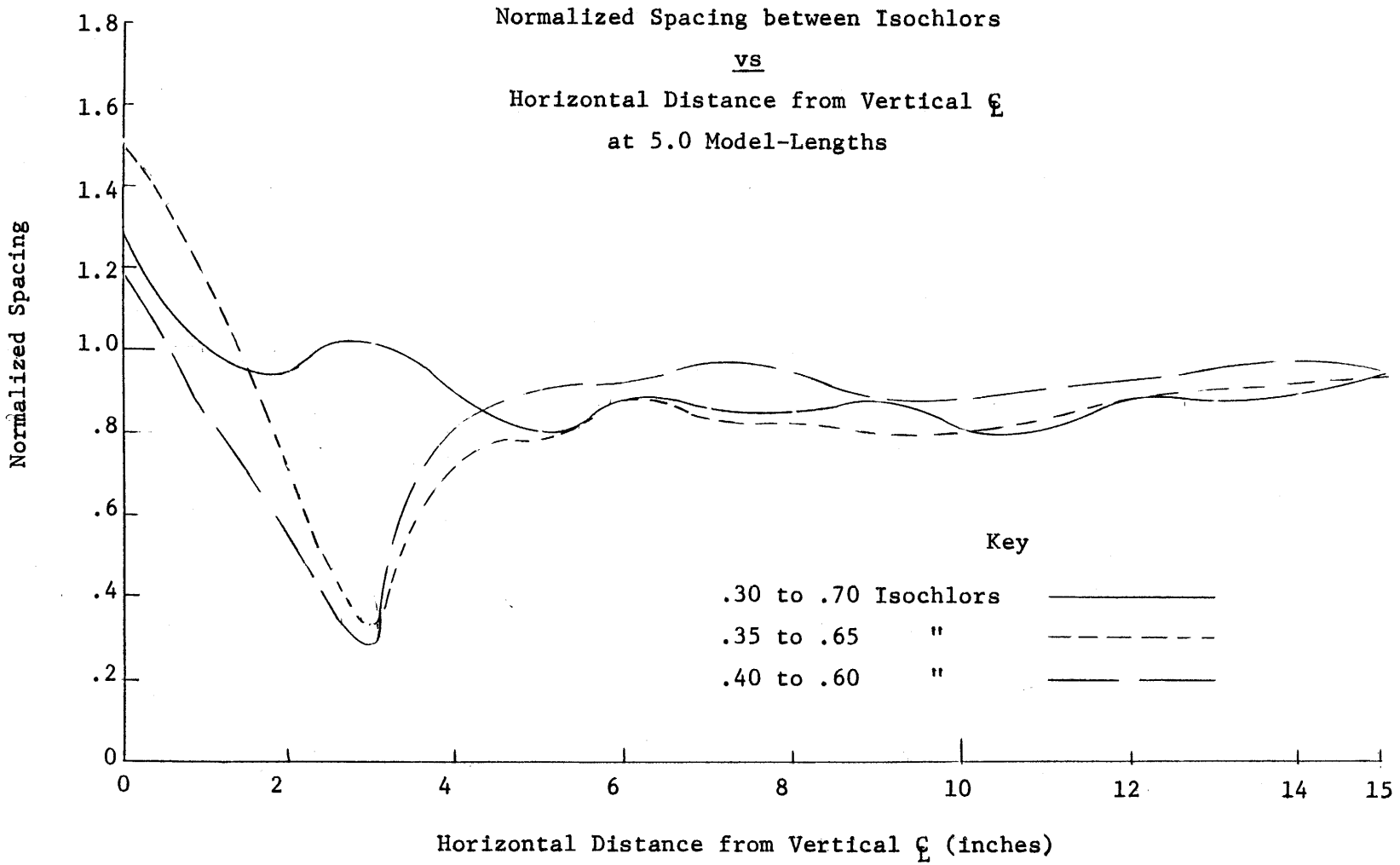
Normalized Spacing between Isochlors
vs
Horizontal Distance from Vertical ℄
at 5.0 Model-Lengths
Normalized Spacing
1.8
1.6
1.4
1.2
1.0
.8
.6
.4
.2
0
0
2
4
6
8
10
12
14
15
Key
.30 to .70 Isochlors
.35 to .65 "
.40 to .60 "
Horizontal Distance from Vertical ℄ (inches)

Figure 21a

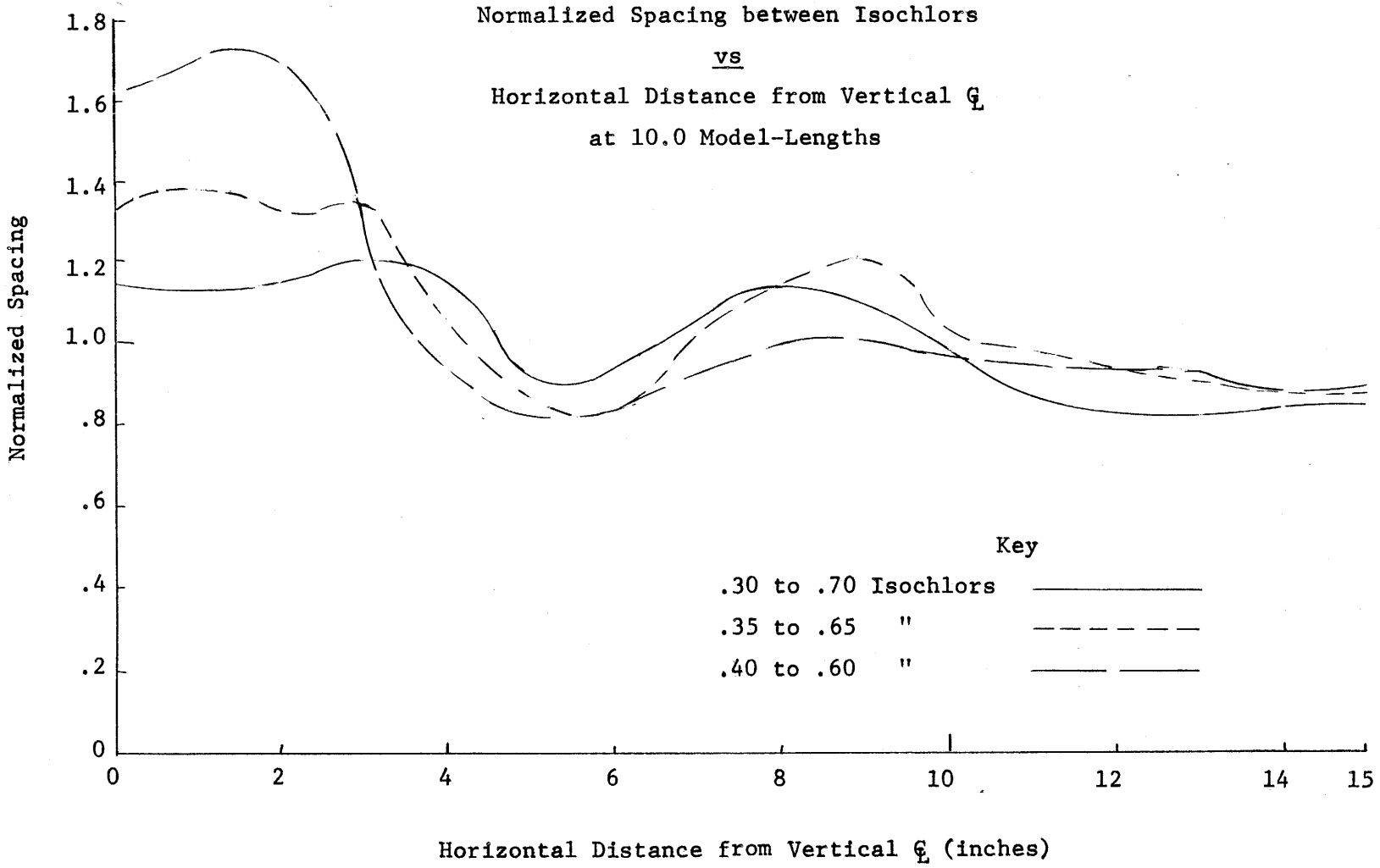
Normalized Spacing between Isochlors
vs
Horizontal Distance from Vertical ℄
at 10.0 Model-Lengths
Normalized Spacing
1.8
1.6
1.4
1.2
1.0
.8
.6
.4
.2
0
0
2
4
6
8
10
12
14
15
Key
.30 to .70 Isochlors
.35 to .65 "
.40 to .60 "
Horizontal Distance from Vertical ℄ (inches)

Figure 21b

Normalized Spacing between Isochlors

vs

Horizontal Distance from Vertical ℄

at 12.5 Model-Lengths

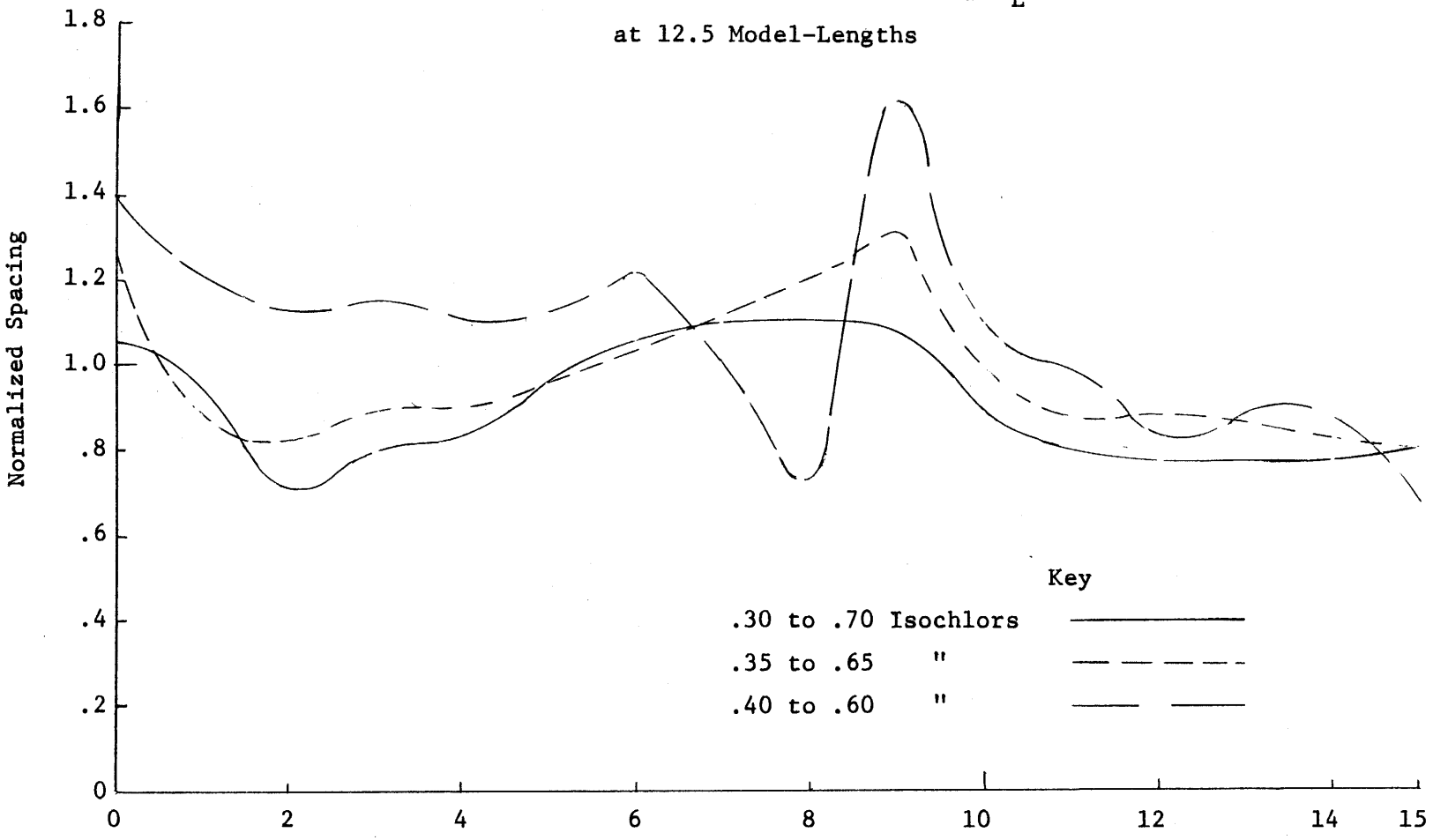

Figure 21c

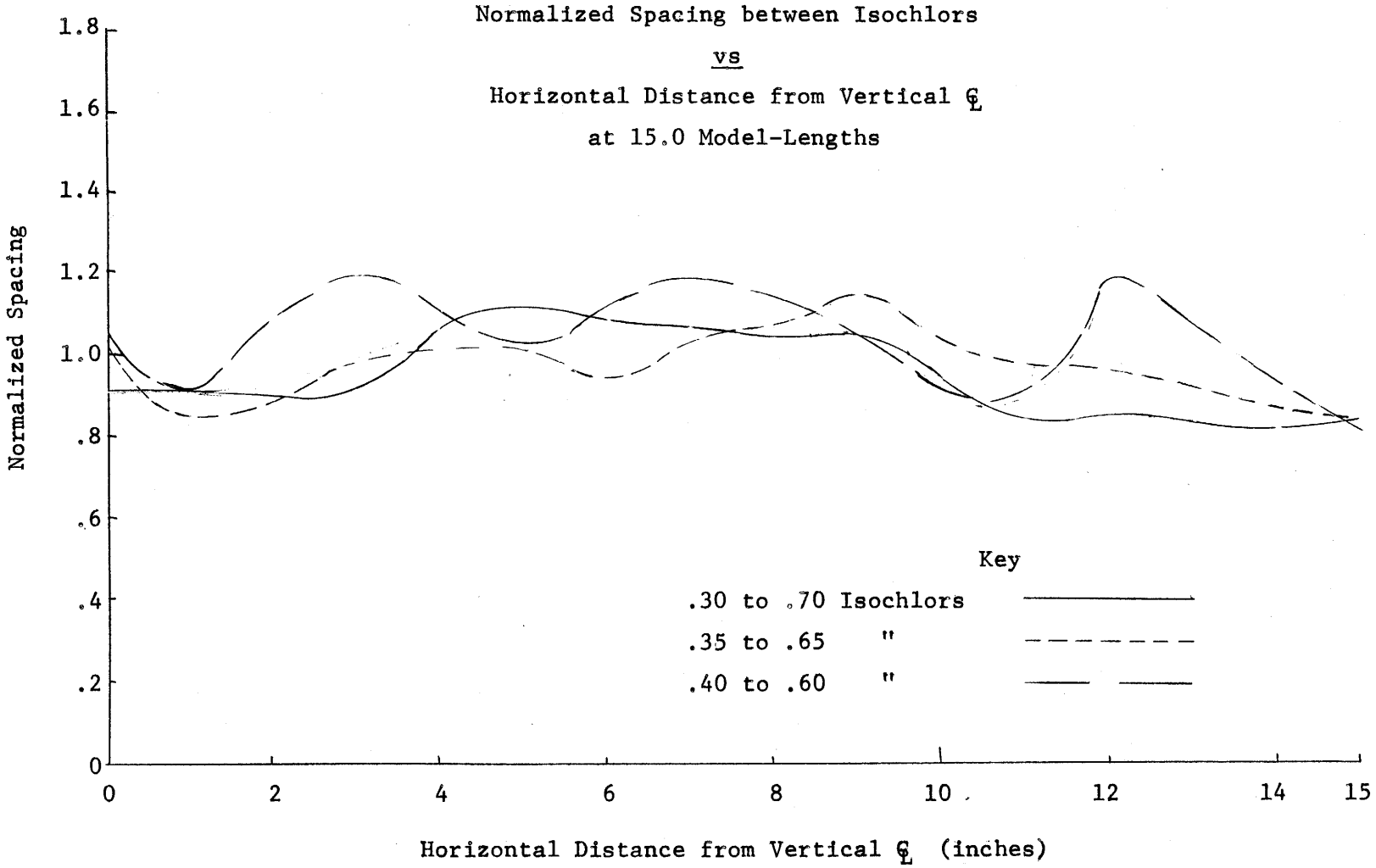
Normalized Spacing between Isochlors
vs
Horizontal Distance from Vertical ℄
at 15.0 Model-Lengths
Normalized Spacing
1.8
1.6
1.4
1.2
1.0
.8
.6
.4
.2
0
0
2
4
6
8
10
12
14
15
Key
.30 to .70 Isochlors
.35 to .65 "
.40 to .60 "
Horizontal Distance from Vertical ℄ (inches)

Figure 21d

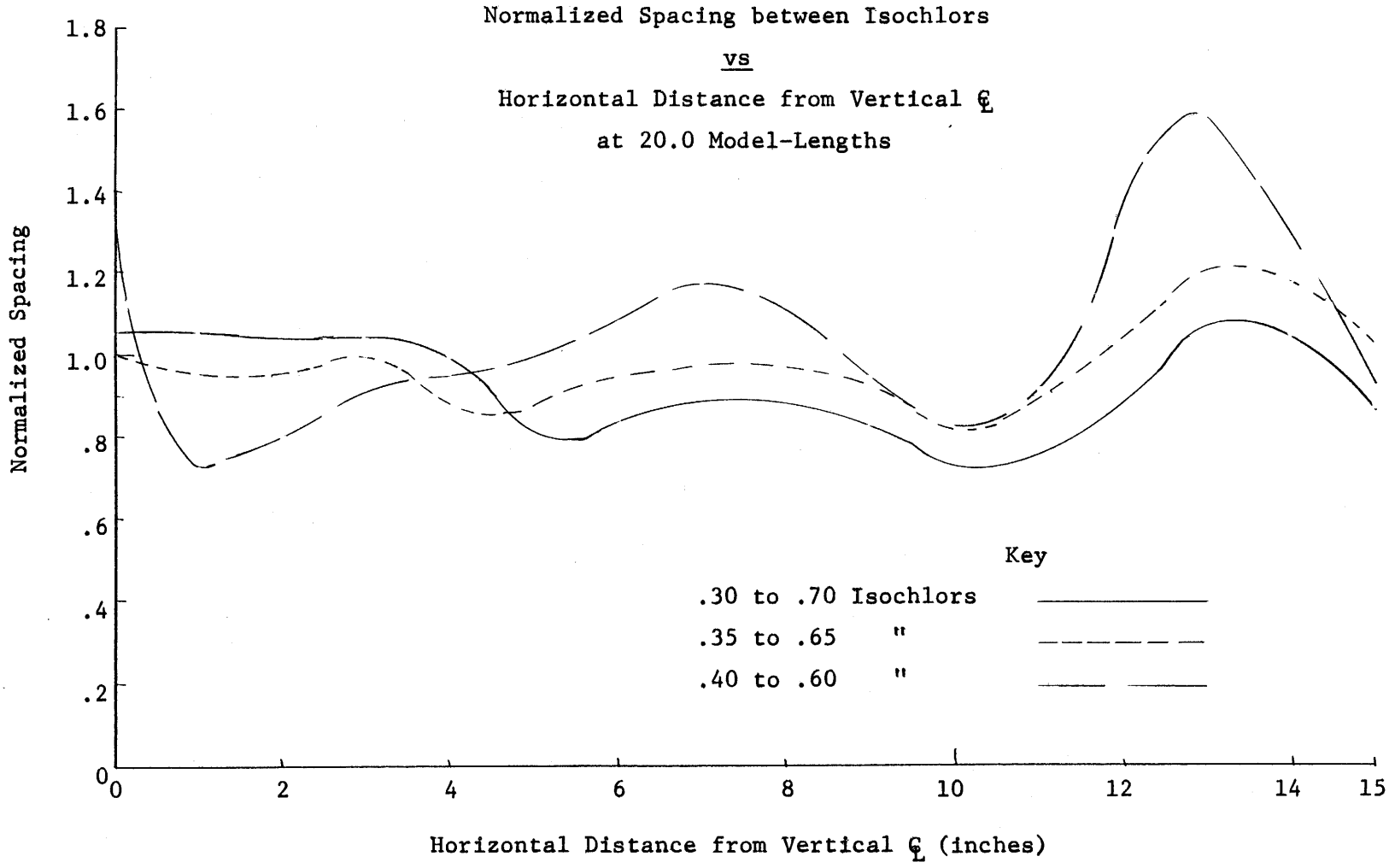
Normalized Spacing between Isochlors
vs
Horizontal Distance from Vertical ℄
at 20.0 Model-Lengths
Normalized Spacing
1.8
1.6
1.4
1.2
1.0
.8
.6
.4
.2
0
0
2
4
6
8
10
12
14
15
Key
.30 to .70 Isochlors
.35 to .65 "
.40 to .60 "
Horizontal Distance from Vertical ℄ (inches)

Figure 21e

Figures 21a through 21e are plots of the normalized distance between isochlors vs distance from the vertical ℄ of the model, for various distances behind the model. These figures show the propagation of the displacement of the isochlors from their initial positions, as the mixed fluid spreads laterally. Again, as with the wake envelope plots on the isochlor maps, the wake influence is seen to increase horizontally as the distance behind the model increases.

C. Surface Effects

In addition to providing information about the motion of fluid at the free surface, it was hoped that the surface motion studies would also yield an independent verification of the time scale of the wake collapse obtained in the density configuration studies discussed in Section B. Two different density gradients, $\frac{1}{\rho_o}\frac{d\rho}{dy} = -0.003\ (ft)^{-1}$ and $-0.0015\ (ft)^{-1}$, in addition to a homogeneous fluid, were investigated in order to determine qualitatively the effect of the density gradient on the time scale and the strength of the wake collapse. The data presented in this section are the time variations of the distance between pairs of particles that were initially equidistant from and on opposite sides of the path of the model, for each of the three different density gradients. Although it is not shown by these data, both a high degree of eddy motion and a forward drift in the direction of the model were present at the surface for every density gradient investigated, indicating that the wake does extend to the free surface. Variations in the salinity configuration near the free surface were not measured.

Shown in Figure 22a are the particle spacings as a function of time for the density gradient, $\frac{1}{\rho_o}\frac{d\rho}{dy} = -0.003\ (ft)^{-1}$, which was also used in the density configuration studies. Recall from Section B that the principal wake collapse occurs between 10 and 15 model lengths (50 to 75 disc diameters) behind the body. Referring to Figure 22a, it is observed that a sharp convergence of surface particles also occurs during this time interval. It is

also noted in Figure 22a that the strength of particle convergence decreases with increasing lateral distance from the path of the model. Some indication of the eddy motion at the surface near the path of the model is shown by the negative spacing between one pair of particles in Figure 22a, indicating that these particles actually crossed paths and then diverged. This pair of particles appeared to be entrained in opposite sides of a strong eddy. Particle convergence on the free surface appears to have ceased approximately 70 seconds (60 model lengths or 300 disc diameters) after passage of the model.

Figure 22b illustrates the results obtained for a density gradient of $-0.0015\ (ft)^{-1}$. As might be expected, the rate of convergence of particles for this series of experiments is noticeably less than for the previous case, the gravity effect being diminished by the reduced gradient. The lateral extent over which the particle convergence can be detected is also reduced, indicating that the wake collapse, which is responsible for the convergence as explained in the next section, has a diminished effect on the surface motion. In some instances, particles far from the centerline actually diverge, a result of random eddy motion in this region. The duration of the effects of the collapse on the free surface appears to be about the same as for the larger density gradient (Figure 22a).

A similar series of surface motion experiments was conducted for homogeneous tap water, the results of which appear in Figure 22c. In the absence of any density gradient and corresponding gravitational effects, the particle motion is quite random, and, if there is any net lateral motion of the surface fluid, it would appear to be a divergence. Comparing the results of the three density gradients investigated, it is apparent that the degree of density stratification is certainly an important influence on the rate and strength of convergence of surface particles.

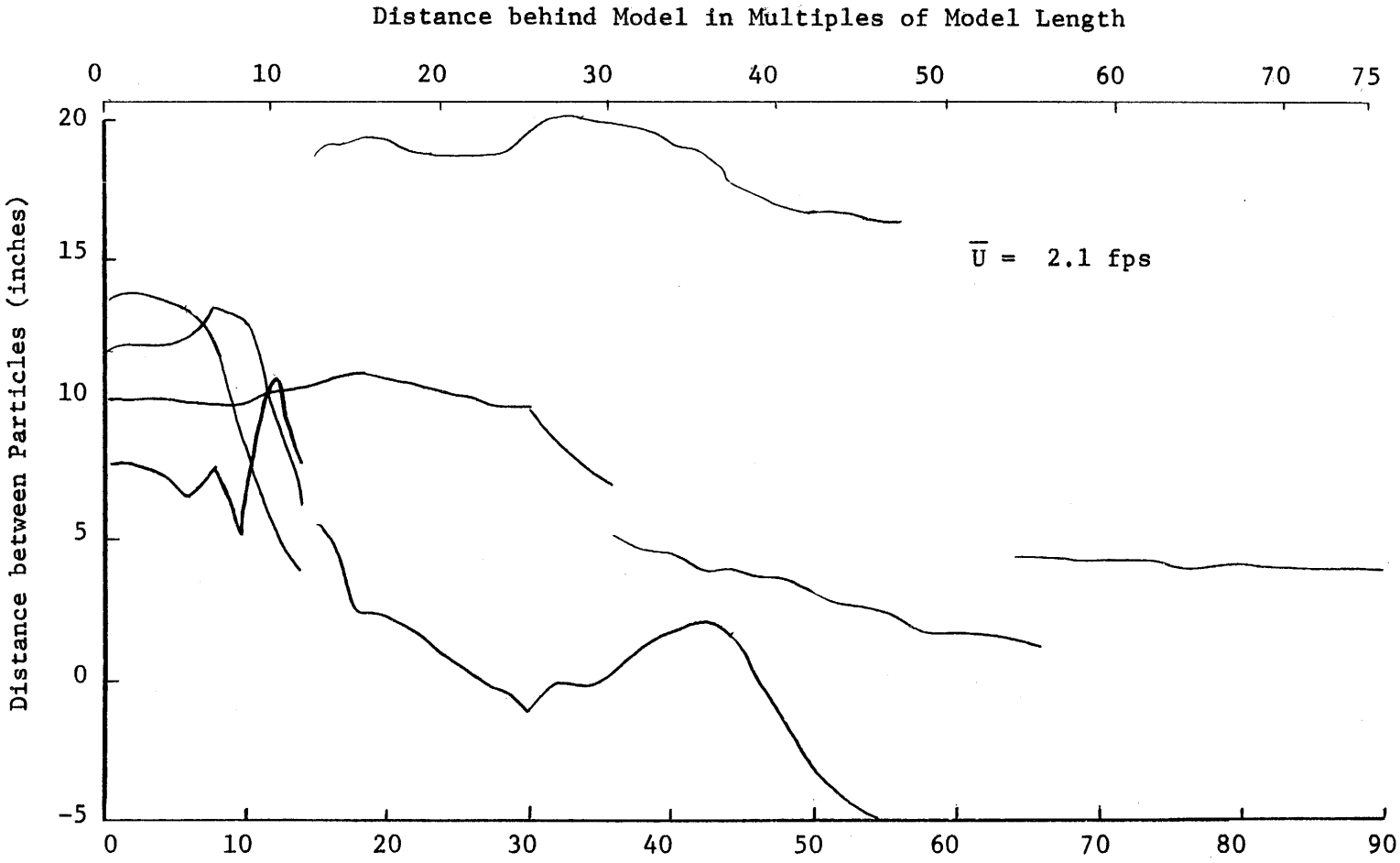

Spacing between Particles which were Initially Equidistant from $\mathbb{C}$ ($\frac{1}{\rho_o}\frac{d\rho}{dy} = -0.003\ ft^{-1}$)

Figure 22a

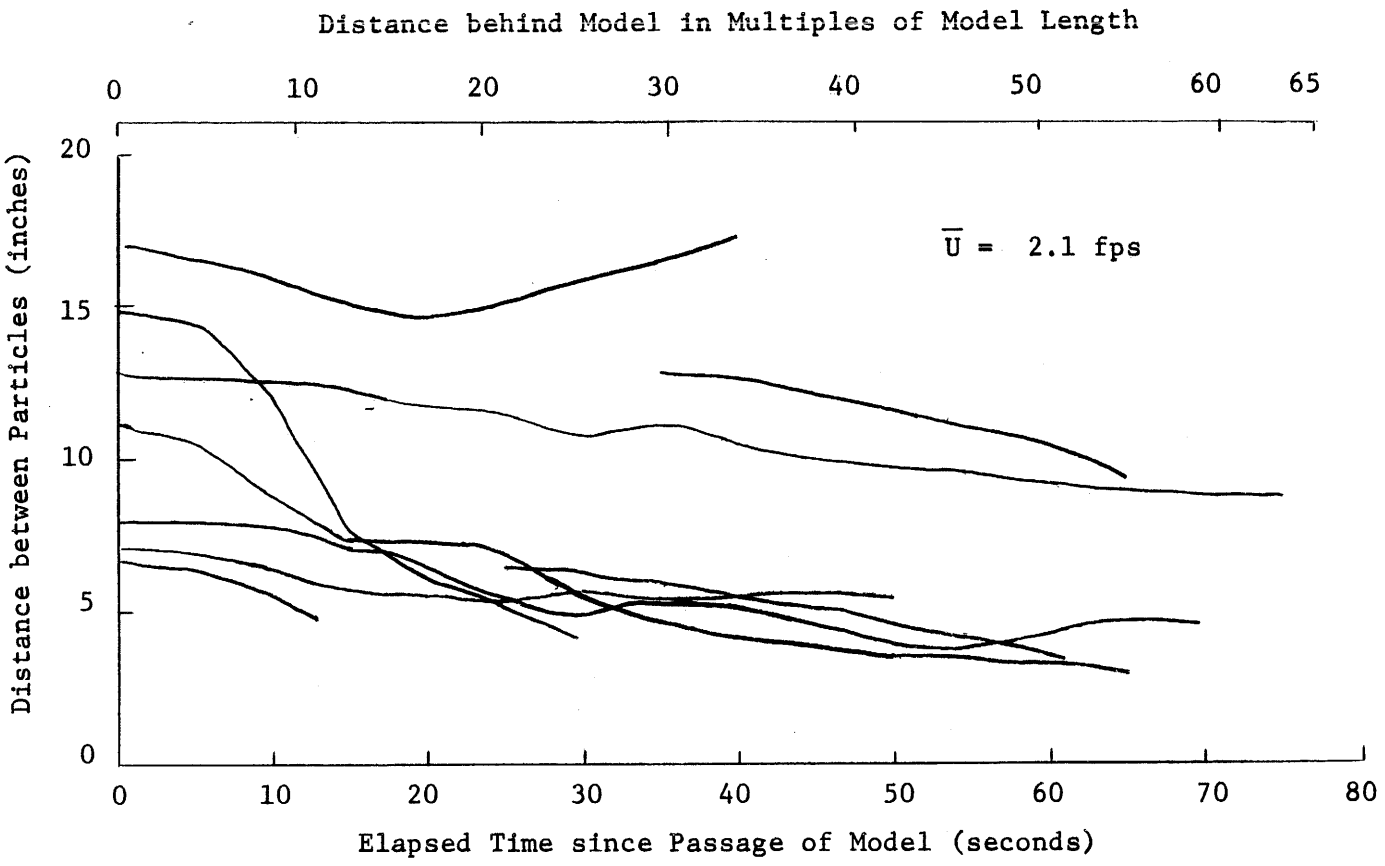

Spacing between Particles which were Initially Equidistant from $\mathbb{Q}$ ($\frac{1}{\rho_o}\frac{d\rho}{dy} = -0.0015\ ft^{-1}$)

Figure 22b

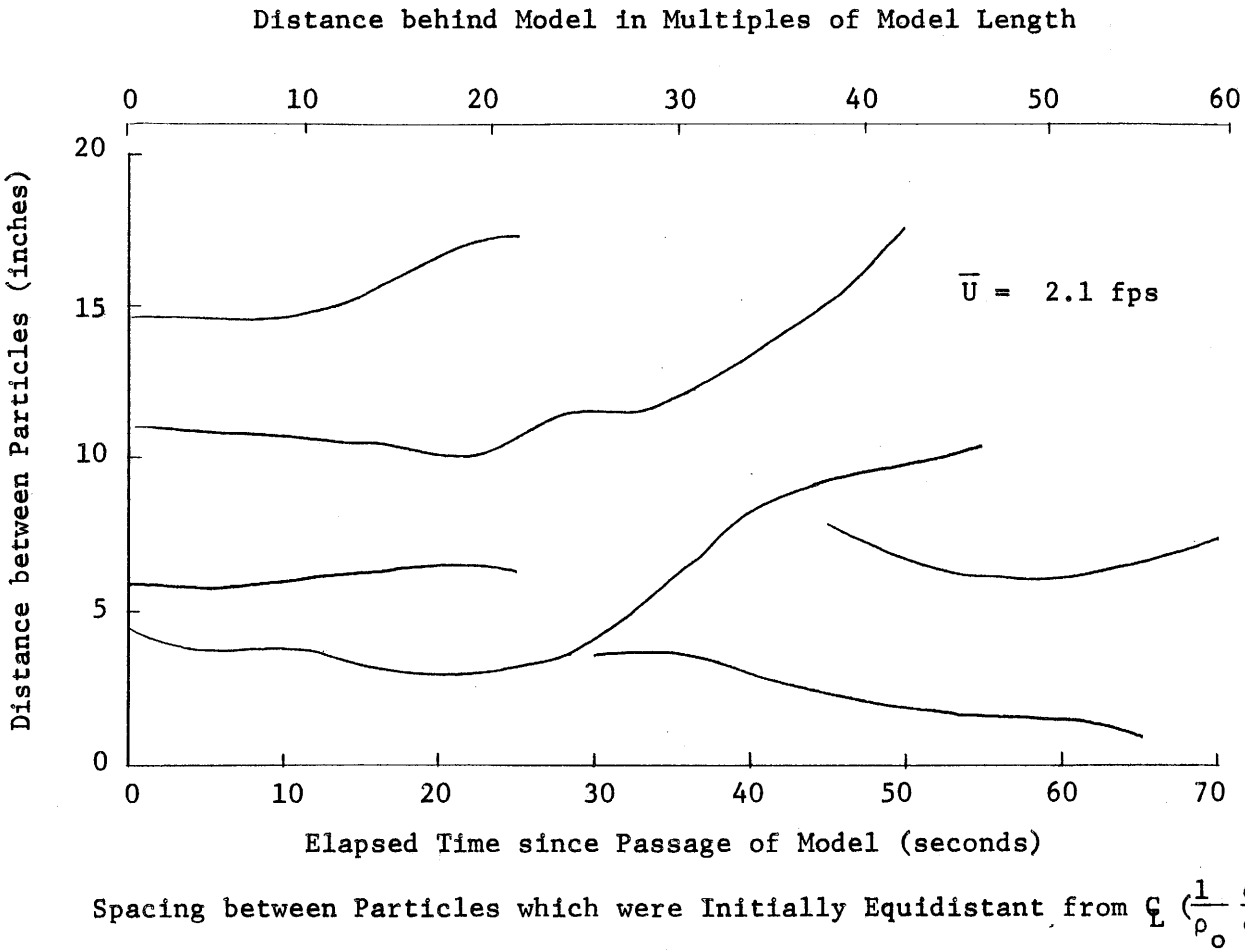

Spacing between Particles which were Initially Equidistant from $\mathcal{C}_L$ ($\frac{1}{\rho_o}\frac{d\rho}{dy} = 0$)

Figure 22c

D. The Physical Mechanism of Wake Collapsing

The experimental results reported in Sections B and C of this chapter provide the basis for a better understanding of the behavior of the mixed region and the turbulent wake of an axi-symmetric self-propelled body travelling in a density-stratified liquid. A general description of the physical phenomena occurring in the region is presented here, with specific reference to the experimental results obtained for the density gradient of $\frac{1}{\rho_o}\frac{d\rho}{dy} = -0.003\ (ft)^{-1}$ used in both the density configuration study and in some of the motion studies.

1. Initial Stage of Wake Growth

In the early wake, at short distances behind the body, turbulent mixing is the dominant feature of the motion, and the outline of the turbulent wake and also the region of significant mixing would be expected to expand at the same rate in all directions, similarly to a wake in a homogeneous fluid. This phase is illustrated in Figure 23a. Note that turbulent diffusion will transport more of the density biasing agent (salt in the present experiments) vertically than horizontally, due to the larger gradients in the vertical direction. This is shown in Figure 23a by the varying lengths of the dashed arrows, which represent salinity transport due to turbulent mixing. Note also that the potential energy of the fluid in the wake is increase by the net upward transport of salinity, which has the effect of raising the center of gravity of the mixed fluid. This is readily seen in the density profile at the centerline of the body, which is also shown in Figure 23a. The duration of this initial phase and the expanse of the mixed region should depend on the strength of the density gradient. Either a very strong or a very weak density gradient would diminish the vertical salinity transport during this period, the former by increasing the stability of the density profile, and the latter by diminishing the rate of vertical transport accomplished by the wake's eddy diffusivity.

In the experiments, this initial phase appeared to extend to a distance of 2 1/2 to 5 model lengths (13 to 25 disc diameters) behind the body. Beyond this distance the shape of the envelope delineating the zone of principal mixing was elongated in the horizontal direction, indicating that the collapse phase of the wake growth had begun.

2. Early Stages of Wake Collapse

As the zone of mixing expands with increasing distance behind the body, the turbulent diffusion subsides, but is still significant at intermediate distances. The mixed region in the wake, in which the lines of constant density are displaced from their initial position, is now in a state of density disequilibrium with the surrounding fluid, and thus gravity forces start to influence the behavior of the mixed region by returning the fluid containing the displaced salinity toward a level of density equilibrium. Viewed from energy considerations, the increase in potential energy that was engendered by the turbulent mixing is transformed into the kinetic energy of the net translational velocities of the fluid in and around the mixed zone. Hence, one has the interesting situation of turbulent mixing, which gives no net fluid displacement in planes transverse to the path, giving rise to a net fluid motion as the mixed fluid seeks levels of density equilibrium. The mixed fluid that spreads laterally outward, at about the level of the body, is displaced by lateral inward flow above and below the body's path. This stage of the wake development is shown in Figure 23b, where the solid curved arrows represent the movement of the fluid moving toward equilibrium and the motion produced in the surrounding fluid. It would appear unlikely that any appreciable vertical motion would occur outside of the mixed zone, because this would change the potential energy of the stratified fluid in the unmixed region and hence would require a source of energy that is not available. This consideration bears the important implication that unless the turbulent wake extends to the free surface and accomplishes some mixing in the vicinity of it, there can be no convergence of the surface fluid. Turbulence was

observed to extend to the surface in the present experiments, as was revealed by the motion pictures of the free surface. If the turbulent field generated by the body is not strong enough to generate some mixing in the region just below the free surface, the wake collapse will have no effect on the free surface, except possibly some wave oscillations.

The experimental results indicate that this phase of the wake's development, in which both turbulent diffusion and gravity-induced motion affect the configuration of the mixed region, occurs in the vicinity of about 10 model lengths behind the body, where the rate of vertical expansion has diminished to almost zero, suggesting that gravitational body forces are suppressing the expansion generated by turbulent diffusion.

3. Later Stages of Wake Collapse

At larger distances behind the body, the turbulence will have decayed to the point where there is no significant diffusive transport. The behavior of the mixed region is then dominated by the gravitational forces which drive the mixed fluid to levels of density equilibrium where it spreads laterally, as shown in Figure 23c. The isochlors return to their initial levels and then oscillate about these levels until the internal waves dissipate. In Figure 23c, the dashed arrows no longer appear, indicating that the turbulent mixing has subsided. There is no longer a turbulent wake as such, but only a mixed region. This mixed region increases in lateral extent but loses its identity as density equilibrium is again reached.

It was concluded that in the present experiments this last stage, in which the lateral spreading of the mixed region is the primary feature, occurs at distances beyond about 15 model lengths (75 disc diameters) behind the body.

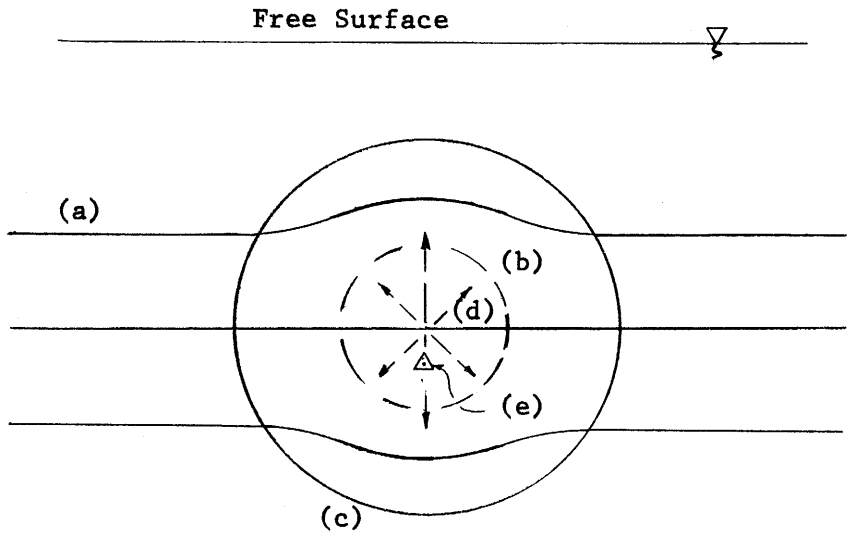

(a) Normalized Isochlors

(b) Outline of Self-Propelled Body

(c) Nominal Limit of Turbulent Wake and Mixed Region

(d) Salinity Transport due to Mixing

(e) Original Center of Gravity

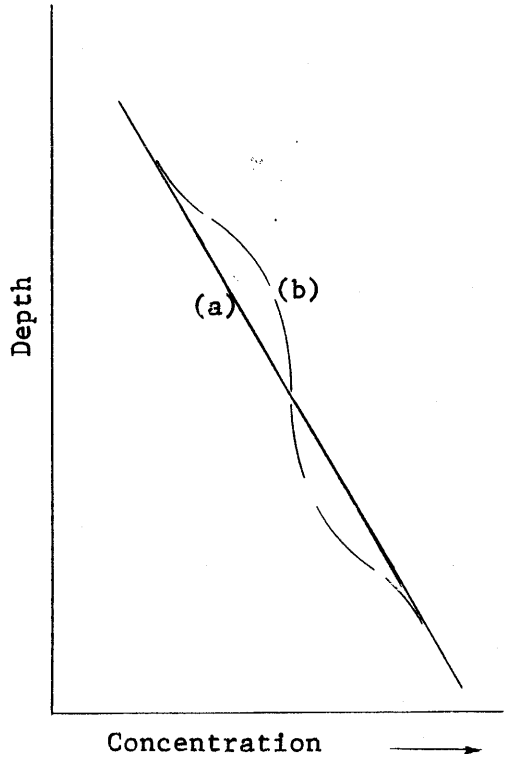

(a) Original Normalized Concentration

(b) Normalized Concentration at Initial Stage of Wake Generation

Initial Stage of Wake Growth

Figure 23a

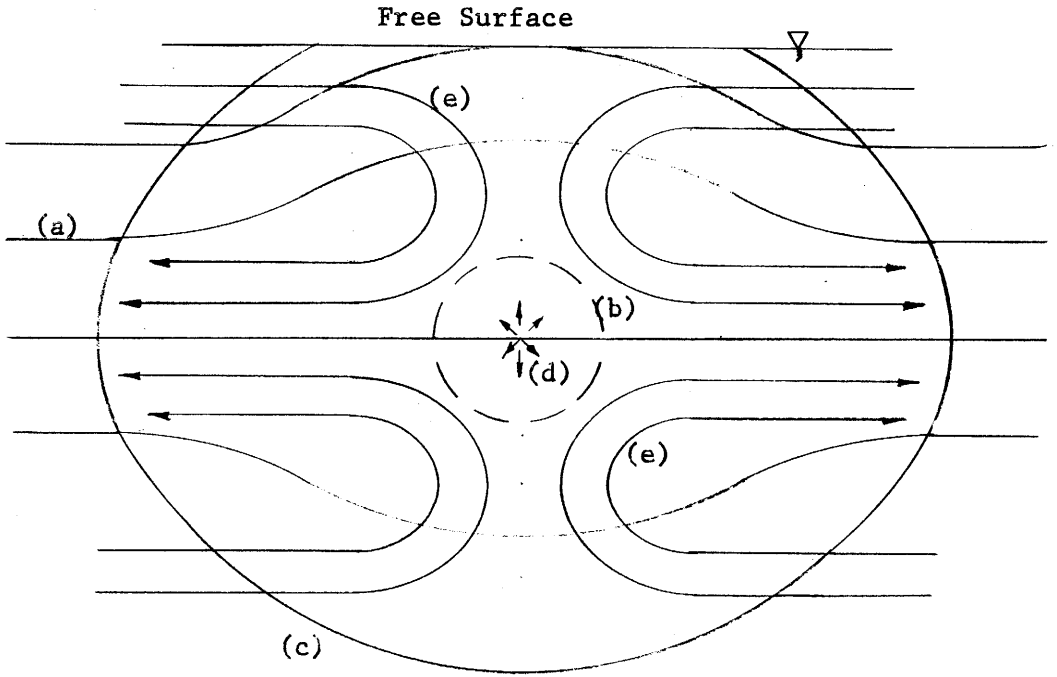

(a) Normalized Isochlors

(b) Outline of Self-Propelled Body

(c) Nominal Limit of Turbulent Wake and Mixed Region

(d) Salinity Transport due to Mixing

(e) Lines of Fluid Motion

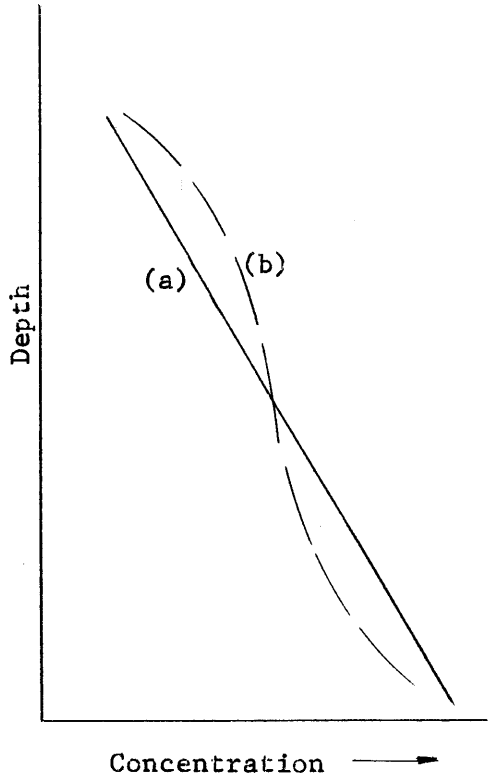

(a) Original Normalized Concentration

(b) Normalized Concentration at Initiation of Wake Collapse

Initiation of Wake Collapse

Figure 23b

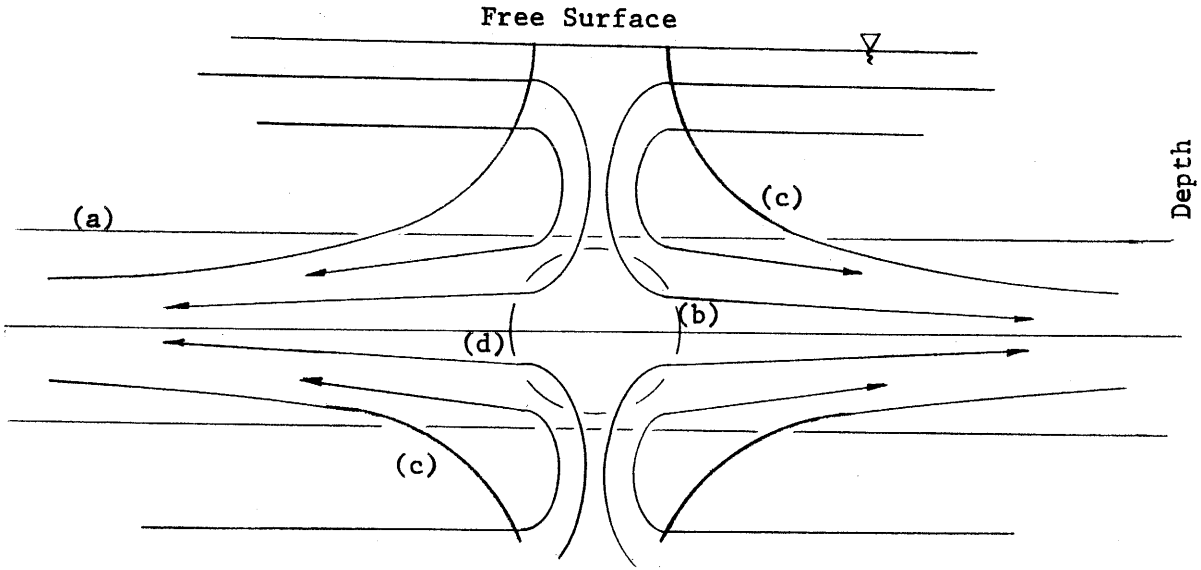

(a) Normalized Isochlors

(b) Outline of Self-Propelled Body

(c) Nominal Limit of Turbulent Wake and Mixed Region

(d) Lines of Fluid Motion

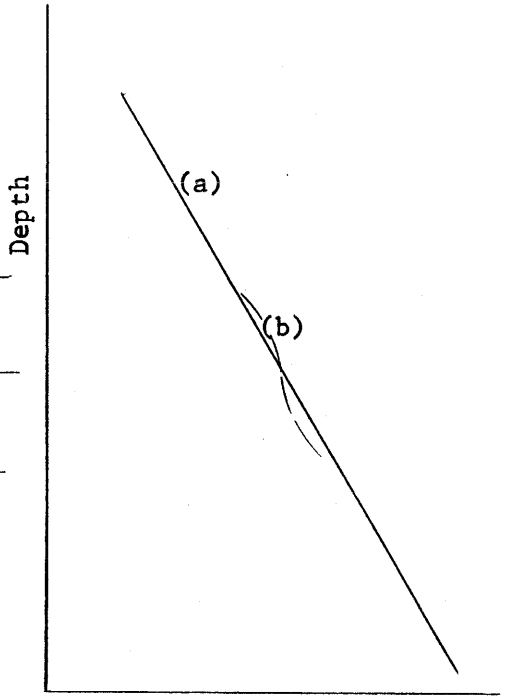

(a) Original Normalized Concentration

(b) Normalized Concentration in Later Stage of Wake Collapse

Later Stage of Wake Collapse

Figure 23c

CHAPTER V

CONCLUSIONS

The purpose of this study was to conduct a comprehensive investigation of the configuration of a three-dimensional axi-symmetric wake generated by a self-propelled body in a linearly density-stratified fluid, and the fluid motion induced at the free surface by the collapse of the wake. The study was approached from two avenues: 1) Identification of the zone of turbulent mixing by studying the variations of the salinity concentration distribution within the mixed region and in the surrounding vicinity, and; 2) Study of the motion induced at the free surface by measuring particle displacements at the surface. Extensive studies in both areas were conducted for a density gradient, $\frac{1}{\rho_o}\frac{d\rho}{dy} = -0.003\ (ft)^{-1}$, and additional studies of surface particle movements were made for gradients of zero and $-0.0015\ (ft)^{-1}$, to determine the dependence of the wake collapse and surface convergence on the strength of the density stratification. All other quantities were held constant throughout the experimental program. The twin-screw, self-propelled body used in the experiments was 30 inches long, 4 1/2 inches in diameter, and had a 6-inch diameter circular disc mounted on its bow. Its average speed was 1.92 fps, giving a Reynolds number of 8.9×10^4, based on the disc diameter.

The conclusions drawn from these experiments can be briefly summarized as follows:

1. For the density gradient of $-0.003\ (ft)^{-1}$ and an average model speed of 1.92 fps, an initial expansion of the wake region was detected immediately behind the model. The growth rate appeared to be about the same in all directions,and not unlike the wake in a homogenoous fluid. The first effects of gravity appeared at a distance of about 10 model lengths or 50 disc diameters behind the model, as elements of the fluid displaced by turbulent mixing moved back toward positions of density equilibrium. This was

followed by a rapid vertical collapse of the mixed region as the turbulent mixing subsided and gravitational effects became dominant. The configuration of the salinity distribution indicated that the vertical collapse was virtually complete at a distance of about 15 model lengths (75 disc diameters) behind the body.

2. A horizontal expansion of the mixed region was associated with its vertical collapse. Although the lateral extent of the mixed region was difficult to define, it could be approximately delineated by comparing charts of the normalized concentration contours for various cross sections behind the model, and noting the displacements of the isochlors from their initial positions. The horizontal expansion was observed to increase almost linearly with time during the period of vertical wake collapse.

3. Concurrent with the vertical collapse of the mixed region, a convergence, toward the path of the model, of fluid at the free surface was measured. This convergence is explained from continuity considerations; above the path of the body, the descending mixed fluid in the collapsing wake is replaced by fluid moving inward from the sides.

4. It was concluded from some energy arguments that there can be convergence of the surface fluid only if the turbulent wake extends to the free surface and generates some mixing in the vicinity of the surface. Lateral convergence can occur only at the sides of a region which has undergone some mixing.

5. A reduced gradient of $-0.0015\ (\text{ft})^{-1}$ had the effect of decreasing the lateral extent over which the surface convergence occurred, and decreasing the rate of convergence. It was concluded that a reduced gradient diminishes the relative strength of the gravitational effects, resulting in a weaker collapse.

6. A field of internal gravity waves was excited by the passage of the body, and presumably also by the collapse of the wake. These waves made it very difficult to experimentally define the extent and geometry of the turbulent wake and the mixed region.

A by-product of this investigation was the development of a quick and efficient method for generating linear density profiles in a large experimental tank. A long 4-inch high plate (athwart to the direction of motion) and a 1 1/2-inch diameter rod, both spanning the width of the tank were towed at a constant speed through an initially two-layered fluid. The plate was positioned at the density interface and the rod slightly below the free surface. The resulting equilibrium density profile was linear over most of the depth of the tank. It was found possible to use each profile for eight to ten experiments before the profile became so disrupted that it was no longer usable.

VI REFERENCES

1. Schlichting, Herman, Boundary Layer Theory, 4th Edition, McGraw-Hill Book Co., Inc., New York, 1960, Chapter XXIII.

2. Prych, E. A., Harty, F. R., and Kennedy, J. F., "Turbulent Wakes in Density-Stratified Fluids of Finite Extent," Technical Report No. 65, Hydrodynamics Laboratory, Massachusetts Institute of Technology, Cambridge, Mass., July, 1964.

3. Kennedy, J. F., and Froebel, R. A., "Two-Dimensional Turbulent Wakes in Density-Stratified Liquids,"A.S.M.E. Publication, 64-WA/UNT-11, 1964.

4. Schooley, A. H. and Stewart, R. W., "Experiments with a Self-Propelled Body in a Fluid with a Vertical Density Gradient," Journal of Fluid Mechanics, Vol. 9, No. 1, 1963.

5. Wu, Jin, "Collapse of Turbulent Wakes in Density-Stratified Media," Technical Report 231-4, Hydronautics, Inc., Laurel, Md., 1965.

6. Prych, E. A., "Mixing of a Stratified Fluid in a Two-Dimensional Turbulent Wake," S.M. Thesis, Course I, Massachusetts Institute of Technology, Cambridge, Mass., 1961.

7. Froebel, R. A., "Two-Dimensional Turbulent Momentum Wakes in Density-Stratified Fluids," S.M. Thesis, Course I, Massachusetts Institute of Technology, Cambridge, Mass., 1964.

8. Yih, Chia-Shun, Dynamics of Nonhomogeneous Fluids, The Macmillan Co., New York, 1965.

9. International Critical Tables, McGraw-Hill Book Co., Inc., New York, 1928.

APPENDIX A

LIST OF SYMBOLS

α	=	constant of proportionality
β	=	constant of proportionality
δ	=	recorder deflection
ν	=	kinematic viscosity
ρ	=	mass density
ρ_o	=	mass density of fresh water
Δ	=	incremental difference
b	=	characteristic wake width
b_o	=	width or diameter of wake generating body
b^*	=	maximum vertical wake width
d	=	model body diameter
d^*	=	depth of submergence
g	=	gravitational constant
x	=	horizontal dimension
y	=	vertical dimension
C	=	concentration
$D^* = \frac{UT^*}{b_o}$	=	distance in body diameters that moving body travels in time T^*
$F = U\sqrt{\frac{-1}{\rho_o g}\frac{d\rho}{dy}}$	=	densimetric Froude number
L	=	length of model

$N = \sqrt{-\frac{g}{\rho_o}\frac{d\rho}{dy}}$ = Väisälä frequency

P = fluid resistance at a point

R = resistance

$R = \frac{\bar{U}b_o}{\nu}$ = Reynolds number

T^* = time necessary to attain maximum wake width

U = horizontal velocity

$\bar{U}$ = average horizontal velocity

APPENDIX B

VALUES OF NORMALIZED CONCENTRATIONS AT DISCRETE DISTANCES BEHIND THE MODEL AND VARIOUS GRID POSITIONS

Values of Normalized Concentrations for 2.5

Model Lengths at Various Grid Positions

Distance from Horizontal ℄ (inches)	Distance from Vertical ℄ (inches)										
	0	1.5	3	4.5	6	7.5	9	10.5	12	13.5	15
6	.27	.320	.305	.265	.210	.185	.170	.200	.195	.190	.205
4.5	.460	.450	.360	.305	.340	.310	.250	.250	.235	.255	.255
3				.345	.320	.350	.350	.340	.310	.300	.330
1.5				.420	.395	.425	.425	.415	.385	.375	.405
0				.34	.41	.455	.44	.495	.485	.48	.485
-1.5				.415	.485	.530	.515	.570	.560	.555	.560
-3				.720	.680	.660	.660	.650	.650	.665	.650
-4.5	.660	.630	.560	.735	.715	.715	.720	.760	.745	.745	.745
-6	.780	.765	.670	.815	.820	.820	.810	.820	.800	.805	.820

TABLE B-I

Values of Normalized Concentrations for 5.0

Model Lengths at Various Grid Positions

Distance from Horizontal ℄ (inches)	Distance from Vertical ℄ (inches)										
	0	1.5	3	4.5	6	7.5	9	10.5	12	13.5	15
6	.385	.210	.360	.355	.160	.150	.150	.195	.170	.170	.185
4.5	.475	.370	.285	.260	.265	.235	.220	.230	.235	.240	.250
3	.505	.480	.360	.315	.335	.295	.310	.305	.330	.330	.325
1.5	.535	.600	.630	.470	.410	.415	.375	.410	.405	.420	.410
0	.700	.615	.765	.340	.415	.410	.505	.480	.480	.470	.550
-1.5	.615	.625	.705	.620	.560	.530	.520	.565	.550	.560	.565
-3	.660	.770	.745	.760	.695	.675	.675	.695	.665	.665	.640
-4.5	.630	.740	.780	.705	.715	.720	.715	.805	.770	.755	.745
-6	.930	.900	.770	.875	.895	.850	.845	.850	.830	.825	.830

TABLE B-II

Values of Normalized Concentrations for 7.5

Model Lengths at Various Grid Positions

Distance from Horizontal ℄ (inches)	Distance from Vertical ℄ (inches)										
	0	1.5	3	4.5	6	7.5	9	10.5	12	13.5	15
6	.220	.300	.325	.180	.120	.120	.140	.150	.170	.165	.175
4.5	.375	.340	.295	.315	.145	.170	.170	.190	.160	.245	.210
3	.485	.440	.370	.300	.315	.320	.325	.310	.355	.280	.325
1.5	.525	.530	.555	.350	.375	.385	.425	.475	.415	.420	.415
0	.535	.515	.615	.455	.425	.390	.470	.465	.460	.460	.460
-1.5	.490	.565	.615	.595	.545	.555	.560	.560	.545	.550	.550
-3	.435	.505	.540	.690	.690	.670	.675	.740	.705	.690	.655
-4.5	.665	.590	.820	.670	.685	.685	.675	.820	.800	.775	.765
-6	.950	.665	.735	.885	.850	.895	.880	.860	.840	.835	.840

TABLE B-III

Values of Normalized Concentrations for 10.0

Model Lengths at Various Grid Positions

Distance from Vertical ℄ (inches)

Distance from Horizontal ℄ (inches)	0	1.5	3	4.5	6	7.5	9	10.5	12	13.5	15
6	.18	.175	.18	.18	.17	.15	.16	.205	.175	.195	.18
4.5	.245	.255	.270	.310	.25	.23	.27	.215	.140	.175	.180
3	.40	.315	.365	.29	.33	.385	.365	.375	.375	.325	.325
1.5	.47	.43	.43	.465	.455	.405	.405	.415	.405	.415	.410
0	.435	.545	.58	.485	.445	.44	.485	.49	.485	.485	.485
-1.5	.44	.495	.49	.63	.615	.585	.555	.595	.580	.575	.57
-3	.57	.585	.595	.655	.655	.645	.62	.66	.68	.68	.66
-4.5	.645	.530	.620	.71	.72	.68	.66	.77	.77	.76	.75
-6	.765	.735	.740	.745	.78	.785	.705	.85	.83	.835	.84

TABLE B-IV

Values of Normalized Concentrations for 12.5

Model Lengths at Various Grid Positions

Distance from Horizontal ℄ (inches)	Distance from Vertical ℄ (inches)										
	0	1.5	3	4.5	6	7.5	9	10.5	12	13.5	15
6	.180	.195	.180	.160	.120	.120	.090	.175	.160	.175	.180
4.5	.400	.310	.260	.205	.315	.285	.320	.255	.175	.185	.195
3	.370	.270	.330	.310	.360	.375	.405	.385	.365	.340	.320
1.5	.635	.555	.450	.425	.470	.390	.390	.440	.400	.425	.400
0	.640	.580	.600	.570	.535	.510	.500	.480	.510	.475	.560
-1.5	.325	.370	.375	.510	.510	.570	.630	.565	.570	.570	.610
-3	.665	.795	.735	.640	.660	.635	.550	.775	.735	.720	.680
-4.5	.680	.680	.690	.715	.725	.695	.735	.935	.875	.850	.780
-6	.730	.700	.730	.770	.805	.745	.690	.820	.810	.820	.825

TABLE B-V

Values of Normalized Concentrations for 15.0

Model Lengths at Various Grid Positions

Distance from Horizontal ℄ (inches)	Distance from Vertical ℄ (inches)										
	0	1.5	3	4.5	6	7.5	9	10.5	12	13.5	15
6	.20	.22	.205	.290	.215	.195	.165	.195	.195	.175	.265
4.5	.330	.315	.295	.305	.280	.300	.310	.230	.165	.180	.170
3	.395	.355	.390	.380	.380	.345	.390	.385	.395	.345	.325
1.5	.560	.490	.475	.455	.485	.455	.405	.385	.430	.440	.395
0	.530	.540	.535	.615	.505	.520	.490	.495	.495	.495	.505
-1.5	.610	.615	.540	.610	.585	.525	.570	.540	.535	.560	.570
-3	.735	.765	.720	.665	.655	.645	.64	.685	.680	.69	.67
-4.5	.66	.580	.720	.700	.705	.730	.74	.81	.815	.775	.770
-6	.765	.720	.755	.850	.830	.80	.80	.88	.765	.805	.825

TABLE B-VI

Values of Normalized Concentrations for 17.5

Model Lengths at Various Grid Positions

Distance from Vertical ℄ (inches)

Distance from Horizontal ℄ (inches)	0	1.5	3	4.5	6	7.5	9	10.5	12	13.5	15
6	.22	.285	.250	.230	.330	.285	.260	.290	.225	.245	.250
4.5	.425	.370	.465	.445	.075	.145	.200	.250	.190	.185	.180
3	.365	.440	.390	.335	.365	.405	.485	.450	.425	.435	.365
1.5	.435	.620	.645	.455	.495	.435	.420	.375	.385	.400	.385
0	.585	.555	.620	.615	.555	.485	.515	.560	.495	.500	.590
-1.5	.695	.700	.650	.530	.575	.575	.580	.565	.475	.545	.550
-3	.610	.670	.700	.645	.620	.550	.655	.780	.590	.670	.730
-4.5	.845	.810	.915	.720	.715	.735	.705	.905	.885	.830	.880
-6	.855	.865	.795	.865	.880	.840	.880	.785	.780	.790	.805

TABLE B-VII

Values of Normalized Concentrations for 20.0

Model Lengths at Various Grid Positions

Distance from Horizontal ℄ (inches)	Distance from Vertical ℄ (inches)										
	0	1.5	3	4.5	6	7.5	9	10.5	12	13.5	15
6	.18	.23	.225	.215	.220	.195	.200	.270	.250	.235	.27
4.5	.350	.325	.335	.320	.165	.195	.205	.280	.260	.370	.195
3	.305	.300	.345	.280	.315	.320	.330	.280	.470	.435	.355
1.5	.490	.475	.540	.525	.500	.575	.430	.405	.420	.420	.400
0	.59	.48	.520	.510	.545	.535	.560	.520	.505	.480	.505
-1.5	.695	.685	.635	.600	.580	.570	.580	.570	.545	.560	.565
-3	.59	.66	.635	.685	.655	.635	.650	.730	.730	.615	.630
-4.5	.86	.820	.885	.790	.760	.765	.760	.825	.785	.790	.795
-6	.92	.94	.880	.840	.830	.805	.820	.735	.73	.76	.780

TABLE B-VIII

Values of Normalized Concentrations for 22.5

Model Lengths at Various Grid Positions

Distance from Vertical ℄ (inches)

Distance from Horizontal ℄ (inches)	0	1.5	3	4.5	6	7.5	9	10.5	12	13.5	15
6	.265	.250	.265	.235	.040	.200	.210	.190	.270	.215	.190
4.5	.370	.330	.345	.330	.205	.195	.365	.260	.265	.240	.205
3	.385	.360	.380	.330	.330	.340	.350	.350	.525	.525	.425
1.5	.495	.530	.520	.330	.415	.430	.425	.430	.425	.435	.390
0	.660	.590	.645	.555	.560	.640	.585	.460	.460	.440	.535
-1.5	.625	.585	.595	.585	.615	.595	.590	.505	.515	.545	.520
-3	.770	.685	.575	.735	.700	.665	.650	.845	.885	.860	.720
-4.5	.680	.730	.765	.845	.800	.765	.790	.845	.860	.875	.910
-6	.870	.940	1.005	.815	.760	.795	.785	.770	.745	.735	.770

TABLE B-IX

Values of Normalized Concentrations for 25.0

Model Lengths at Various Grid Positions

Distance from Vertical ℄ (inches)

Distance from Horizontal ℄ (inches)	0	1.5	3	4.5	6	7.5	9	10.5	12	13.5	15
6	.21	.18	.17	.24	.22	.210	.245	.185	.18	.18	.215
4.5	.295	.285	.290	.280	.305	.325	.335	.290	.265	.255	.200
3	.345	.350	.360	.315	.380	.385	.300	.345	.420	.410	.360
1.5	.315	.395	.410	.395	.475	.500	.465	.430	.435	.395	.370
0	.565	.565	.590	.545	.520	.530	.500	.460	.500	.505	.500
-1.5	.600	.575	.650	.595	.590	.580	.595	.580	.580	.575	.575
-3	.66	.68	.68	.685	.670	.670	.655	.630	.635	.660	.680
-4.5	.78	.80	.76	.775	.770	.755	.760	.730	.790	.800	.800
-6	.96	.935	.905	.800	.825	.805	.80	.87	.82	.815	.815

TABLE B-X

Values of Normalized Concentrations for 30.0

Model Lengths at Various Grid Positions

Distance from Horizontal ℄ (inches)	Distance from Vertical ℄ (inches)										
	0	1.5	3	4.5	6	7.5	9	10.5	12	13.5	15
6	.205	.205	.165	.18	.15	.13	.155	.225	.265	.240	.185
4.5	.295	.310	.305	.290	.250	.255	.20	.295	.340	.305	.290
3	.335	.315	.330	.360	.370	.360	.365	.345	.525	.650	.540
1.5	.430	.425	.430	.420	.475	.425	.430	.425	.430	.425	.465
0	.515	.505	.55	.505	.55	.55	.53	.42	.465	.48	.495
-1.5	.545	.555	.525	.565	.575	.580	.60	.555	.565	.575	.590
-3	.72	.83	.735	.71	.685	.68	.685	.73	.73	.755	.715
-4.5	.715	.67	.645	.785	.745	.755	.720	.665	.725	.720	.715
-6	.815	.745	.795	.790	.785	.785	.825	.87	.645	.735	.83

TABLE B-XI

Values of Normalized Concentrations for 35.0

Model Lengths at Various Grid Positions

Distance from Horizontal ℄ (inches)	Distance from Vertical ℄ (inches)										
	0	1.5	3	4.5	6	7.5	9	10.5	12	13.5	15
6	.235	.235	.205	.180	.22	.195	.190	.29	.21	.235	.165
4.5	.315	.270	.270	.280	.255	.255	.215	.285	.285	.190	.350
3	.385	.360	.395	.435	.375	.380	.40	.380	.360	.350	.405
1.5	.430	.430	.485	.475	.390	.390	.360	.375	.390	.435	.420
0	.52	.495	.515	.495	.505	.480	.565	.465	.475	.465	.470
-1.5	.540	.555	.590	.570	.560	.555	.570	.585	.570	.575	.570
-3	.765	.80	.78	.655	.65	.65	.655	.67	.680	.655	.635
-4.5	.840	.82	.845	.725	.720	.725	.710	.725	.745	.755	.765
-6	.86	.795	.715	.805	.76	.81	.835	.90	.895	.87	.885

TABLE B-XII

Values of Normalized Concentrations for 40.0

Model Lengths at Various Grid Positions

Distance from Vertical $\mathbb{C}_L$ (inches)

Distance from Horizontal $\mathbb{C}_L$ (inches)	0	1.5	3	4.5	6	7.5	9	10.5	12	13.5	15
6	.195	.225	.22	.205	.195	.165	.165	.21	.265	.235	.215
4.5	.30	.305	.275	.330	.280	.270	.250	.210	.355	.295	.225
3	.37	.33	.355	.35	.355	.42	.40	.39	.405	.360	.370
1.5	.415	.485	.445	.460	.425	.445	.370	.405	.385	.40	.390
0	.540	.520	.515	.50	.50	.515	.535	.485	.480	.485	.490
-1.5	.580	.605	.605	.60	.595	.580	.555	.580	.605	.595	.60
-3	.65	.695	.72	.71	.715	.71	.700	.710	.715	.700	.655
-4.5	.695	.740	.685	.720	.730	.740	.755	.715	.730	.715	.700
-6	.86	.81	.855	.820	.820	.785	.800	.82	.83	.85	.87

TABLE B-XIII